UNIVERSITY OF OKLAHOMA

GRADUATE COLLEGE

ULTRA-HIGH PERFORMANCE CONCRETE FOR CONNECTIONS OF PRECAST, PRESTRESSED GIRDERS MADE CONTINUOUS FOR LIVE LOAD

A THESIS

SUBMITTED TO THE GRADUATE FACULTY

In partial fulfillment of the requirements for the

Degree of

MASTER OF SCIENCE

By

CONNOR WILLIAM CASEY

Norman, Oklahoma

2019

ULTRA-HIGH PERFORMANCE CONCRETE FOR CONNECTIONS OF PRECAST, PRESTRESSED GIRDERS MADE CONTINUOUS FOR LIVE LOAD

A THESIS APPROVED FOR THE

SCHOOL OF CIVIL ENGINEERING AND ENVIRONMENTAL SCIENCE

BY

Dr. Royce Floyd, Chair

Dr. Jeffery Volz

Dr. Chris Ramseyer

Acknowledgments

First, I want to thank my advisor Dr. Royce Floyd for giving me such a great opportunity to work for him, as an undergrad, and then as a graduate student. I appreciate all of the knowledge and guidance you gave me during the years of working on your research, and most importantly the admiration I gained from you towards prestressed concrete.

I would like to thank, Stephen Roswurm, Jacob Roswurm, and Dakota Gennings for their help in the initial phases of this research. Whether it was staying late at the lab tying rebar cages, or helping mix and pour the concrete for the prestress girders, I truly cannot express enough gratitude for your efforts on this project.

I would also like to thank the rest of my thesis committee members, Dr. Jeffery Volz, and Dr. Chris Ramseyer.

I would like to thank the Oklahoma Department of Transportation for funding this project

I'm truly thankful for the financial support, and encouragement from my parents Robert and Faith Casey, and Grandparents Ron and Jenny Morton.

Lastly, I would like to thank my friends, Antonio Guardado, Joel Pickard, Robert Gilstrap, and Mathew Freeze for their continued support and encouragement during my academic career.

Table of Contents

List of Tables

List of Figures

ABSTRACT

Continuity joints have often been employed in bridges with precast, prestressed girders to increase the overall ability of bridges to distribute live loads by making two simple spans continuous. However, if the continuity connection cracks due to time-dependent effects in the girders, continuity can be lost, resulting in simply supported conditions for the girders and subjecting the joint reinforcement to potential corrosion damage. A potential solution to prevent cracking in the continuity joint is using Ultra-High Performance Concrete (UHPC). UHPC has been studied to determine how effective the material is in a number of bridge applications, but not for continuity joints. Six specimens consisting of two precast girders made continuous with a UHPC joint were constructed and tested. Three of the six specimens focused on continuity joint detailing for new bridge construction and followed the AASHTO LRFD 2014 Specifications for design. The three remaining specimens focused on retrofit continuity joint detailing for existing bridges. Both designs consisted of the same reinforcement ratio determined for newly constructed continuity joints. Each specimen was tested using a static point load at mid-span of each girder in order to produce the maximum negative moment in the continuity joint. In addition, a positive moment test was conducted on the joint for the third specimen of each joint type. The results from the tests to failure showed an increase in girder capacity compared to the design values, similar crack development for both joint types, and limited flexural cracking in the joint compared to the girders. Though the joints did not fail, this indicates that the failure would likely be pushed out of the joint and into the girders for both types of connections. Overall, the retrofit specimens exhibited better performance than the newly constructed specimens, with higher ultimate capacity, less deflection under the load points, and the reinforcing bars yielding

within the joint. The retrofit connection is a potential option for strengthening existing simple span bridges in service by making the girders continuous for live load.

1.0 Introduction

Poor performance of continuous concrete bridges formed from simply supported precast concrete girders constructed as continuous for live load can often be at least partially traced back to the integrity of the continuity connection between the precast prestressed girders. Integrity issues can arise from multiple types of loads occurring on the bridge. One loading concern is the time dependent effects due to creep and shrinkage in the prestressed girders. These effects can lead to cracking in the continuity joint and cause the joint to be susceptible to corrosion. In addition, the corrosion effects can extend to the ends of prestressed girders. Ultra-high performance concrete (UHPC) is a possible solution to prevent cracking and improve durability of the connection.

UHPC is defined by FHWA as "a cementitious composite material composed of an optimized gradation of granular constituents, a water-to-cementitious materials ratio less than 0.25, and a high percentage of discontinuous internal fiber reinforcement" (FHWA, 2013). This combination of material allows UHPC to exhibit superior mechanical properties compared to typical concrete. Some of the mechanical properties are compressive strength exceeding 20 ksi, tensile strength exceeding 0.9 ksi, low permeability and a high resistance to freeze thaw. UHPC also has high flowability in the fresh state allowing it to fill complicated formwork. These advantages would significantly increase resistance to stresses caused by time dependent effects in the positive moment regions in the joint to help prevent cracking, and UHPC has the added benefit that it can be easily used to repair existing continuity connections. This not only would fix one major concern in bridges made continuous for live load but can also be implemented on in-service bridges containing simply supported beams with no continuity. These bridges can be retrofit by adding continuity joints into the configuration, which have the potential to increase live load capacity and replace the expansion joint in the deck in the process. UHPC has been used in

bridges, from connecting precast deck panels together for accelerated bridge construction, to completely making prestressed girders out of UHPC. However, there is limited to no test data for the application of UHPC to continuity joints and exploring UHPC for this application in continuity joints could potentially lead to more effective methods of bridge construction and rehabilitation of current bridges.

Three key goals were tested in this research.

- UHPC is an effective method for connecting precast, prestressed girders for live load continuity in both new construction and bridge retrofits.
- UHPC is more effective for continuity joint compared to values calculated for conventional concrete.
- Bond behavior is more efficient in UHPC resulting in shorter required splice lengths.

To explore these hypotheses, research was conducted to investigate UHPC type connections between pairs of prestressed concrete girders. Two types of connections were examined: newly constructed and retrofit of existing bridges. The specimens tested consisted of two approximately half scale AASHTO Type II girders with UHPC continuity connections. They were tested as two-span specimens with one point load at each beam mid-span to develop the maximum negative or positive moment in the joint. This testing was done to examine the feasibility of using UHPC for continuity connections of precast concrete girders, to characterize deflection and cracking behavior of the joint, and to observe the failure type that may occur in the joint, the interface between the girder and the joint, or the beam.

There are two objectives that were addressed by this research.

- Create a plan for retrofit/new construction of continuity joints with UHPC
- Characterize cracking and strength level performance of UHPC continuity joints for retrofit and new construction

2.0 Literature Review

2.1 Continuity Joints

A continuity joint is the connection of two simply supported beams that allows the transfer of subsequent superimposed dead loads and live loads. This type of connection has been used occasionally in pretensioned prestressed concrete girder bridges since the 1960's. Continuity joints for prestressed concrete girders are established with composite concrete decks and the use of diaphragms at pier caps and abutments. Establishing the continuity joint allows for any future loads, beyond the self-weight of the members, to be transferred through the structure as a continuous beam, improving the durability and strength of the whole bridge. In addition, continuity between the girders helps reduce maintenance costs, improve the appearance, and the riding qualities of the bridge (Freyermuth 1969). Figure 1 shows a typical continuity connection between two girders.

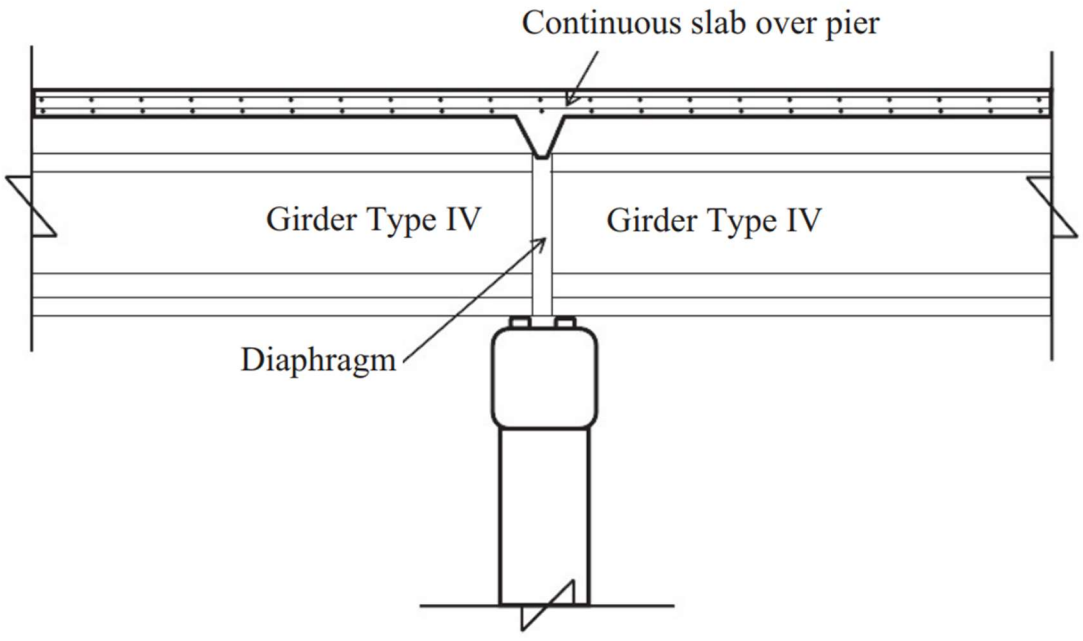

Figure 1. Typical continuity joint between girders (Eamon Et. al., 2016).

As a vehicle drives over a bridge, it acts as a set of point loads moving across the girders. In response the girders bend and create moments within the girders. Within the continuity joint, two types of moments occur. The first type is the negative moment that occurs in the composite deck portion over the pier and abutments when the girders are loaded. The second type is the positive moment, which occurs in the diaphragm between girders due to time dependent effects within the girders. These time dependent effects are concrete shrinkage of the girders and creep effects related to the amount of prestress in the girders. Figure 2 shows the effects from creep and shrinkage causing upward deflection to each induvial span. Once the girders are connected to each other with a continuity joint the ends become restrained, and additional creep effects can cause a restraint moment within the connection preventing the girder ends from rotating.

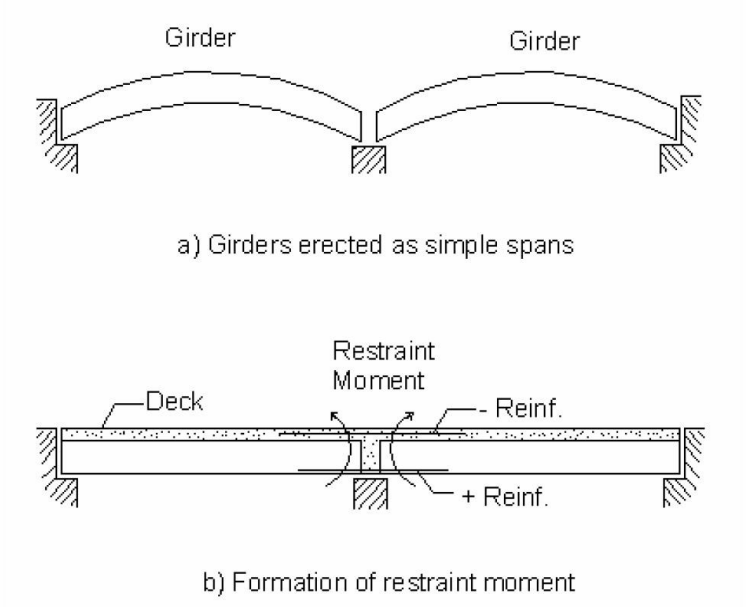

Figure 2. Formation of positive restraint moment under time dependent effects (Saadeghvaziri et. al. 2004).

Early studies done by the Portland Cement Association (PCA) state that the reinforcement in the composite deck properly accounts for the negative moment, but these studies also showed that the positive moment can lead to cracking of the diaphragm if not properly detailed (Miller 2004). If the connection at the diaphragm cracks, the positive moment is released, the joint acts as a hinge, and continuity is lost. However, if the positive moment connection is properly detailed using reinforcement within the joint, the connection maintains continuity despite cracking and the joint still performs as designed with the reinforcement transferring the moment through the joint (Miller 2004). There are two types of reinforcement typically used for the positive moment connection. The first type of reinforcement is prestressing strands extending out of the girder for the specified length and bent upwards to form a 90-degree angle creating a hook. The second type of reinforcement is mild steel embedded into the girder and extending into the joint for a set distance and bent at a 90-degree angle to form a hook.

The study described in "Connection of Simple-span Precast Concrete Girders for Continuity" was conducted on six types of joint detailing for the positive moment connection (Miller 2004). Figures 2, 3, and 4 show the joint detailing tested. The study was to further explore the findings in an analytical study on the positive moment connection presented in the NCHRP 322 report (Oesterle et al. 1989), since the analytical study in NCHRP 322 found that the positive moment connection for continuity had no structural benefit in bridges. The NCHRP 322 authors' reasoning for this conclusion was if the positive moment due to time dependent effects becomes restrained at the continuity connection, the effects then also occur along the girder creating a second positive moment in the girder. As a result, the same secondary moment was observed in the typical simple span case without a continuity joint, thus no structural benefit was gained. The authors of NCHRP 519 stated that any type of analytical study performed has a set of

parameters, and the results observed do not necessarily reflect other types of situations. Thus, Miller (2004) concluded that continuity joints still can be useful as they can still provide structural benefits by providing a connection point between girders, in case of supports being damaged, and protecting girder ends from erosion.

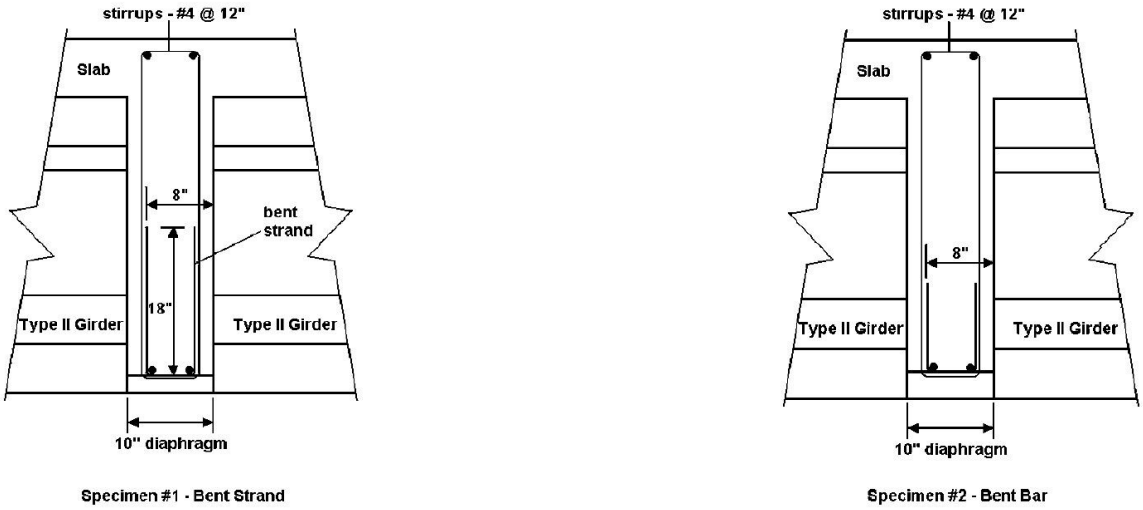

Figure 3. Details of the specimen #1 and # 2 connection (Miller 2004).

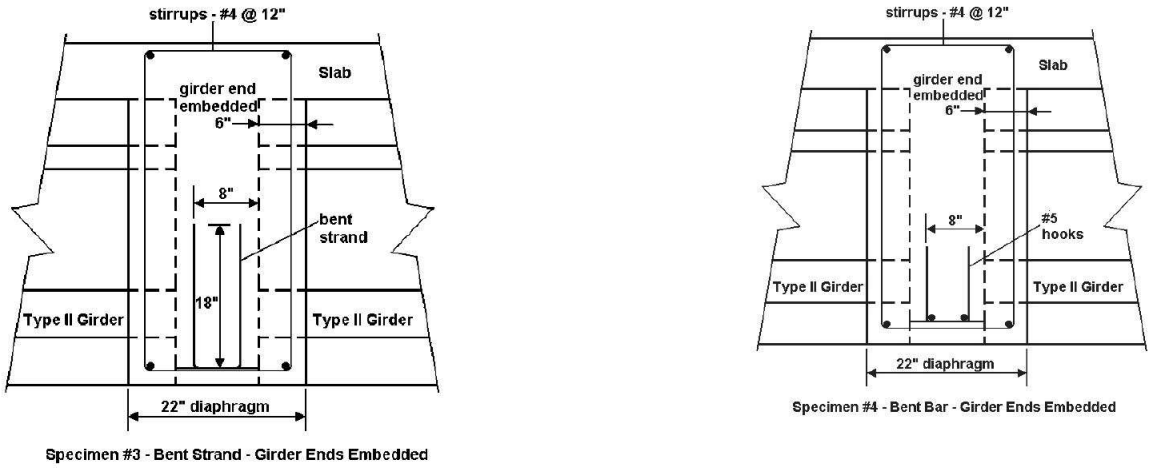

Figure 4. Details of the specimen #3 and # 4 connection (Miller 2004).

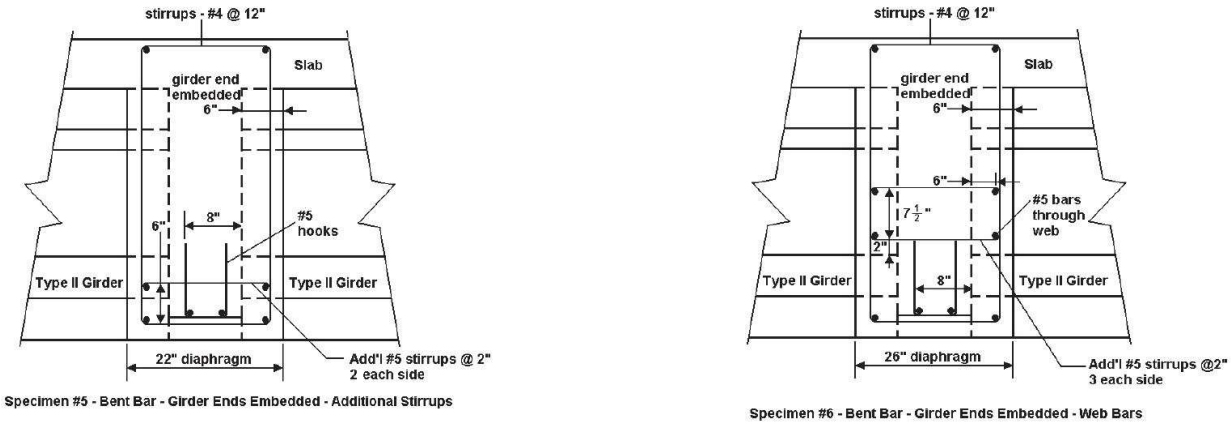

Figure 5. Details of the specimen #3 and # 4 connection (Miller 2004).

Another study was carried out by Saadeghvaziri, Spillers, and Yin (2004) "Improvement of Continuity Connection over Fixed Piers". The initial part of this study was to monitor three bridges in New Jersey to determine the degree of continuity for different configurations of anchor bolts fixing the superstructure to the piers. The study found the continuity in these bridges ranged from 0 to 90 percent for service load transfer between multiple continuity connections in one span for each bridge. With only three bridges being examined for the level of continuity, and since the range of continuity for those bridges was not consistent, this study shows that the level of continuity in all continuity connections within any given bridge could be inconsistent. The researchers concluded that the difference in the level of continuity in bridges is dominated by time dependent effects. The age of the girder when continuity was established had the largest impact on continuity for the three bridges investigated. This further supported the authors theory that, if the girders were embedded into the continuity joint using elastomeric pads with little lateral deformation and have anchor bolts in each continuity joint connecting the girders to the pier, the supports act like a fixed end preventing rotation and sliding to occur. This fixed end behavior leads to the time dependent deformation effects being completely restrained and

causing cracking in the continuity joint. The authors recommended to not use anchor bolts, not embed girder ends into the diaphragm or joint, and to design only one support in the continuous span as a pin with the rest designed as "rollers" to prevent the girders acting as a fixed connection (Saadeghvaziri et. al. 2004).

A finite element study was also conducted as part of the same research to determine the range of girder age when continuity should be established between prestressed girders. The finite element model results further supported that establishing continuity between girders at an early age significantly increased the positive moment created by time dependent effects. The modeling also showed the time dependent effects of creep dominated when continuity is established at an early age with shrinkage not contributing substantially at the early age. However, when continuity is established at a later age shrinkage dominated the time dependent effects, and creep did not contribute as much at the later age. The age of the girders at the time of establishing continuity found to have the largest impact on reducing these effects was at an age between 45 and 90 days (Saadeghvaziri et al 2004).

2.2 Ultra High-Performance Concrete

Ultra-High Performance Concrete (UHPC) is defined by the FWHA as "a cementitious composite material composed of an optimized gradation of granular constituents, a water-to-cementitious materials ratio less than 0.25, and a high percentage of discontinuous internal fiber reinforcement" (FHWA, 2013). This combination of material allows UHPC to have improved material properties compared to normal concrete, which could be useful in the highway bridge industry for many types of applications, specifically for connections of discrete elements. In order for UHPC to be a more valid material for everyday practice in the bridge community, the

Federal Highway Administration (FHWA) did a full material property characterization of a proprietary UHPC called Ductal® (Graybeal 2006). The authors followed the American Society for Testing and Materials (ASTM) and the American Association of State Highway and Transportation Officials (AASHTO) recommended procedures for the material characterization tests that would typically be done on normal concrete. In some cases the author had to modify or develop new tests to adequately test specimens to get useful information due to the vast differences in material properties.

In addition, Graybeal (2006) examined four different curing regimens on specimens for each of the material characterization tests. The first regimen was the control specimen that followed the manufactures recommendation for steam curing the UHPC at 194 ºF (90 ºC) and 95 percent relative humidity for 48 hours. The second regimen was not steam cured, but cured at the standard laboratory environment from demolding until testing. The third regimen was tempered steam curing, which was similar to the steam curing recommended by the manufacturer, but the temperature was limited to 140 ºF (60 ºC). The fourth regimen was a delayed steam curing that did not begin until the 15th day after initial casting, and used the same recommended specifications for steam curing by the manufacture. Table 1 shows the average UHPC material properties found after testing was concluded. Based on all the results the author concluded that UHPC had enhanced material properties when compared to normal concrete (Graybeal 2006).

Table 1. Average UHPC material properties (Graybeal 2006).

Material Characteristic	Steam	Untreated	Tempered Steam	Delayed Steam	Supplemental Description
Compressive Strength (MPa)	193	126	171	171	ASTM C39; 28-day strength
Modulus of Elasticity (GPa)	52.4	42.7	51.0	50.3	ASTM C469; 28-day modulus
Split Cylinder Cracking Strength (MPa)	11.7	9.0	11.7	11.7	ASTM C496
Prism Flexure Cracking Strength (MPa)	9.0	9.0	10.3	9.7	ASTM C1018; 305-mm span; corrected
Mortar Briquette Cracking Strength (MPa)	8.3	6.2	9.7	6.9	AASHTO T132
Direct Tension Cracking Strength (MPa)	9.7–11.0	5.5–6.9	7.6–9.0	9.0–11.0	Axial tensile load
Prism Flexural Tensile Toughness (I_{30})	53.0	48.3	43.1	48.3	ASTM C1018; 305-mm span
Long-Term Creep (C_{cu})	0.29	0.78	0.66	0.31	ASTM C512; 77-MPa sustained load
Long-Term Shrinkage (microstrain)	766	555	620	657	ASTM C157; initial reading after set
Total Shrinkage (microstrain)	850	790	–	–	Embedded vibrating wire gage
Coeff. of Thermal Exp. ($x10^{-6}$ mm/mm/°C)	15.6	14.7	15.4	15.2	AASHTO TP60-00
Chloride Ion Penetrability (coulombs)	18	360	39	18.00	ASTM C1202; 28-day test
Chloride Ion Permeability (kg/m^3)	< 0.06	< 0.06	< 0.06	< 0.06	AASHTO T259; 12.7-mm depth
Scaling Resistance	No Scaling	No Scaling	No Scaling	No Scaling	ASTM C672
Abrasion Resistance (grams lost)	0.17	0.73	0.20	0.13	ASTM C944 2x weight; ground surface
Freeze-Thaw Resistance (RDM)	96%	112%	100%	99%	ASTM C666A; 600 cycles
Alkali-Silica Reaction	Innocuous	Innocuous	Innocuous	Innocuous	ASTM C1260; tested for 28 days

1 MPa = 145 psi
1 GPa = 145,000 psi
1 psi = 6.895 Pa
1 mm = 0.039 inch
1 mm/mm/°C = 1.8 inches/inches/°F
1 kg/m^3 = 1.69 lb/yd^3
1 g = 0.035 oz

2.3 UHPC Bond Behavior

2.3.1 Bond Behavior of Mild Steel in UHPC

A critical consideration for connections of concrete elements is bond of reinforcement with the concrete material used for the connection. FHWA conducted pull out testing on a tension-tension lap splice configuration to characterize the bond behavior of mild steel reinforcing bar in UHPC (Yuan and Graybeal 2014). To recreate the tension-tension lap splice configurations, the specimens consisted of a precast concrete slab with multiple rows of No. 8 reinforcing bar extending 8 inches from the face of the slab. Reinforcing bars to be tested were placed between the No. 8 reinforcing bars in each row, and rectangular strips of UHPC were cast around the reinforcing bar configurations, with the line of reinforcing bars being on the center line of the strips, as shown in Figure 6. To recreate tension that would occur in an actual structural configuration with lap splices, a steel frame with two hydraulic rams was used to put the testing

reinforcing bar into direct tension with the frame pushing against the precast concrete deck, as shown in Figure 7 (Yuan and Graybeal 2014).

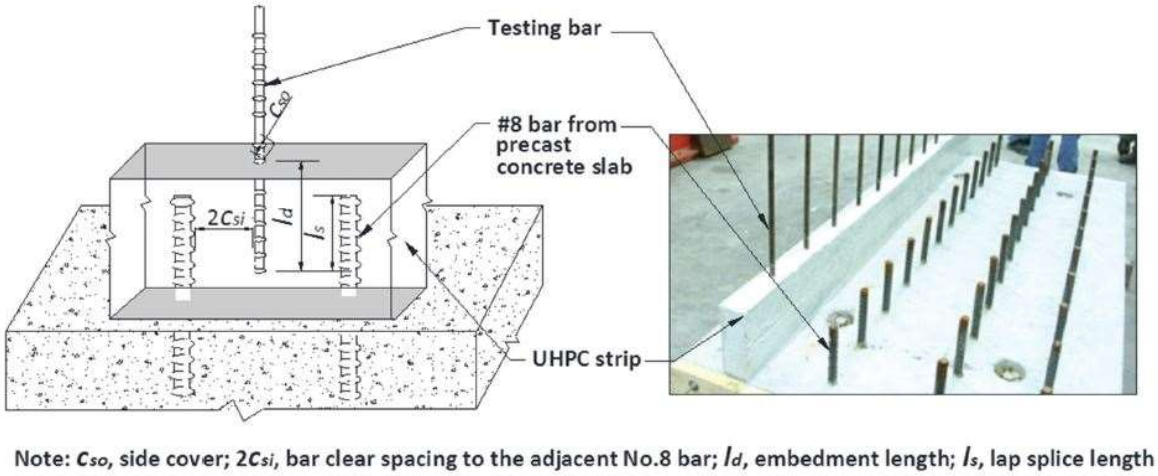

Figure 6. Overall configuration of FHWA reinforcing bar bond test specimens (Yuan and Graybeal 2014).

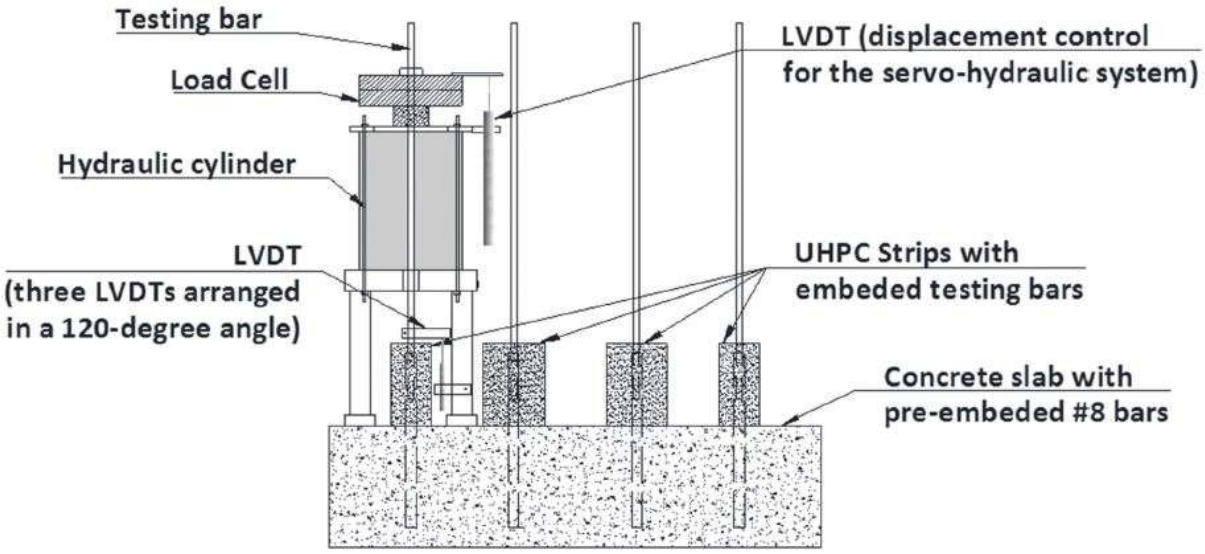

Figure 7. FHWA reinforcing bar bond test loading setup (Yuan and Graybeal 2014).

The parameters that were examined for the bond behavior of reinforcing bars in UHPC were the embedment length, concrete side cover, bar spacing, concrete compressive strength, reinforcing bar size, reinforcing bar yield strength, and casting orientation. After conducting over 200 tests with the various parameters, the results showed a difference in bond behavior for reinforcing bars embedded in UHPC compared to normal concrete. The author concluded that increases in embedment length, side cover, and compressive strength increased the bond strength. Characteristics that decreased bond strength were epoxy-coated reinforcing bars and reinforcing bar with a larger diameter. It was also noted that a non-contact lap splice had an increased bond strength over a contact lap splice. The author stated that this was most likely due to the non-contact splice allowing fibers to fully engage around the reinforcing bar, thereby increasing bond strength, as the contact lap splice would not allow fibers to fully engage around the portion of the bars that were in contact with one another, thus decreasing the bond strength (Graybeal 2014).

Based on the results from the bond behavior tests in UHPC, the authors presented design recommendations to obtain deformed bar yield strength before bond failure. The recommendations are for bar sizes ranging from No. 4 to No.8, either uncoated or epoxy-coated, and clear spacing of greater than $2d_b$ and lap splice length (l_s). Minimum requirements were an embedment length of $8d_b$, side cover of $3d_b$, and UHPC compressive strength of 13.5 ksi (93.1 MPa). Additionally, a lap splice length of 75 percent of embedment length was recommended, as this was the percentage used for the majority of tests conducted in this study. There was also guidance for when the side cover was between $2d_b$ and $3d_b$ to use $10d_b$ for the embedment length. The possibility to reduce the minimum embedment length of $8d_b$ was noted for cases having an increase in side cover or an increase of compressive strength, and the possibility of increasing

embedment if decreasing side cover and compressive strength. This allows designers to have potential flexibility in connection design with UHPC (Yuan and Graybeal 2014).

2.3.2 Bond Behavior of Untensioned Prestressing Strands

FHWA conducted pull out testing on a tension-tension non-contact lap splice configuration to determine the development length of untensioned prestressing strands cast in UHPC (Graybeal 2014). The test specimen was created using the standard prestressing strand grid pattern of 2 inches center to center spacing, with adding a splice strand in-between. This was done to recreate a splice connection that would be used for splicing prestressed members together using 0.5 and 0.6 inch prestressing strands. Figure 8 shows the geometry of the UHPC test specimen, and the strand location within the UHPC for a 0.5 inch strand (Graybeal 2014).

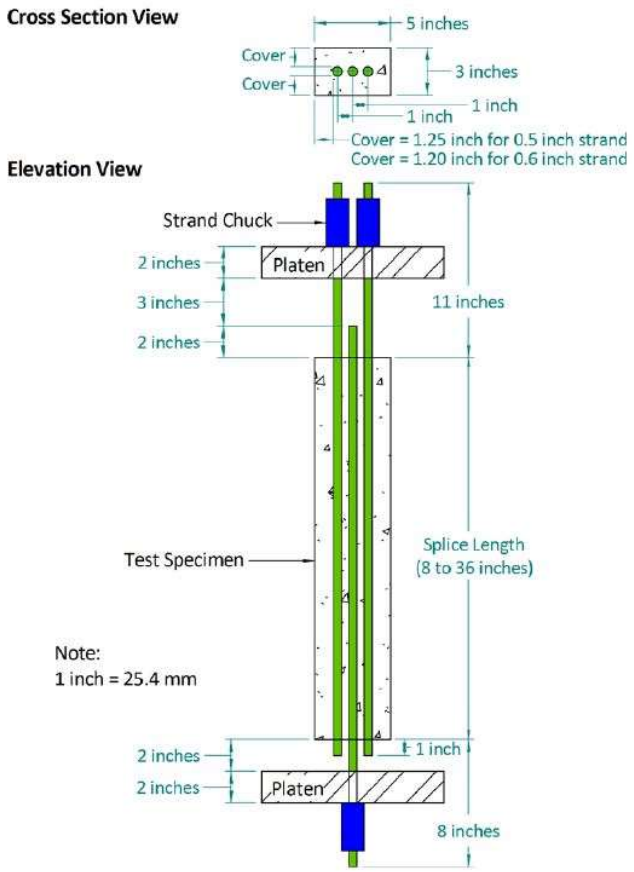

Figure 8. Geometry of FHWA prestressing strand-UHPC bond test specimen with 0.5 in. diameter strands (Graybeal 2014).

The non-contact lap splice lengths tested for the 0.5 and 0.6 inch prestressing strands ranged from 8 to 24 inches. The specimens were tested using a servo-hydraulic testing machine to allow for displacement control. Tension was applied to the end with two prestressing strands (live end). Slippage and load resistance were measured at the single prestressing strand located at the dead end of the testing machine. The test was stopped for each specimen upon reaching the peak resistance, or until the strand ruptured. Figure 9 shows one of the specimens in the testing frame. The authors concluded from the test results that the 0.5 inch diameter strand can be fully developed within a splice length 20 inches, and the 0.6 inch diameter strands can be approximately developed within 24 inches (Graybeal 2014).

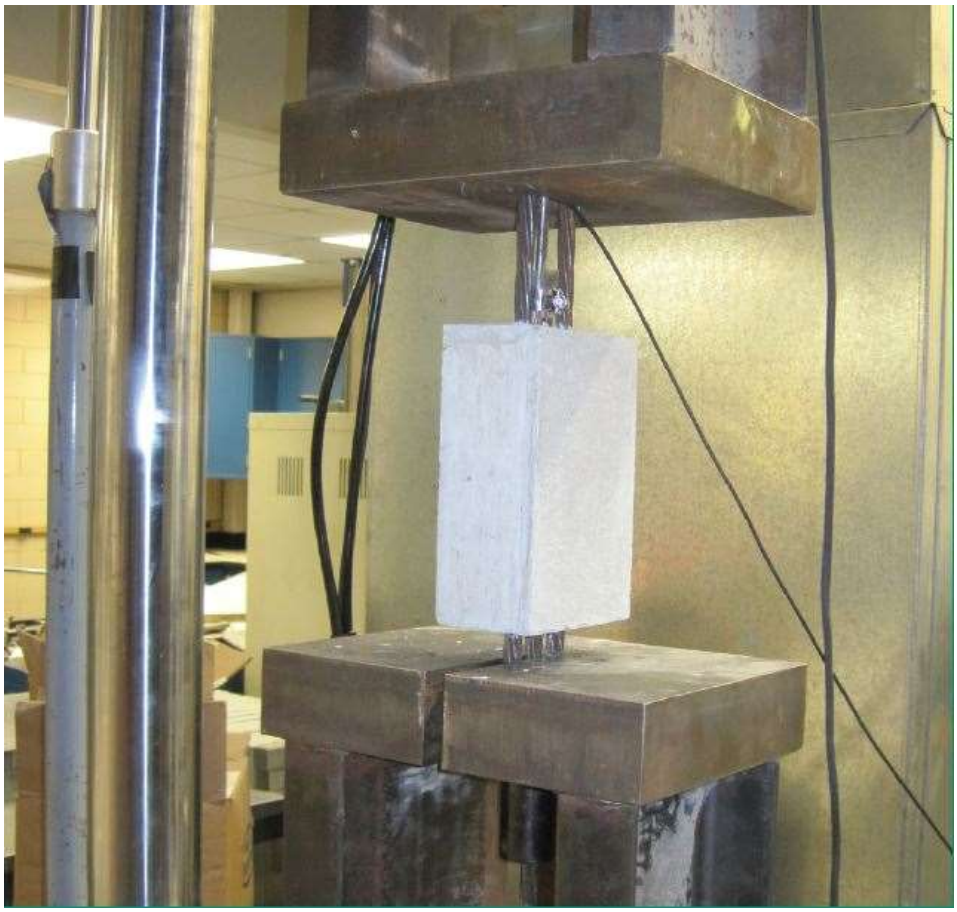

Figure 9. FHWA prestressing strand-UHPC bond test specimen in load frame (Graybeal 2014).

2.4 UHPC Applications

2.4.1 UHPC Slab Joint Connections

The use of modular bridges has become more and more popular due to the advances in UHPC. In the past, modular bridge construction was much more difficult because regular concrete was not ideal for connecting segmental bridges together, as the development length for reinforcing bar would require large joints and the high amount of reinforcement would lead to poor consolidation of normal concrete in the joints. UHPC has a much higher strength which allows a

reduced development length, a more feasible joint length, and has high flowability to prevent consolidation issues.

To understand the behavior of using UHPC in joints for modular bridges, FHWA conducted tests on slabs with UHPC joints having several different types of reinforcement detailing (Graybeal 2010). Cyclic and static loading conditions were applied to the joint specimens. Cyclic loading was used to model actual roadway conditions for a vehicle driving over the connections and to achieve fatigue failure, and a single point load was used to test the ultimate capacity. The results from the dynamic loading tests on the joints indicated far better performance than expected, and the overall ultimate failure capacity of the joints also exceeded expectations. As a result, using UHPC as a type of connection proved to be favorable, since in most cases the load path going through a connection is the weak link in the overall structure. Having a robust connection allows concrete around the connection to fail, which is much more desirable from a design standpoint. Figure 10 depicts the test layout of the slabs used in the 2010 FHWA study (Graybeal 2010).

Figure 10. FHWA UHPC slab connection test (Graybeal 2010).

2.4.2 UHPC Splice Connection Between two Precast Girders

Splicing precast concrete members at mid-span with post-tensioning has been a common practice but the need for post-tensioning could potentially be avoided through the use of a spliced connection between precast prestressed concrete members. To make this possible the spliced connection would use UHPC, combined with the un-tensioned prestressing strands extending from the precast members. To better understand how this type of connection would behave under loading, FHWA conducted two flexural tests with two precast prestressed AASHTO Type BII-36 box beams in tandem connected with a splice at mid-span using UHPC (Maya and Graybeal 2017). The connection detail for the first test used a splice length of 24 inches ($40d_b$) for the un-tensioned strands. In addition, six No. 4 reinforcing bars were included in the bottom half of the connection with 6 inches extending into the joint, and 6 inches extending into the beam. Figure 11 shows the cross-sectional view of the box beams.

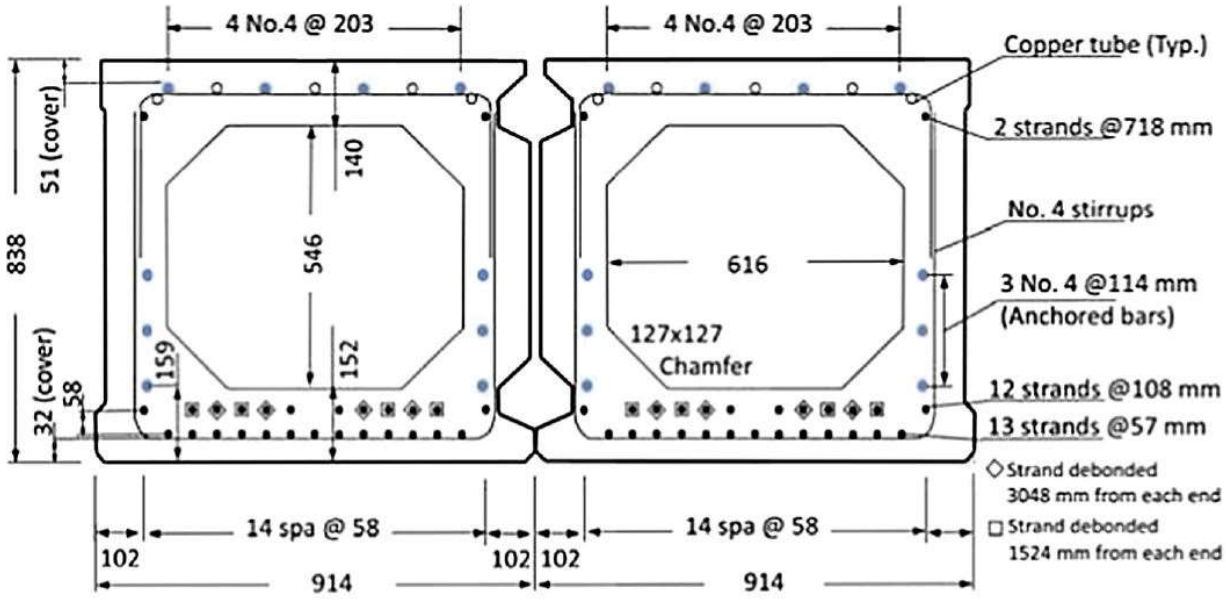

Figure 11. Cross-sectional view of box girders used for FHWA beam splice test (Maya and Graybeal 2017).

The first test conducted on this connection detail reached 77 percent of the anticipated ultimate flexural capacity of the tandem beams when a load drop-off occurred. A truncated pyramid failure type had occurred in the UHPC joint, indicating bond failure of the strands, but the authors stated that cracking in the joint led to no flexural capacity loss. The specimen was then reloaded up to 85 percent of the ultimate flexural capacity of the tandem beams, when failure occurred due to concrete crushing. The loading configuration for the box beam test is shown in Figure 12 (Maya and Graybeal 2017).

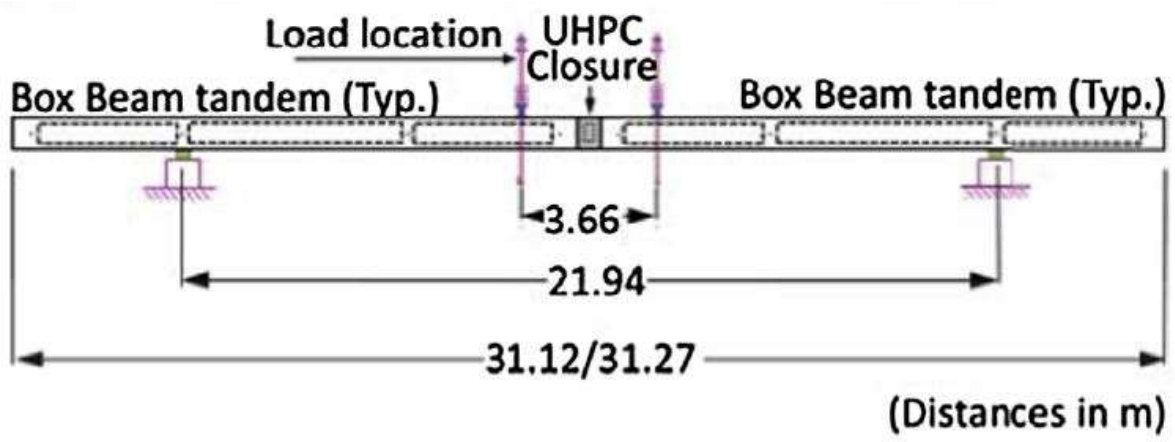

Figure 12. FHWA box beam splice test loading configuration (Maya and Graybeal 2017), Note: 1 ft = 0.3048 m.

The authors conducted a second test intended to further improve the flexural capacity of the spliced connection. The second connection detail used a splice length of 30 inches ($50d_b$), and debonded alternating stands by 1 inch going into the joint. With the new detail changes from the first connection tested, the test specimen reached 90 percent of the anticipated ultimate flexural capacity of the tandem beams when failure occurred due to flexural cracking and concrete crushing. In addition, the authors noted in the second detail had no bond failures in the un-

tensioned prestressing strands, which led them to suggest debonding alternating strands by 1 inch in the joint reduced the outcome of bond failure. The flexural stiffness reported was similar for both connection details, and both had an initial reduction in stiffness at the beginning of each test. The authors recommend spliced connections for mid-span to use a splice length of $50d_b$ for prestressing strands in order to achieve higher flexural capacities than that resulting from using the recommended splice length of $40d_b$. The flexural capacity could potentially be improved even greater with proper detailing strategies and debonding strands in the joint (Maya and Graybeal 2017).

2.4.3 UHPC pi-girder

UHPC has been examined for complete replacement of normal concrete in structural members instead of only connecting normal concrete structural members in a bridge. A prototype pi-shaped girder was developed to best use the advanced material properties of UHPC while also taking advantage of prestressing forces. The idea behind using UHPC in this application would allow long spans with an efficient cross section and including the deck portion of the bridge within a single element. This would allow for modular bridge construction using the enhanced prototype pi-girders. The prototype was developed through an analytical study completed at the Massachusetts Institute of Technology (Park 2003 and Soh 2003). The prototype was analyzed in one, two and three dimensions respectively, to show the predicated response of the girder from the loadings specified by the AASHTO LRFD Bridge Design Specifications (AASHTO 2014). Figure 13 shows the cross-sectional view of the prototype pi-girder after the analytical study had been completed (Graybeal 2009).

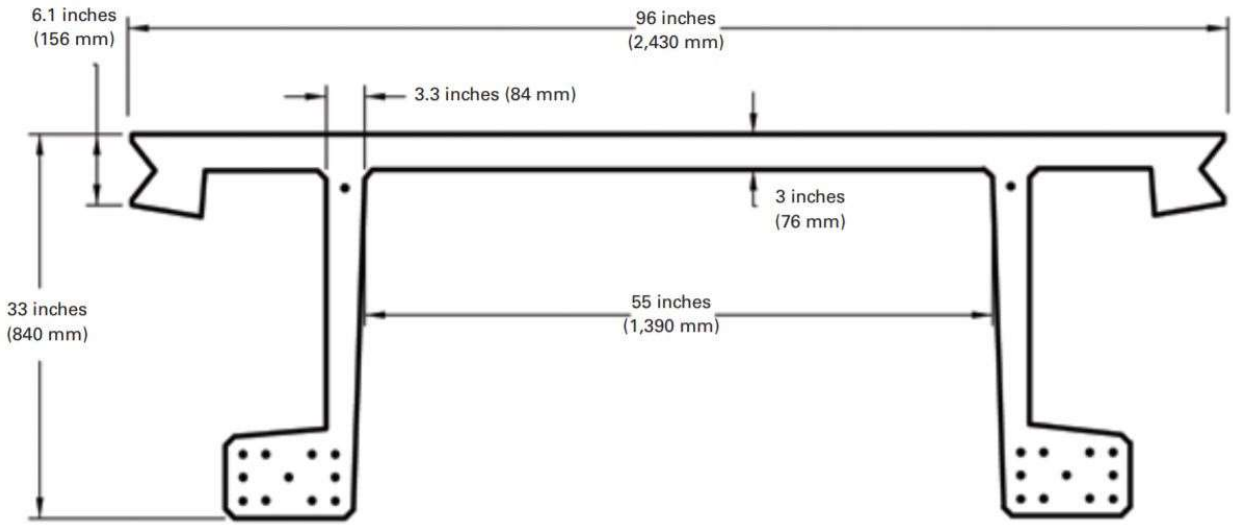

Figure 13. Cross sectional view of the prototype UHPC pi-girder (Graybeal 2009).

The next phase was to do physical full scale testing on the prototype pi-girder with a span of 70 feet. The pi-girder was fabricated at a precast plant and then transported to the testing facility. The tests conducted examined flexural, shear, transverse flexural, and load distribution behaviors. Shown in Figure 14 is the prototype pi-girder set up in the load frame for shear testing (Graybeal 2009).

Figure 14. Prototype pi-girder in load frame for shear testing (Graybeal 2009).

The results of the physical tests showed that this type of decked UHPC girder is possible, as the prototype met all design requirements in the primary flexural and shear tests. However, the load distribution was limited, and the transverse flexural capacity was not able to elastically resist service-level wheel loads. In response to the prototype not meeting all of the design requirements, the prototype was modified to not only increase the structural capacity, but to allow for ease of fabrication and simplify modular construction. Shown in Figure 15 is the cross-sectional view of the 2nd generation pi-girder (Graybeal 2009).

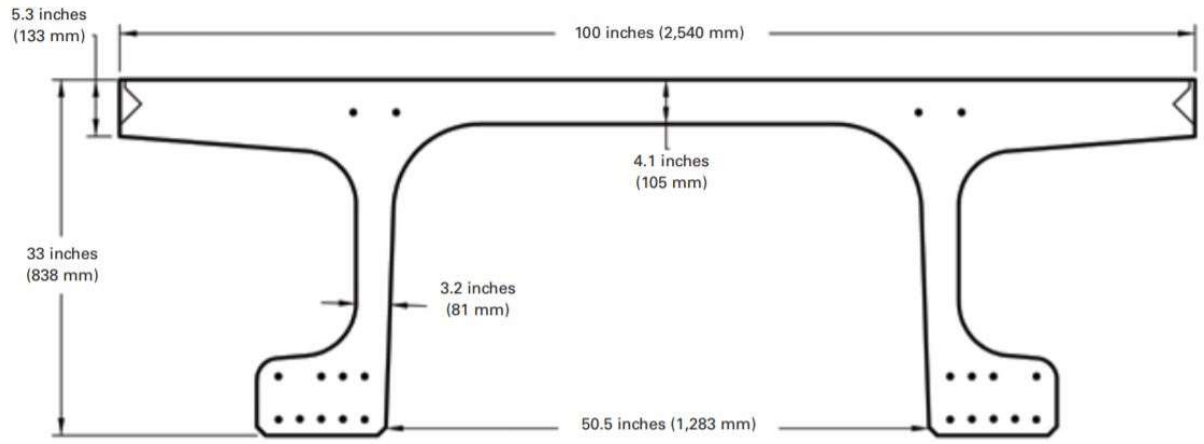

Figure 15. Cross-sectional view of the 2nd generation pi-girder (Graybeal 2009).

The new pi-girder was not retested for primary flexural and shear capacities, as the researches expected similar portion to the prototype in these areas and wanted to focus on the transverse flexural response when subjected to increasing simulated wheel loads. This allowed a reduction of specimen's span length to 25 ft for testing. Shown in Figure 16 is the 2nd generation pi-girder in a load frame for the transverse flexural test (Graybeal 2009).

Figure 16. 2nd generation pi-girder setup in the load frame for a transverse flexural test (Graybeal 2009).

The results of the transverse flexural tests showed an overall improvement of the transverse flexural capacity from the prototype pi-girder and met the AASHTO LRFD bridge standards (AASHTO 2014). With the improvements done to the prototype pi-girder in the 2nd generation girder would allow the pi-girder to be used in service with a maximum span length of 87 ft. This generation of pi-girder was initially deployed in Buchanan County, IA and went into service in late 2008 with three adjacent pi-girders being used (Graybeal 2009).

2.5 Literature Review Summary

Recently UHPC has increased in popularity in the bridge community due to the advanced mechanical properties it has to offer for new construction and rehabilitation projects. These properties have been demonstrated in UHPC's testing in slab connections, mid-span beam splices, and in complete girders, but has not been considered in continuity joints for live load distribution. Continuity joints would greatly benefit from the advanced mechanical properties UHPC has to offer in place of normal concrete. The joint would be able to utilize the short development length and high tension strength to make the connection less susceptible to cracking when subjected to the moments caused by time dependent effects such as creep and shrinkage

and improve the overall capacity of the joint for the negative moment from live loading. The research described in this thesis was intended to begin filling the gap in knowledge related to use of UHPC for connections of precast prestressed concrete girders made continuous for live load.

3.0 Methods and Approach

To recreate continuity connections between prestressed girders in a controlled lab environment, the specimens were scaled down to approximately half scale. A total of six specimens were constructed through three key building phases. Phase 1 consisted of the design and casting of the prestressed girders. Phase 2 consisted of the design and construction of a composite concrete deck on top of the girders. Phase 3 consisted of the design and construction of the two types of continuity connections. Phase 4 included the setup and testing of each specimen.

3.1 Phase 1. Prestressed Girders

3.1.1 Prestressed Girder Design

The design of the prestressed girder specimens involved selecting a desired geometry, location and number of prestressing strands, designing shear reinforcement, and designing the concrete mix. All three design aspects had to be feasible with current prestressing beam capabilities at Donald G. Fears Structural Engineering Laboratory. The chosen geometry was an approximately half-scale AASHTO Type II girder with a length of 18 ft used in previous research projects at Fears Lab (Mayhorn 2016, Murray 2018). This design met the needs of a representative bridge-like girder and the formwork was readily available at Fears Lab. Prestressing strand location, initial prestress, and the number and size of the strands were considered to obtain the maximum flexural capacity with the chosen geometry. The strand location was chosen to be 2 in. on center from bottom the beam, which provided the largest moment capacity. The strand type selected was based on readily available 0.5 in. special grade 270 low relaxation strands. The design also required mild steel to be placed in the top portion of the girder to resist tension stress caused by the prestressing force applied to the beam. Shear reinforcement design was based on previous

students' work with the same type of geometry (Mayhorn 2016, Murray 2018). The final design used for all the prestressed girder specimens is shown in Figure 17 and 18.

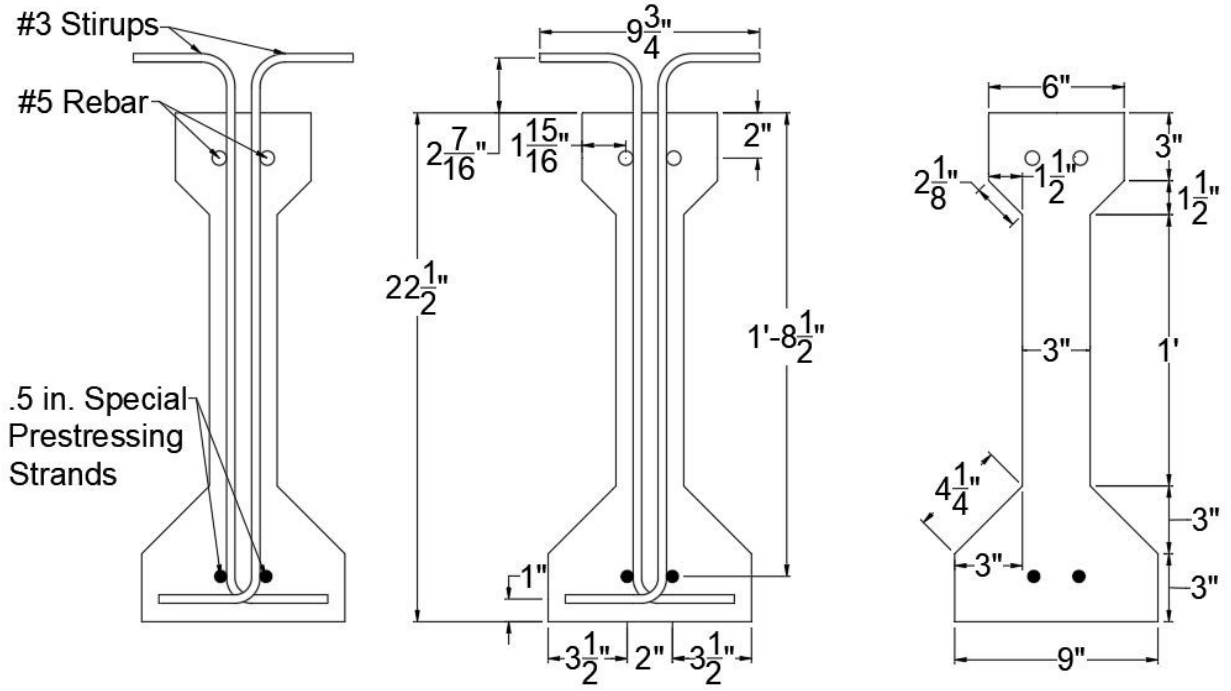

Figure 17. Cross-section of half-scale prestressed girder.

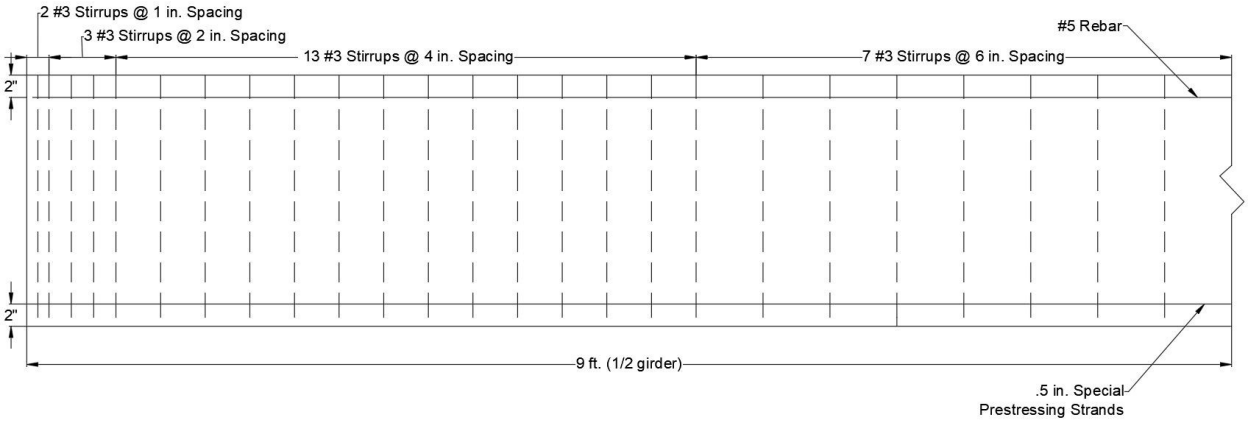

Figure 18. Shear reinforcement spacing

Several trial batches were done to develop a mix design to meet the fresh property, and compressive strength requirements. A minimum compressive strength at 1 day of 4 ksi, and a minimum 28 day strength of 6 ksi were required for the concrete mix design. The minimum compressive strength of 4 ksi at 24 hours was required for release of the prestressing strands. The fresh property tests conducted were the slump, air content, and temperature with a target slump of 6 in., and target air content of 2 percent. Table 2 lists the mix proportions for the final mix design based on a cubic yard.

Table 2. Mix design at saturated surface dry used in prestressed girders

Mix Proportions	**Weight (lb.)**	**Volume (ft^3)**	**Ratio**
Cement	750	3.82	0.141
Sand	1250	7.62	0.282
Rock	1850	11.06	0.410
Water	248	3.97	0.147
Air	0	0.54	0.020
Total	4098	27.00	1.000
Unit Weight ($lb./ft^3$)	151.8		

3.1.1 Prestressed Girder Construction

The construction process for the prestressed girders involved two main building activities. The first activity was the setup of the prestressed girders. The first step was preparing the prestressing bed for prestressing strands and the two sided steel formwork. Figure 19a shows the prestressing bed, which is made from five 8 ft. wooden tables, and two steel prestressing abutments. This configuration allows the construction of two prestressed girders at a time. The next step involved running the prestressing strands through both abutments and using strand chucks to hold the prestressing strands against the abutments. The strands were then tensioned to 2 kips each to pull the strands to the correct elevation. After the strands were tensioned half of the formwork was put into place to allow for the top longitudinal mild steel to be placed. Following this the shear

stirrups were placed and tied in place. The remaining formwork was then put into place, and the prestressing strands were tensioned slightly past 75% of the ultimate capacity, to account for seating losses from the nuts holding the strands in place after tensioning. When the hydraulic rams were released the target load was75% of the ultimate capacity, or 202.5 ksi (33.4 kips) per strand. The load was monitored on one prestressing strand using a through hole load cell that the strand chuck would react against. The formwork during construction and after completion is shown in Figure 20. The second building activity consisted of mixing and placing the concrete. All concrete was mixed at Fears Lab in order to properly maintain quality control of the concrete mix design. The largest capacity mixer available at the lab was a Praschak spiral blade mixer with a 21 ft^3 capacity. Each girder required 16 ft^3 of concrete, and two back to back batches were done for each set of two specimens, one for each girder. As a result of having a separate batch for each girder, the time difference between girder placements was up to 30-60 minutes affected the actual age of each girder when prestress was released. After the concrete was placed in both sets of formwork, the concrete was left to cure for 24 hours. Upon reaching the 24 hour mark after casting the second girder cylinders were tested from each batch to verify the 4000 psi compressive strength required for prestressing strand release had been reached. Once the strength was verified, the prestressing strands were de-tensioned gradually using the hydraulics included in the prestressing abutment shown in Figure 19b, allowing the prestressing force from the strands to transfer into the concrete creating two prestressed girders. A completed set of girder specimens is shown in Figure 21.

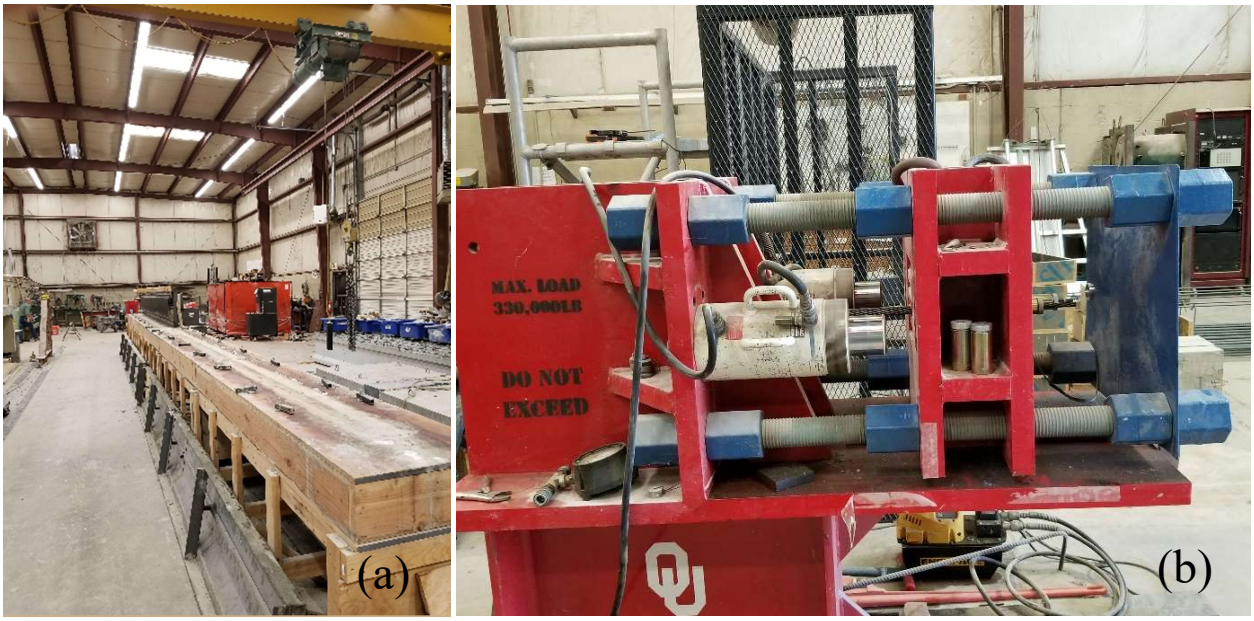

Figure 19. Prestressing bed (a) and active abutment (b).

Figure 20. Prestressing bed with formwork showing reinforcement (a) and exterior formwork in place (b).

Figure 21. Finished prestressed girder before Detensioning.

3.2 Phase 2. Composite Deck Slab

3.2.1 Deck Slab Design

The design of the composite concrete deck involved scaling down the geometric dimensions from a full-scale bridge to half-scale. The same bridge system considered in previous research (Murray 2017) was used as the considered case. The geometric dimensions of the full scale tributary width over a typical beam line used was 96 in., which was scaled down to 46 in. for half-scale. The concrete deck depth at full scale was 8 in., which was scaled down to 4 in. for

half-scale. The tributary width at half-scale presented some problems for construction due to restrictions in a lab setting. The restrictions include limited space for staging specimens and the amount of construction time required to build the formwork. Considering these restrictions, the tributary width was reduced by optimizing the depth of the deck relative to the tributary width. This was done by using the calculated moment capacity of the half-scale prestressed concrete beam with the half-scale concrete composite deck attached to determine the required depth to get a matching moment capacity from the half-scale beam and reduced deck width. This allowed a large reduction in the tributary width, from 46 in. to 9 in., with only a small increase to the depth of the deck, from 4 in. to 4.625 in. No flexural, temperature, or shrinkage steel was designed for the composite deck to prevent congestion from the shear steel hooks and the negative moment reinforcement for the joints due to the smaller dimensions of the revised composite deck. The final dimensions of the composite deck are shown in Figure 22.

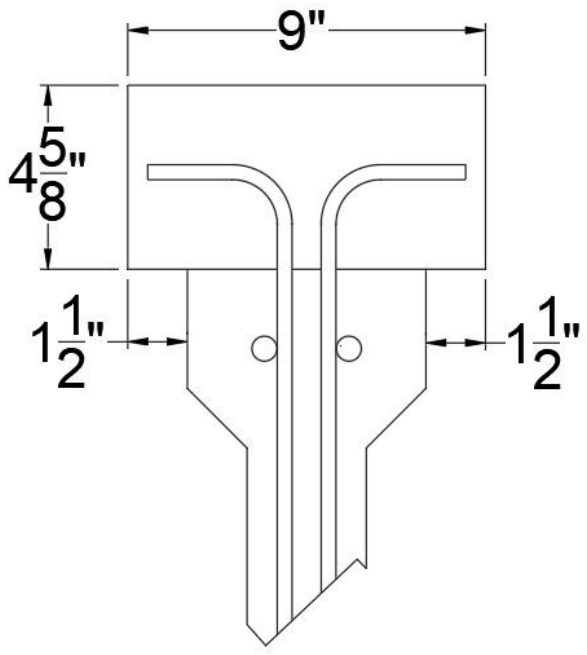

Figure 22. Composite deck dimensions.

3.2.2 Deck Slab Construction

The construction of the composite deck involved two activities; construction of formwork and casting the concrete. The slab construction consisted of making unshored wood formwork for each individual prestressed concrete beam. Unshored formwork was chosen to model actual composite deck construction that occurs on full scale bridges. To achieve this type of formwork, 2 x 4 dimensional lumber was first attached to each side of the flange of each beam using concrete screws, to obtain the designed tributary width. The top of each 2 x 4 was made flush with the top of the beam flange. Plywood was then attached to the 2 x 4's to obtain the required depth of the slab. The required negative moment reinforcing steel for the continuity joint was then tied at the desired elevation near the end of the beam to be connected. At the same end of the deck where the negative moment reinforcing steel goes into the joint, a portion of the deck was blocked off from normal concrete to allow UHPC to go into a portion of the deck slab as shown in Figure 11b. After the formwork was finished the next step was to place concrete into forms. To further model full scale bridge construction, ODOT Class AA concrete was delivered in a concrete ready mix truck. This type of concrete mix has a design 28 day compressive strength of 4000 psi and is used by ODOT in their full scale bridge deck construction. After the concrete was cast into the forms, covered, and cured for 24 hours, the slabs were surface water cured for 7 days using wet burlap before removing the formwork. The various stages of construction of the slabs are shown in Figures 23-25.

Figure 23. Initial composite deck formwork.

Figure 24. Composite deck formwork prior to casting.

Figure 25. Concrete being placed (a) and finished composite deck (b).

3.3 Phase 3 Continuity Joints

Two types of continuity joints were designed and constructed. One type intended for new bridge construction, and the other type intended for retrofitting an in-service bridge with a continuity connection. Both joints used the same type of commercially available UHPC produced by LafargeHolcim called Ductal®. In addition, both joints were designed using normal concrete properties to recreate the same type of reinforcement that is currently in use, but with the added benefit of using UHPC in place of normal concrete.

3.3.1 Newly Constructed Continuity Joint Design

This section will discuss each component of the joint design using AASHTO LRFD 2014, and includes the detailing of the joint. An overview of the newly constructed continuity joint is shown in Figures 26.

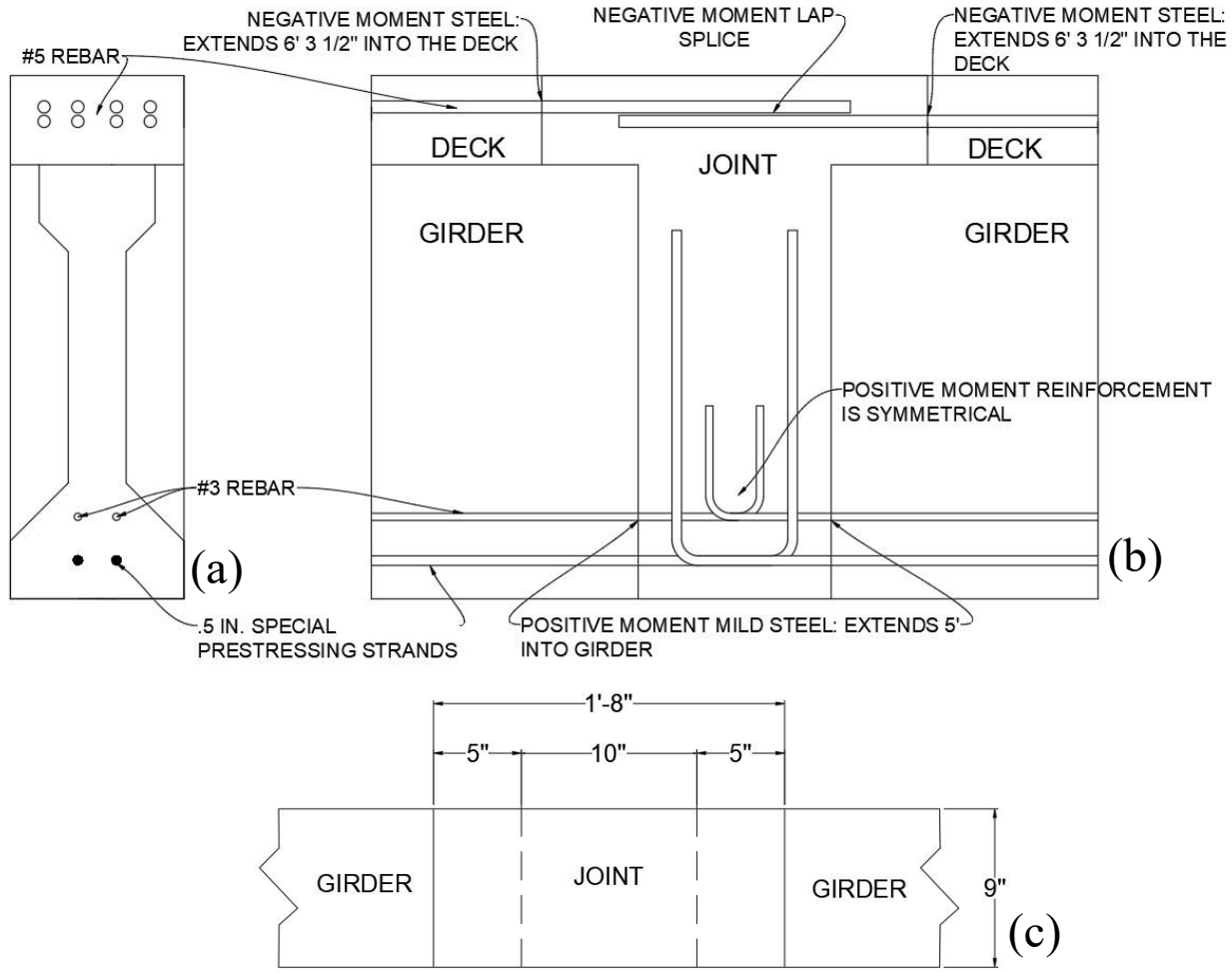

Figure 26. Newly constructed continuity joint cross-section (a), elevation view, (b), and plan view (c).

3.3.1.1 Positive moment Design

The design of the positive moment region of the continuity joint was based on AASHTO LRFD 2014 5.14.1.4.9a. This section allows the use of section 5.14.1.4.4 to determine the magnitude of positive moment for the steel reinforcement design. Section 5.14.1.4.4 specifies a minimum precast girder age of 90 days before establishing continuity to allow restraint moments caused by creep and shrinkage to be taken as zero. The section then allows the use of the cracking moment (M_{cr}) with a factor of 1.2 for the design positive moment value. The equation used to calculate the cracking moment is Eq. 5.7.3.6.2-2. Three variables are needed to calculate the cracking moment of the joint: distance from the neutral axis to the extreme tension fiber, moment of inertia, and the modulus of rupture of the concrete. The width of the joint cross-section was set at 9 in. to match the width of the bottom flange of the girder and was kept constant throughout the girder depth up to the deck. The deck width was set at 24 in., and the depth of the deck set at 4 in. The distance from the bottom of the joint to the neutral axis was then calculated to be 15.5 in. using a T-shaped cross section. The moment of inertia of the joint was then calculated to be 20,105 $in.^4$. The full half-scale dimensions of the beam were used to calculate the section properties for design as it was done before the deck width was reduced. The modulus of rupture was calculated in accordance with article 5.4.2.6 using a compressive strength of 5 ksi. The modified cracking moment ($1.2M_{cr}$) was 69.6 kip-ft. After obtaining the design cracking moment value, the moment capacity provided by the reinforcement to be used was compared to the cracking moment.

AASHTO LRFD 2014 section 5.14.1.4.9 allows the use of prestressing strands extending from the beam to be used for joint reinforcement, but the strands to be used cannot be de-bonded at the end of the girder. The strands must also extend at least 8 in. from the end of the girder into the

joint, and then have a 90 degree bend pointing the strand straight up for adequate development. With only two strands provided in the girder specimens, this was the only reinforcement used to calculate the moment capacity for comparison with the design cracking moment. The strain compatibility method and Whitney stress block were used to calculate the moment capacity of the joint. The tension and compression resultant forces were calculated, along with the distance between the forces. The tension force was calculated using the stress in the strand at the strength limit state and the area of the strand. AASHTO LRFD Equation 5.14.1.4.9c-2 was used to calculate the stress developed in the strand at the strength limit state based on the length after the 90 degree bend. The length of the strand after the bend was taken to be 16 in. giving a stress in the strands of 98 ksi. Figure 27 shows the dimensions of the prestressing strands in the newly constructed joint. The compressive force was calculated using the depth of the compression block, effective width, and the compressive strength of the concrete.

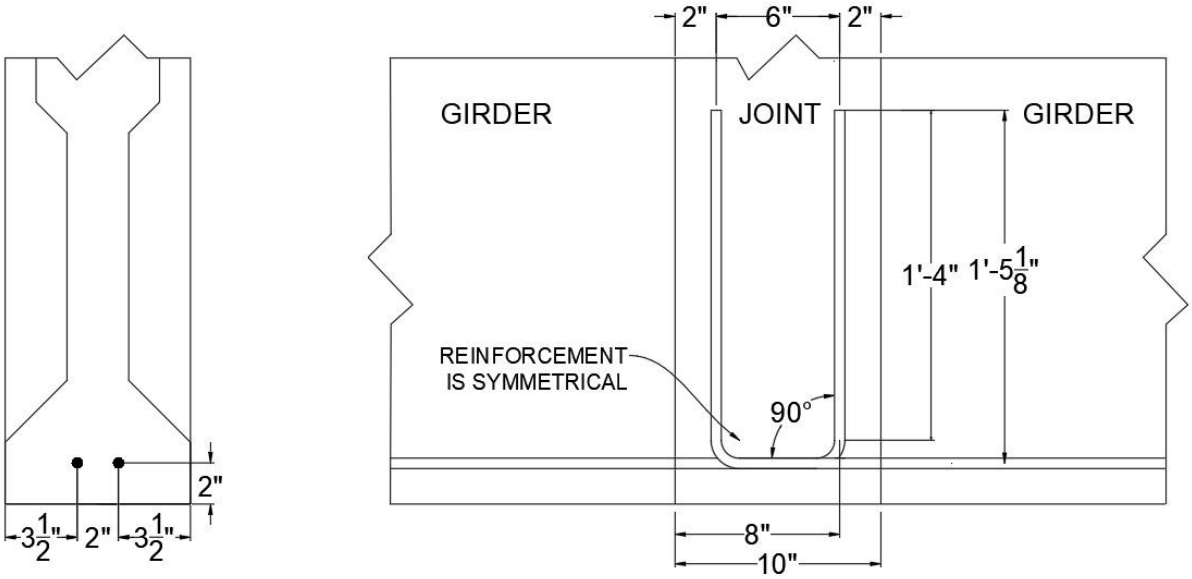

Figure 27. Newly constructed continuity joint prestressing strands detail for positive moment.

The area of two 0.50 inch special strands is 0.334 in^2. The resulting force calculated by multiplying the area by the stress is 32.8 kips. To calculate the compressive force, the depth of the compressive block was calculated using the assumption that the compression force must equal the tension force (C=T) to satisfy equilibrium. The known concrete compressive strength and section width were multiplied together and then divided into the tension force to solve for the unknown depth. After obtaining both forces, a moment was taken at the compression resultant force, with the moment arm taken as the effective depth of 25.125 in. minus half of the depth of the compression block. The moment arm was then multiplied by the tension force to obtain the moment capacity of 60.73 kip-feet. Figure 28 shows the distance between the resultant forces and their location on the joint.

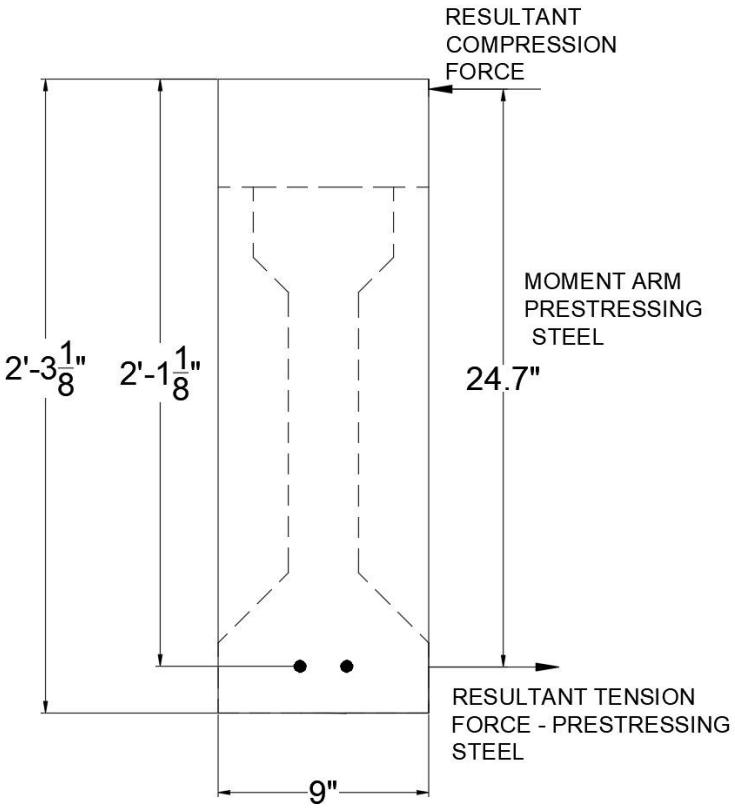

Figure 28. Positive moment resultant forces with prestressing strands at the joint.

This value did not exceed the cracking moment indicating inadequate steel reinforcement for the positive moment region of the joint. In order to increase the moment capacity, two No. 3 rebar were included in the calculation. The bars were placed 2 in. on center above the prestressing strands. The compression block depth was recalculated using the added steel, based on the assumption of C=T. By having an additional tension force, a second moment was added, which increased the available moment capacity to 82.60 kip-ft. This value exceeds the design cracking moment, indicating adequate reinforcement. Figure 29 shows the distance between the resultant forces and their locations in the joint.

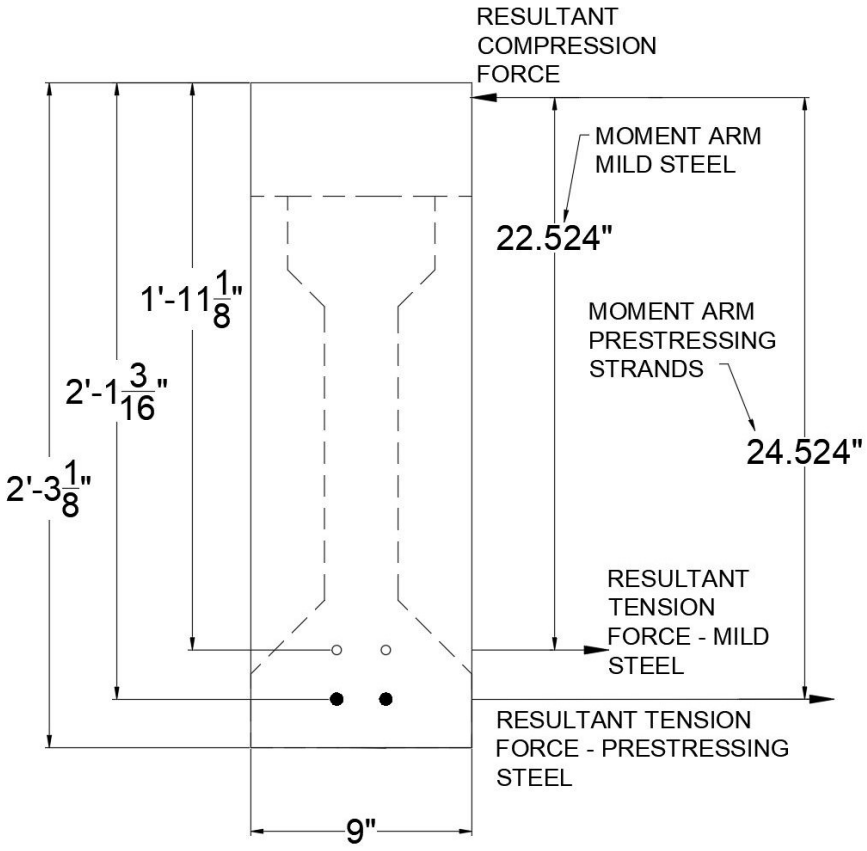

Figure 29. Positive moment result forces location for mild steel and prestressing strands.

To have adequate development length for the added mild steel, a standard 90 degree hook was used inside the joint. The hook detail followed article 5.11.2.4 from AASHTO LRFD 2014. As

this detail is based on the compressive and tensile strengths of normal concrete, the reinforcement will have adequate development length into the UHPC joint. Figures 30 and 31 show the details of the positive moment mild steel within the joint and the hook geometry. It should be noted that this reinforcement was included together with the strands shown in Figure 15, with the mild steel hooks spaced 2.25 in. from the vertical portions of the prestressing strands in the direction of the beams.

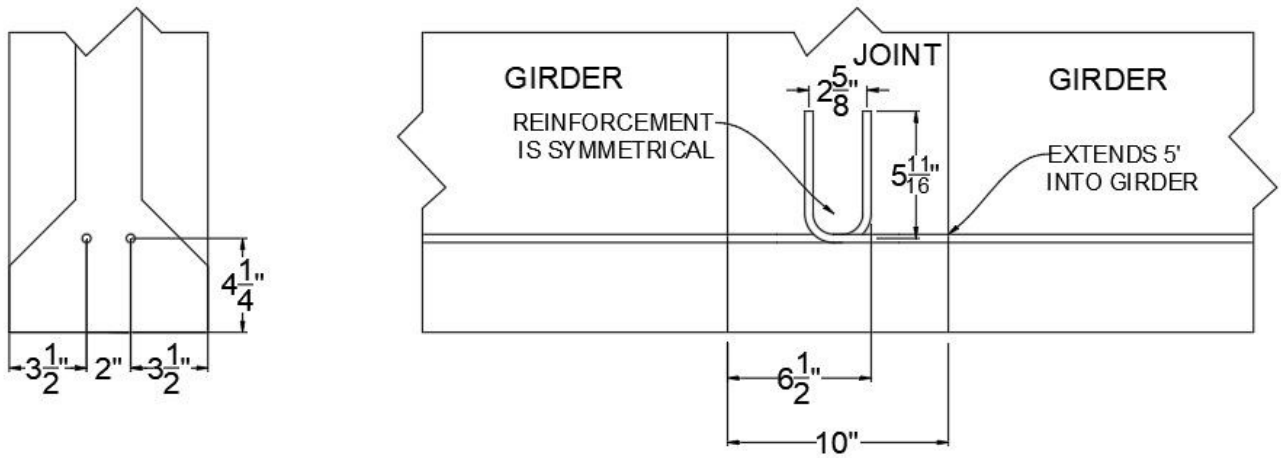

Figure 30. Newly constructed continuity joint mild steel detail for positive moment.

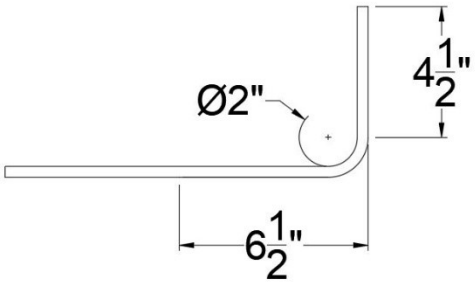

Figure 31. Mild steel hook detail for positive moment.

3.3.1.2 Negative moment Design

The design for the reinforcing steel required in the negative moment region of the continuity joint was determined based on the worst loading case applied on a two span continuous girder configuration that would lead to flexural failure of the beams. This was done according to AASHTO Section 5.14.1.4.8. The determined worst load case was a single point load at mid-span for each girder. The magnitude of each individual point load was back calculated from the maximum moment capacity of each girder with the composite concrete deck with the self-weight moment subtracted out to calculate the point load using strain compatibility. The point load calculated would then act as a live load that could be applied to the girder as a live load resulting in beam failure. This then gave a two point load configuration applied simultaneously to each girder to obtain a maximum negative moment at the continuity joint. The structural analysis software RISA® was used to model the two point loads applied to the continuous girder configuration giving a maximum negative moment of 132 kip-ft at the joint. It should be noted that only one support was used at the joint connection to simplify the model. The actual test had two supports at the joint located at the girder ends. Figure 32 shows the moment diagram from the structural analysis software model.

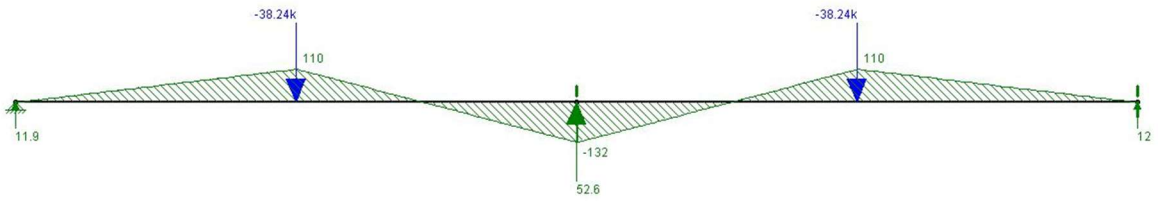

Figure 32. Moment diagram for continuity joint.

The negative moment given by the model was then used to calculate the required area of steel needed to resist the moment using the assumption that the compression force must equal the

tension force for equilibrium (C=T). The compressive strength of the joint material, yield strength of the rebar, effective section width, effective depth, and depth of the compression block were needed for this calculation. A compressive strength of 5 ksi for normal concrete and Grade 60 steel were used. The effective width of the compressive side of the joint was 9 in. The effective depth was calculated based on a 2 in. rebar cover from the top of the joint to the center of rebar location, subtracted from the total height of the joint of 27.125 in., resulting in the effective depth of 25.125 in. The depth of the compression block was then calculated by taking a moment at the resultant tension force, where the rebar will be located, by multiplying the moment arm by the resultant compressive force. The depth of the compressive block was the only unknown value, and was determined by setting the moment taken at the resultant tension force equal to the negative moment from the model. The Excel function Goal Seek was used to solve for the depth of the compression block by trying multiple iterations for the compression block depth until the applied and internal moments equaled one another. After solving for the compression block depth, the assumption C=T was used to solve for the required area of steel reinforcement, which came out to be 1.11 in^2. Four No. 5 rebar (A_s = 1.24 in^2) were needed to obtain the area of steel required to resist negative moment in the joint. Figure 33 shows the distance between the resultant forces and their location on the joint.

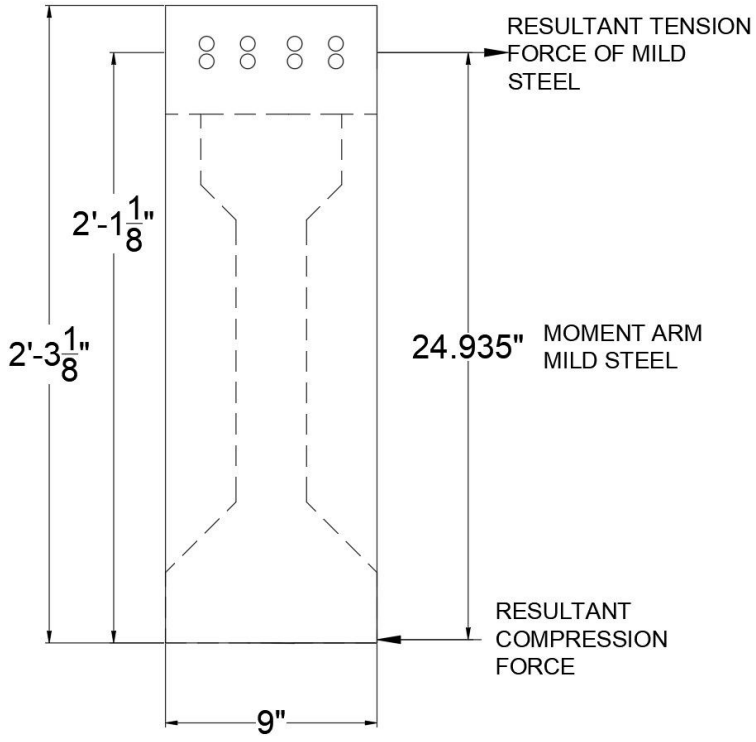

Figure 33. Negative moment resultant force location for mild steel reinforcement calculation.

The negative moment reinforcement development length in the concrete deck followed section 5.11.1.2.3 of the AASHTO LRFD Bridge Design Specifications. The article states that the negative moment reinforcing steel must extend past the inflection point by more than the effective depth of the member, 12 times the nominal diameter of the bar, and 0.0625 times the clear span. The reinforcement only extends 24 in. beyond the inflection point, which is less than the effective depth of the member, 25.125 in. However, the article states that only 1/3 of the reinforcement needs to extend past the inflection point, where in this case all the negative reinforcement passes through the inflection point. Thus, the development length was considered to be adequate.

The negative moment reinforcement was designed using requirements for normal concrete. However, for the development and lap splice length of the reinforcement, requirements for both normal concrete and UHPC were taken into consideration. The development and lap splice lengths for normal concrete were calculated using sections 5.11.2.1.1 and 5.11.5.3.1 in the AASHTO LRFD Bridge Design Specifications. The calculated development length was 15 in., and the lap splice length of 19.5 in. The only issue arising from using these two values was that the end of the splice length would be ½ in. from the concrete deck on the opposite side, which would lead to problems during construction. The development and lap splice lengths for UHPC were calculated using the recommendations of Yuan and Graybeal (2014) of $8d_b$ for the development length and $0.75l_d$ for the splice length. These resulted in values of 5 in. and 3.75 in., respectively. However, the cover recommendation of $3d_b$ for development length in UHPC (Yuan and Graybeal 2014) did not meet the reinforcement detail for the joint on the outside bars. Additionally, the use of contact lap splices limits the ability of the fiber reinforcement to increase the UHPC mechanical properties in the contacted portion of reinforcement (Yuan and Graybeal 2014). A modification was made to account for the cover and contact lap splice by significantly increasing the development and lap splice lengths within the joint to 16 in. and 12 in. respectively. Figure 34 shows the negative moment reinforcing steel dimensions within the joint.

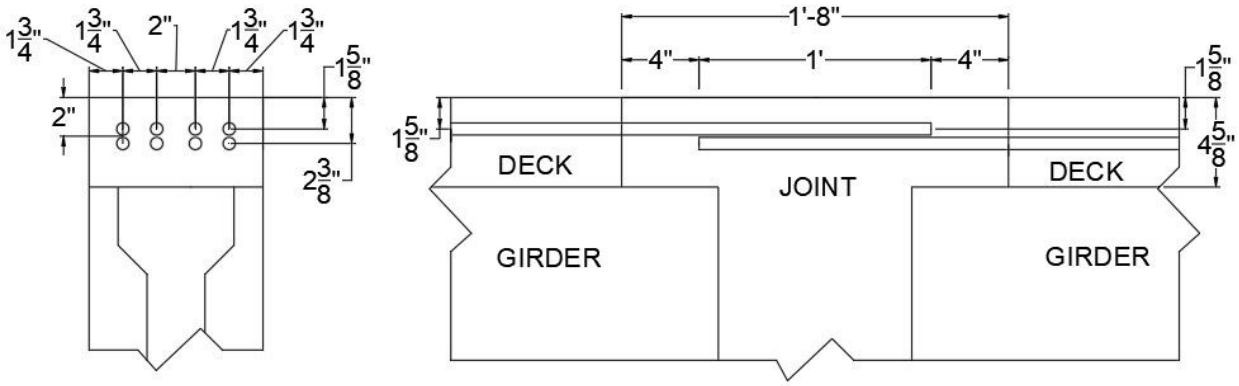

Figure 34. Newly constructed continuity joint mild steel detail for negative moment.

3.3.2 Retrofit Continuity Joint Design

This section discusses each component of the retrofit joint design, and includes the detailing of the joint. An overview of the retrofit continuity joint is shown in Figure 35.

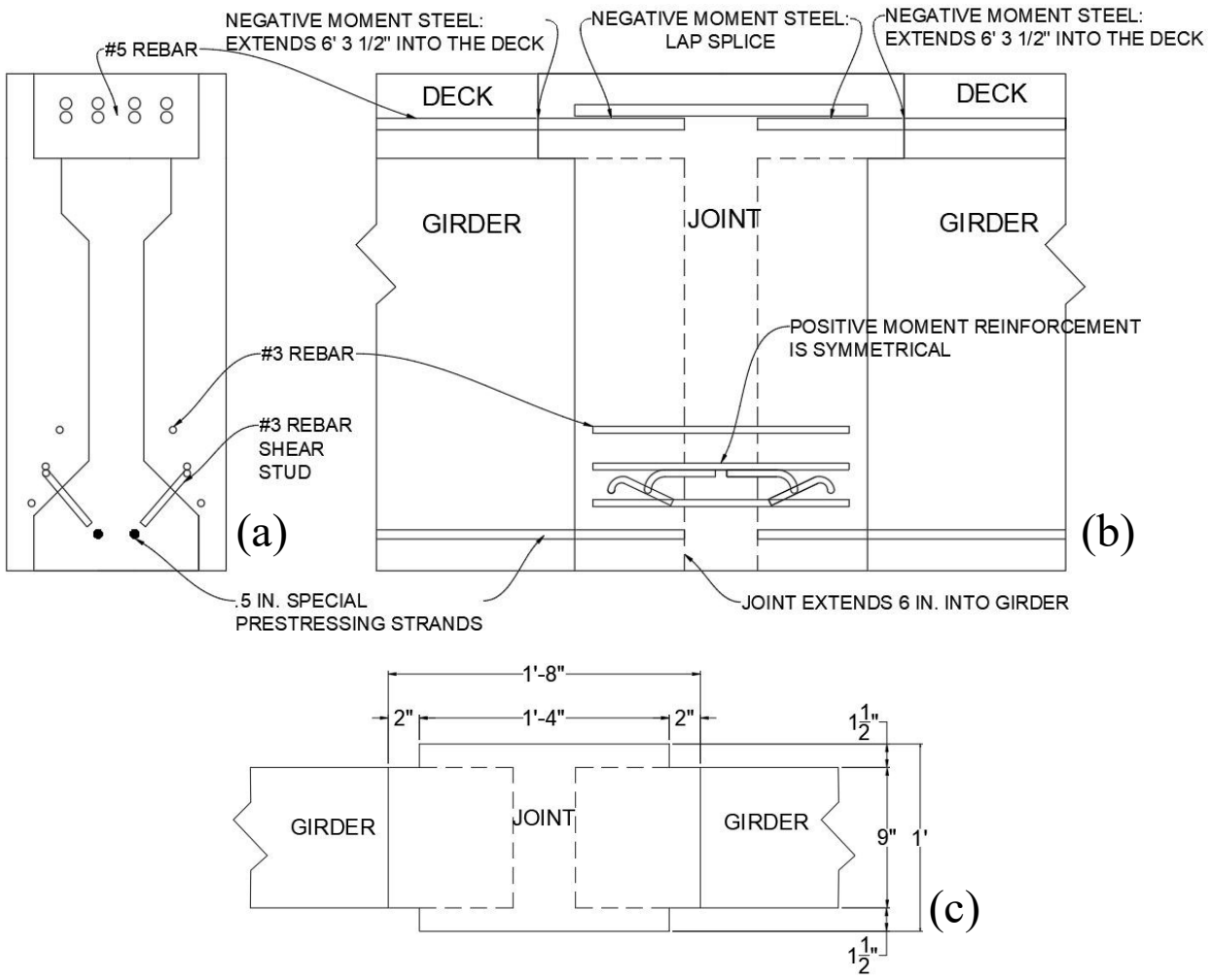

Figure 35. Retrofit continuity joint cross-section (a), elevation view (b), and plan view (c)

3.3.2.1 Positive moment Design

The retrofit continuity joint was designed with the intention that it could be implemented on existing bridges in service with a simple span configuration. ODOT standard detailing sheets showed a 4 in. gap between girder ends in simple span configuration, which does not allow

positive moment steel to be added in the end face of the girders. A solution had to be created for attaching reinforcing steel in another location on the girder at the required elevation. The solution decided on was to attach rebar shear studs on the outside surface of each side of the flange near the end of the girder. This would allow the steel required to resist the positive moment induced at the joint to be transferred into the girders as if the steel was fully developed into the girders as in the newly constructed joint design.

The positive moment value used for determination of the required reinforcing steel was based on the same method as used for the newly constructed joint design since the age of the girders would far exceed 90 days for pre-existing girders to be retrofitted in the field. Because the newly constructed joints used preexisting prestressing strands and mild steel, the same tension force calculated for those joints could not be used for the retrofit design. The required tension force was instead back calculated from the required cracking moment similarly to what was done for the new construction design. The compression block depth was again the unknown in this case and had to be solved for to determine the tension force. This was done by taking a moment at the predicted resultant tension force using the resultant compression force equation, and dividing into the cracking moment to solve for the unknown compression block depth. Once the compression block depth and resulting moment arm were determined, the moment arm was divided into the cracking moment resulting in a required tension force of 33.74 kips. The force was then divided by the tensile yield strength of 60 ksi to get the required 0.56 in^2 area of steel. Six No. 3 rebar were used to obtain the required area of steel with three on each side of the joint. Figure 36 shows the positive moment reinforcing steel location and dimensions within the joint.

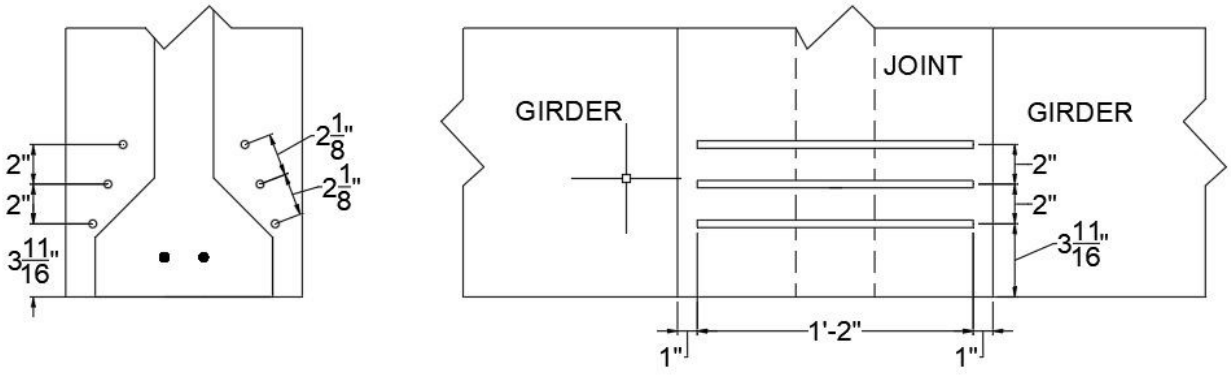

Figure 36. Retrofit continuity joint mild steel detail for positive moment.

The required tension force was then used to determine the required number of rebar shear studs to be embedded into the girder bottom flange for adequate transfer of load. The number of rebar shear studs required was determined using the HILTI epoxy adhesive HILTI HIT-RE 500 specification sheet that gave shear strength values for a No. 3 rebar embedded at multiple embedment lengths with various concrete compressive strength values. The highest compressive strength given (6 ksi) combined with the shortest embedment of 3-3/8 in. had a listed shear value of 12.2 kips. The embedment length of 3-3/8 in. was not possible, however, because a hole of this length would interfere with the location of the prestressing strands. Instead a 2-½ in. embedment length was chosen to avoid interference with the prestressing strands and still meet the 2-3/8 in. minimum embedment length listed for the epoxy. Linear interpolation was then used to estimate the shear strength for the new embedment length as 9.09 kips. This value was then divided into the tension force of 33.74 kips to determine a required total of four rebar shear studs for each girder end, with two on each side if using the epoxy HILTI HIT-RE 500. A 2 in. clear cover from the girder end and anchor spacing was used to satisfy the geometry of the joint and follow the minimum requirements from the epoxy specification sheet. The geometry of the joint limited the ability to include a straight rebar shear stud extending from the face of the bottom

flange. To account for this and ensure proper development of the rebar shear studs, a 90 degree hook with a tail based on the recommendation of $8d_b$ (3 in.) for a No. 3 rebar (Yuan and Graybeal 2014) was applied. Figure 37 shows the positive moment rebar shear stud placement within the joint, and Figure 38 shows the rebar shear stud hook dimensions.

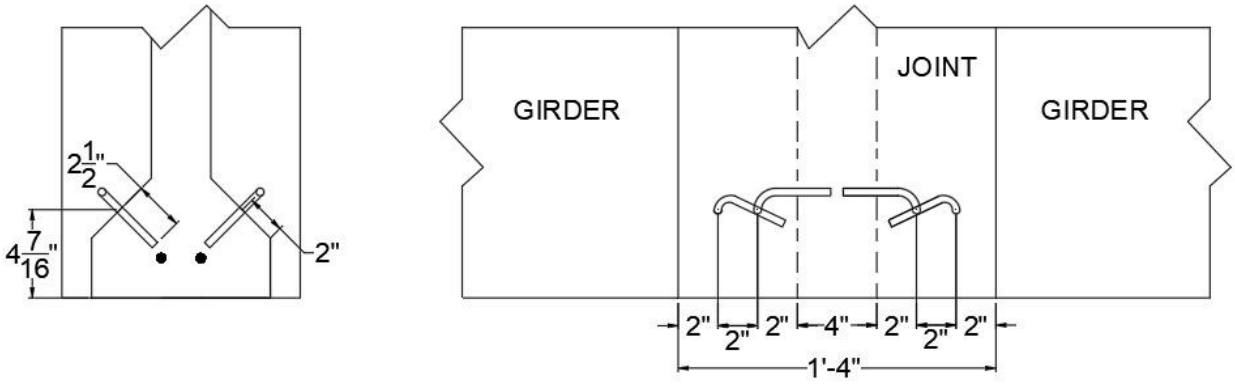

Figure 37. Retrofit continuity joint rebar shear studs detail for positive moment.

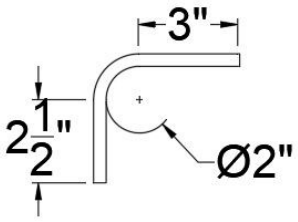

Figure 38. Rebar shear stud detail.

3.3.2.2 Negative moment design

The negative moment design for the retrofit connection was done using the same method as for the newly constructed joint. The only difference that had to be checked was that the length of the joint in the model was decreased by 6 in. However, since this resulted in no significant change in

the negative moment calculated from the model, the same reinforcement was used to resist the moment as for the newly constructed joint: four No. 5 rebar. The only difference in the detailing was using splice bars in the lap splice connection, as this method of splicing bars together would be used to connect pre-existing slabs. With the different type of splice detail used in this joint configuration, the development and splice lengths were adjusted to meet the geometric dimensions of the joint. As in the newly constructed joint, normal concrete was considered for the development and splice lengths, but for this configuration the available splice length was not adequate for the 19.5 in. required for normal concrete. It should be noted that the concrete deck could have been cut back more to meet the splice length connection, but the joint length was kept consistent to the newly constructed joint length of 20 inches. The available splice length in total was 8 in., but only 6 inches was used to meet the recommended 3.75 in. for UHPC (Yuan and Graybeal 2014), and to account for using a contact lap splice with the addition of the clear cover not meeting the recommended distance (Yuan and Graybeal 2014). This resulted in a splice bar length of 16 in. including the effect of gap between the beam ends. Although this splice length did not match the 12 in. from the newly constructed joint, it exceeded the recommendation by 2.25 in. Figure 39 shows the negative moment reinforcing steel dimensions within the joint.

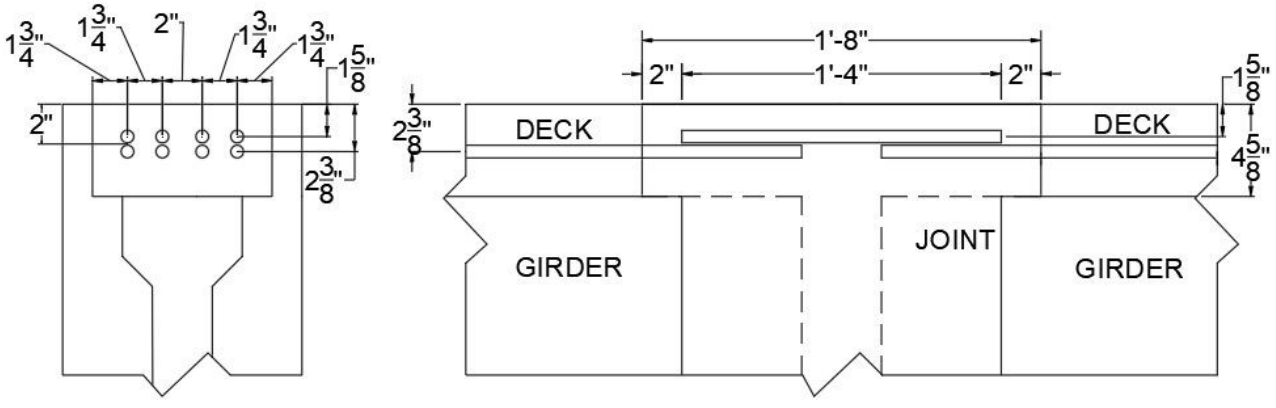

Figure 39. Retrofit continuity joint mild steel detail for negative moment.

3.3.3 Continuity Joint Construction

Continuity joint construction for both types of joints was very similar. The only difference was that the retrofit connections extended 6 in. beyond the end of the girder, and the joint was 3 in. wider, which resulted in different formwork requirements. The first step in the construction was aligning the pairs of prestressed concrete girders constructed together such that the ends with the negative moment and positive moment steel were placed together in the required joint configuration. A survey transit and level rod were used ensure the girders were in a straight line. Figures 40 and 41 show the transit and survey rod.

Figure 40. Transit.

Figure 41. Survey rod.

A reference point was taken at the far end of the first girder, then the opposite end was adjusted until it was in line with the reference point. The second girder was then set to an estimated position with the ends placed with correct gap space for the joint. Then, the joint end of the second girder was adjusted to line up with the reference point, and finally, the opposite end of the second girder was adjusted to line up with the reference point. This was done for all 6 pairs of girders.

After the beams were lined up with the correct gap for the given joint, formwork was constructed for the joint. A plywood cut out matching the geometric perimeter required for each joint type was used to produce a joint with a uniform dimension from top to bottom. The plywood cut out was attached to a piece of dimension lumber that was connected to the top flange of the beam and attached to the formwork at the bottom of the beam. The formwork at the bottom of the joint was supported by the lab floor to mimic field conditions where the girders would already be sitting on the piers, which would be able to support the bottom formwork. For the retrofit

connections, the 16 in. long No. 5 rebar splice bars were tied in between the bars extending from each beam to make connection in the negative moment region. Holes were also drilled into the bottom flange of the girders to attach the rebar shear studs. After the rebar studs had been attached with the Hilti epoxy the positive moment rebar was tied into the positive moment region of the joint. For the newly constructed joints, the only adjustments to the steel reinforcement required were adjusting the prestressing strands to make sure they were vertical at the 90 degree bend. This was done by inserting the prestressing strand into a pipe, clamping the strand down near the face of the girder, and lifting in an upward motion with the pipe to make the bend. The method gave a near 90 degree bend, and bailing wire held the strands in the correct orientation for casting, as shown in Figure 42a. Square plywood sides were then attached to the formwork to enclose each of joints. Figure 42 shows the completed formwork construction, minus one of the formwork sides, for both types of connections.

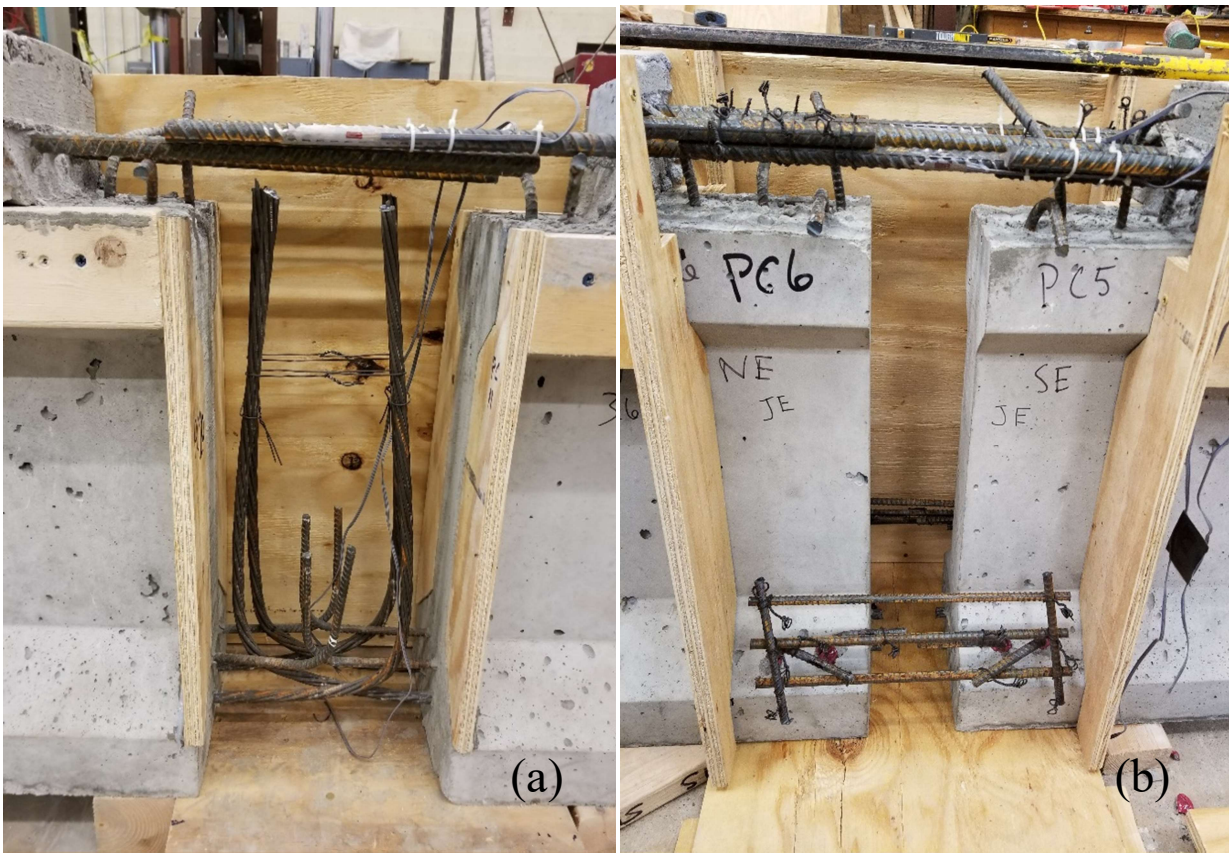

Figure 42. Newly constructed joint (a) and retrofit continuity joint (b).

The next step was to mix and place the UHPC into the joints. Table 3 shows a typical mix design of the UHPC proprietary mix Ductal®. The mixing took place at Fears lab using a Praschak spiral blade mixer with the capacity of 21 cubic feet. The spiral blade configuration of this mixer provided the high shear mixing action necessary to mix UHPC similarly to the typical vertical axis high shear mixer available at Fears Lab but was large enough to meet the quantity demand for one pour. Two 10 ft^3 batches were mixed for each set of three joints. The mixing procedure provided for the proprietary UHPC mixture used, Ductal®, was followed. The procedure consisted of mixing the dry ingredients in the mixer for 2 minutes followed by pouring the water into the mixer over the course of 2 minutes, and then finally adding the water reducing admixture

over the course of 1 minute. The UHPC was mixed until flowable with a consistency similar to cake batter. Upon reaching the correct consistency, the steel fibers were added into the mixer. After the steel fibers mixed thoroughly in the UHPC, a flow test was conducted using the methods of ASTM C1437 and C1856 to check for proper flowability before placing the UHPC into the joints. UHPC was transported from the mix and placed in the joint formwork using a transfer bucket. After UHPC placement pieces of plywood and plastic sheeting were placed on top of the joints to prevent moisture loss. Twelve 3 in. x 6 in. cylinders were made to test the UHPC compressive strength at 3 days, 7 days, 28 days and day of specimen testing. The UHPC was cured for 7 days before removing the formwork around the joint. Figures 43 and 44 show the UHPC being placed, and the formwork being removed after the 7 day curing time.

Table 3. Typical mix design of the UHPC proprietary mix Ductal®

Material	lb/yd^3	kg/m^3	Percentage by Weight
Portland Cement	1,200	712	28.5
Fine Sand	1,720	1,020	40.8
Silica Fume	390	231	9.3
Ground Quartz	355	211	8.4
HRWR	51.8	30.7	1.2
Accelerator	50.5	30.0	1.2
Steel Fibers	263	156	6.2
Water	184	109	4.4

Figure 43. UHPC being poured into the joint formwork for one of the retrofit specimens.

Figure 44. Removing formwork from a newly constructed joint specimen.

3.3.4 Specimen Nomenclature

The labeling of the specimens for the newly constructed and retrofit continuity joints uses two letters followed by a number, and then a second letter. The first two letters represent which joint type is being referenced. The letters would either be NC for newly constructed continuity joint, or RC for retrofit continuity joint. The number following NC and RC would be 1, 2, or 3 to represent the order of testing was done. Lastly the letter N or S will follow the specimen number to describe which girder is being referenced, the girder north of the joint (N) or south of the joint (S). For example: NC1-N would reference newly constructed continuity joint, the first specimen tested, and the girder north of the joint. If the N and S is not present, the specimen as a whole is being represented, e.g. NC1 would represent the entire specimen.

3.4 Phase 4

3.4.1 Testing Procedure

The final phase of the research was to test each continuous beam specimen with a point load applied at midspan of each girder to create a negative moment in the joint. Observations and data were collected at various loads to characterize behavior of the two joint configurations and gain a better understanding of UHPC as a continuity joint material. Two load frames available at Fears lab were used to create the individual point loads. The load frames were attached to the strong floor in the lab spaced at a distance equal to the distance between the mid-spans of each girder with the joint in the middle. Two identical hydraulic rams were attached to each load frame with hydraulic hoses running from the rams to the same pump to create a parallel system. This was done to ensure the same load would be applied to each of the girders at the same time to obtain a

symmetric loading. In the case of a girder failing prematurely, a series of hydraulic valves were installed between the hydraulic pump and rams. This would allow one set of valves to be shut off to maintain hydraulic pressure in the ram on the prematurely failed girder and allow the continuation of loading on the other girder. Figure 45 shows the hydraulic pump, and valves.

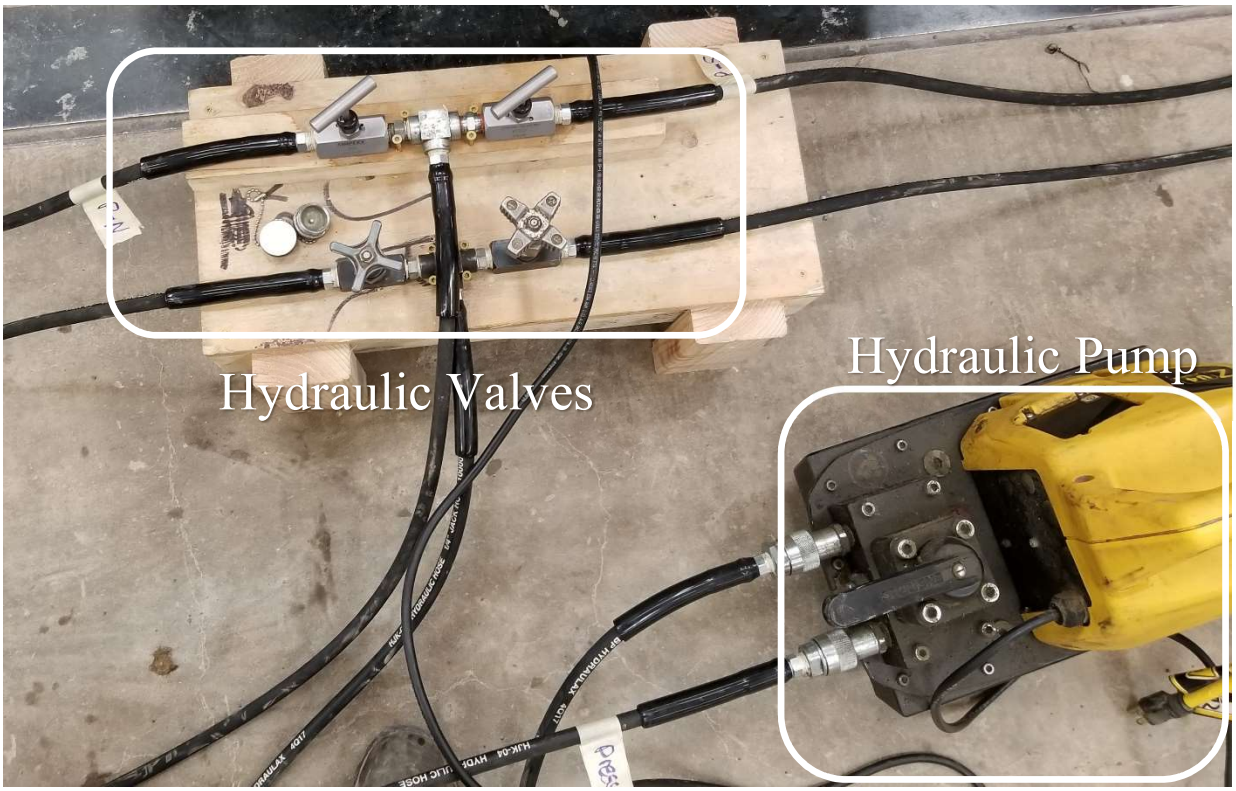

Figure 45. Hydraulic pump and valves.

Cylindrical washers were used at each load point to allow for rotation during loading. Load cells were placed directly under each hydraulic ram to record the applied load and to monitor both loads during the test to verify both were within the same loading range. Figure 46 shows the load cell and hydraulic ram set up on one of the specimens on the north and south ends.

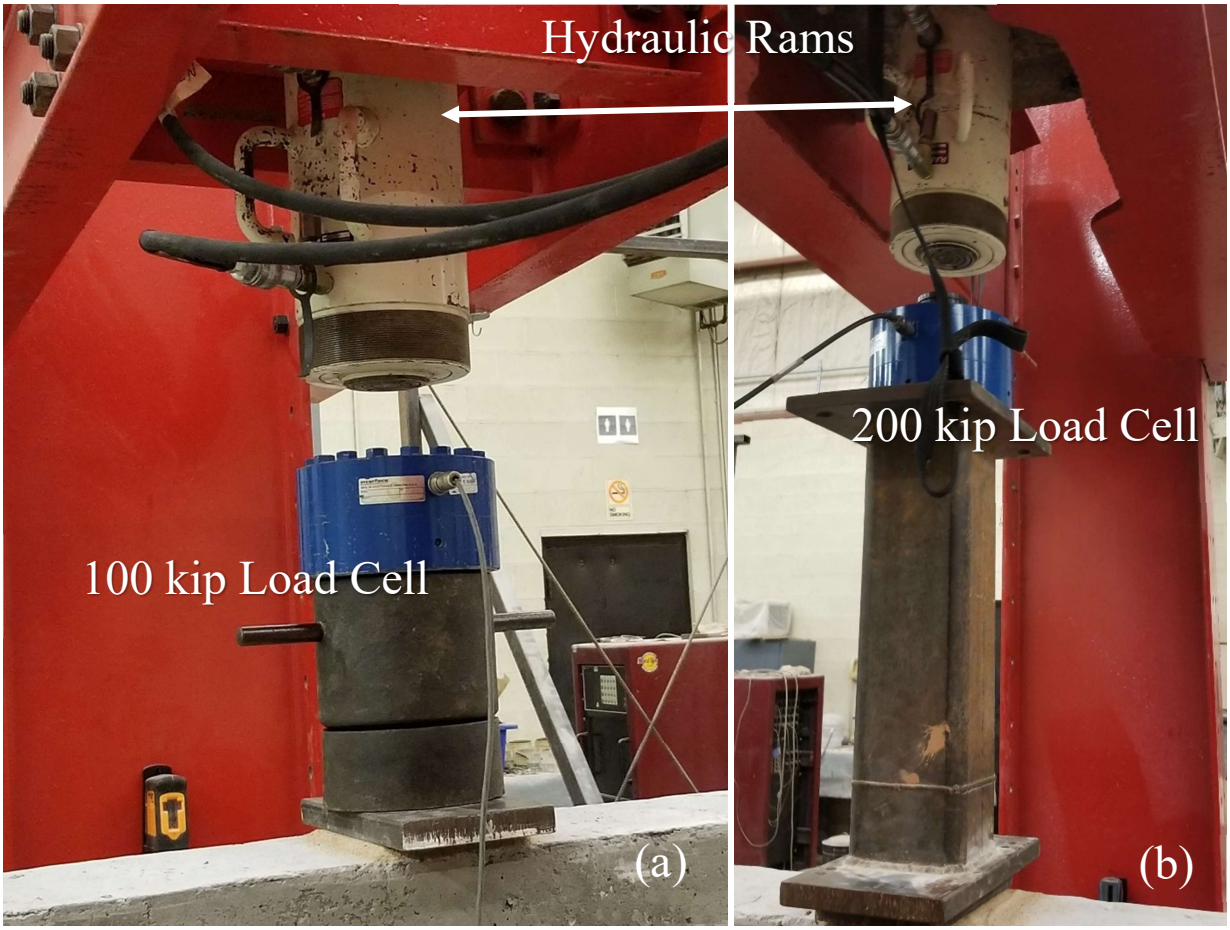

Figure 46. 100 kip load cell and hydraulic ram on the North beam (a) and 200 kip load cell and hydraulic ram on South beam (b).

One wire potentiometer (pot) was placed directly under the beam at each load point to measure the deflection of each beam at mid-span. Linear voltage differential transformers (LVDTs) were placed under the girder center line at each of the supports. These LVDTs were used to measure the deflection of the neoprene pads supporting the girders during loading to subtract from the wire pot readings to get a true deflection of the girder at mid-span. Figure 47 shows a wire pot set up at midspan of the girder, and the LVDT set up at one of the supports.

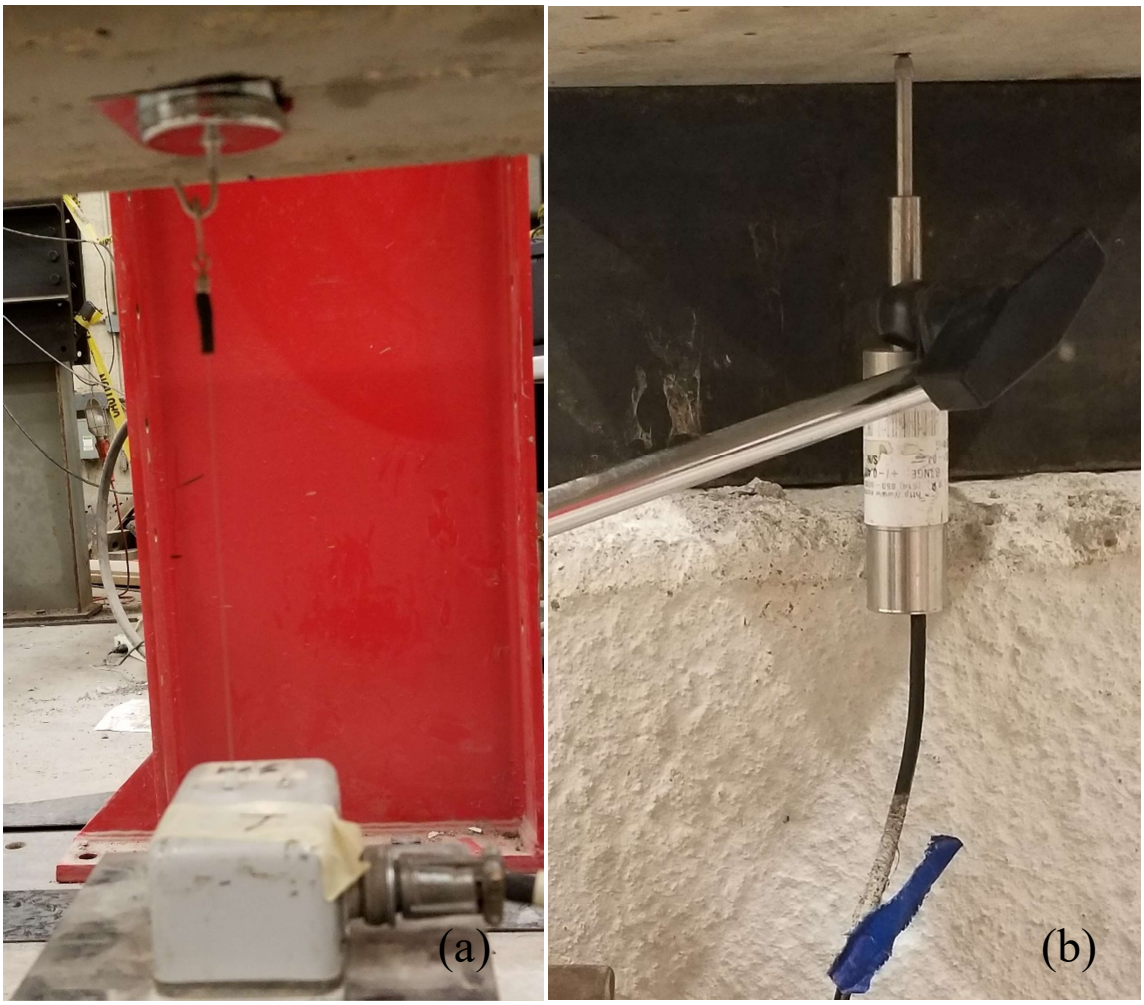

Figure 47. Wire potentiometer (pot) attached to bottom of girder at midspan (a) and linear voltage differential transformer (LVDTs) placed under girder near the support (b).

Four more LVDTs were attached around the negative moment region of the joint to measure joint separation at the interface of the connection if it occurred. One LVDT was attached directly to the concrete deck 2 in. below the top of the deck on each side of the joint on each side of the specimen using two conduit clamps and concrete screws. The LVDTs pushed against an aluminum angle attached to the UHPC joint. This allowed the LVDT to measure joint separation at the top portion of each interface on the side of the joint. Figure 48 shows two LVDT's attached to one face of the continuity joint.

Figure 48.Figure 48. LVDTs used to measure joint separation attached to the girder.

Location of all the external sensors for the newly constructed joint is shown in Figure 49. For the retrofit connection tests, the LVDTs 3 and 5 were adjusted to 11 inches from the end of girder due to the joint length being shorter.

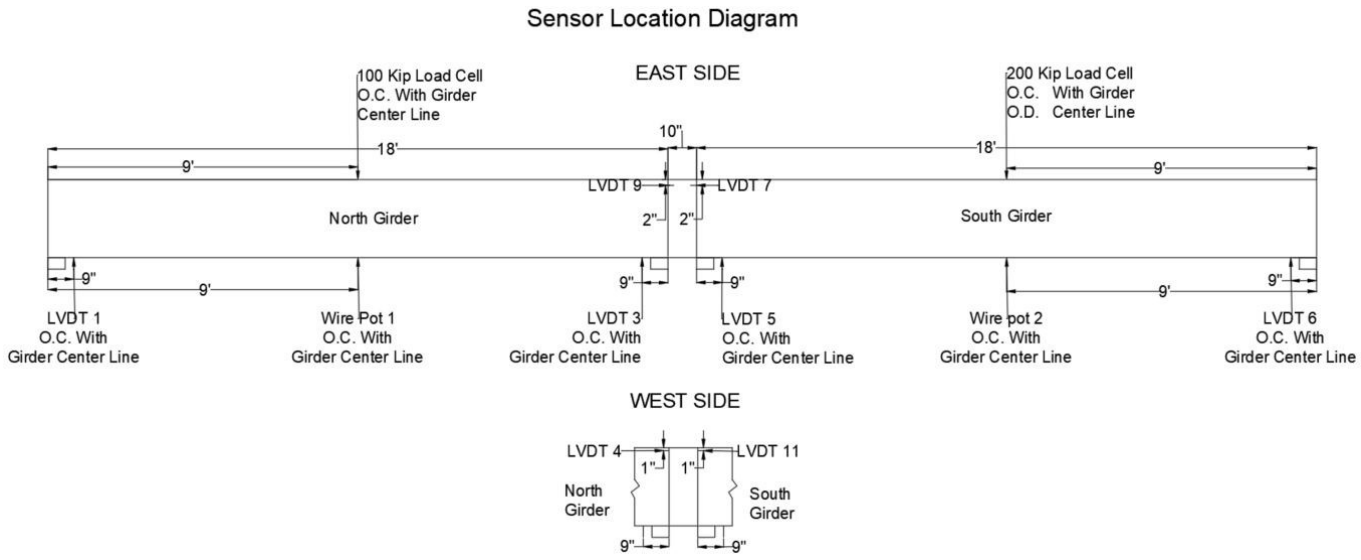

Figure 49. Sensor locations for each test.

Two internal strain gauges with a 6 mm gauge length were attached to the negative moment reinforcing steel in the joint were used to measure strain in the maximum moment region and determine if the steel began to yield during the test. The strain gages were attached in the same location for the newly constructed and retrofit connection. They were attached at the middle of the joint on the rebar, with one strain gauge being attached to and interior bar, and the second gauge to the outer bar not next to the interior bar with the strain gauge. The gauges were coated in silicon to prevent them from getting damaged from the concrete pour. Figure 50 shows a strain gauge attached to a reinforcing bar.

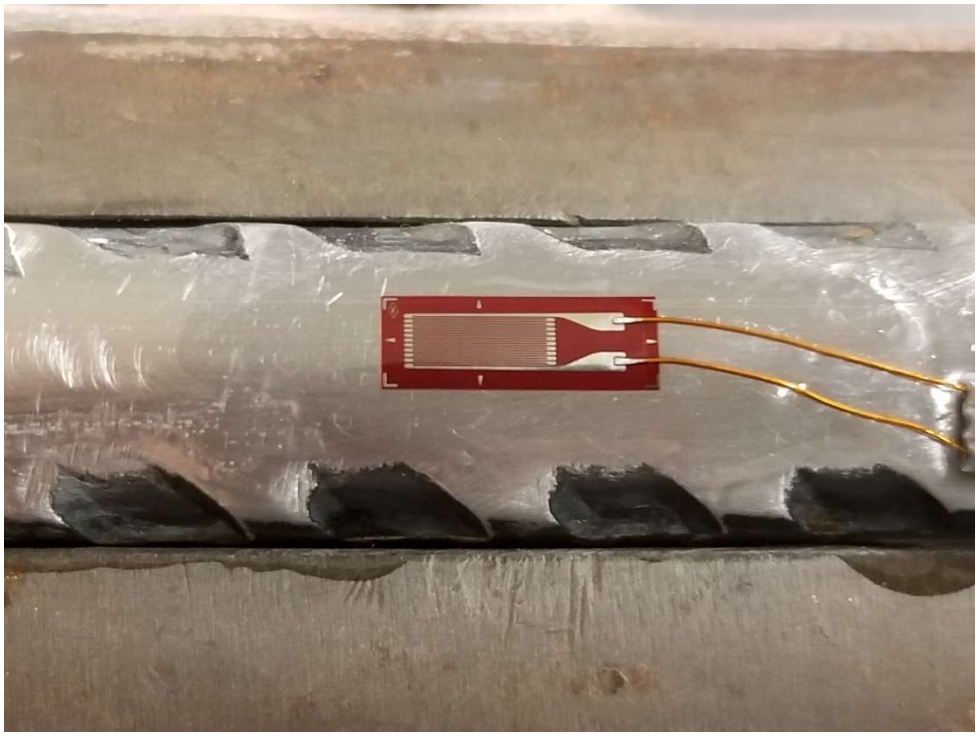

Figure 50. Strain gauge attached to a rebar.

The procedure to begin testing a new specimen started with moving the specimen into the load frames and aligning the specimen on the supports to ensure each girder was in line with the

hydraulic ram. After the specimen was correctly aligned, the load cells, wire pots, and LVDTs were attached/placed into the correct position based on the sensor diagram. Once the sensors were in place, each sensor was tested to verify a signal change was being read on the data acquisition system, and all sensors were zeroed. Load was applied to each specimen in 5 kip increments until initial cracking. The specimen was inspected for initial cracking between each load increment. Upon finding initial cracking, the cracks were traced with a black marker, and the corresponding load increment was written at the end of the crack. Loading increments were changed from 5 kips to 2 kips after initial cracking occurred to allow a more precise crack tracking on the specimen. When the specimen was deemed failed or unsafe to continue loading the specimen was unloaded to end the test.

4.0 Results

Compressive Strengths

The concrete compressive strength data for the prestressed girders associated with the new construction (NC) joint specimens is listed in Table 4. The compressive strength data for the concrete decks associated with each NC specimen is listed in Table 5. The compressive strength data associated with each NC specimen UHPC continuity joint is list in Table 6. All compressive strength data presented is the average between two to three specimens tested. It should be noted that the blanks in Table 4 are missing data that was not collected by mistake. All specimens described in Tables 5 and 6 share the same compressive strengths for 1, 7, and 28 days.

Table 4. Concrete compressive strengths for the NC prestressed girders

Girder	NC1-N	NC1-S	NC2-N	NC2-S	NC1-N	NC1-S
1 Day, psi	4670	4910	5010	5410	5360	5200
7 Day, psi	7110	7070			7310	7090
28 Day, psi			8730	9270	8220	8210
Day of Test, psi	7840	8000	8650	8790	8130	8630

Table 5. Compressive strengths for the NC concrete decks

Deck	NC1	NC2	NC3
1 Day, psi		3970	
7 Day, psi		5090	
28 Day, psi		4930	
Day of Test, psi	4860	4740	5200

Table 6. Compressive strengths for the NC UHPC joints

Joint	NC1	NC2	NC3
3 Day, psi		12870	
7 Day, psi		18000	
28 Day, psi		23390	
Day of Test, psi	23790	25880	24620

The concrete compressive strength data for the prestressed girders associated with the retrofit construction (RC) joint specimens is listed in Table 7. The compressive strength data for the concrete decks associated with each RC specimen is listed in Table 8. The compressive strength data associated with each RC specimen UHPC continuity joint is listed in Table 9. All compressive strength data presented is the average between two to three specimens tested. It should be noted that the blanks in Table 7 are missing data that was not collected by mistake. All specimens described in Tables 8 and 9 share the same compressive strengths for 1, 7, and 28 days.

Table 7. Concrete compressive strengths for the RC prestressed girders

Girder	RC1-N	RC1-S	RC2-N	RC2-S	RC3-N	RC3-S
1 Day, psi	4990	4910	4660	4790	4320	4630
7 Day, psi	6870	7230	6980	7440		
28 Day, psi	8640	8500	7890	8320	7640	8200
Day of Test, psi	8750	8140	7350	7500	7530	8510

Table 8. Compressive strengths for the RC concrete decks

Deck	RC1	RC2	RC3
1 Day, psi		3970	
7 Day, psi		5090	
28 Day, psi		4930	
Day of Test, psi	5460	5510	5160

Table 9. Compressive strengths for the RC UHPC joints

Joint	RC1	RC2	RC3
3 Day, psi		16430	
7 Day, psi		22100	
28 Day, psi		25020	
Day of Test, psi	24850	23980	24790

4.2 Newly Constructed (NC) Specimens

The primary focus of testing the NC specimens was to get a better understanding of how a newly constructed UHPC joint configuration would perform under loading causing negative moment at the joint. To characterize the performance and behavior of this joint configuration, initial cracking for each region of each specimen, cracking occurring at ultimate load, load-deflection curves for each girder in the specimen, and load versus joint separation curves for each joint interface are presented for each NC specimen. The order results are presented is the order in which testing occurred.

4.2.1 Test NC1

During the loading of the NC1 specimen, the data acquisition system crashed approximately two thirds through the loading. The system crashed from over collecting data from the sensors, which resulted in the data file being too large to open with any program and deeming it unusable. The data accusation system was adjusted to reduce the incoming data before reloading the NC1 specimen. On the second loading the file size was significantly smaller and could be opened with no difficulty. Cracks that formed during the reload test were labeled with an R with the load amount.

Initial flexural cracking was observed during the first loading near the joint interface on the NC1-S girder at a load of 35 kips, shown in Figure 52b. The next flexural crack was observed directly under the load point on the NC1-N girder at a load of 43 kips, shown in Figure 51a. In addition, two more cracks had developed at a load of 43 kips, a flexural crack near the joint interface on the NC1-N girder, shown in Figure 52a, and a flexure-shear crack near the joint interface on NC1-S, shown in Figure 52b. On the next load increment a flexural crack was

observed on the NC1-S girder directly under the load point at a load of 45 kips, shown in Figure 51b. A flexure-shear crack had also developed near the joint interface on the NC1-N girder at the same load, shown in Figure 52a. Asymmetrical hairline flexural cracks were observed in the continuity joint at a load of 52 kips during the first loading, as indicated with dark lines in Figure 53. During the reload test a flexural crack was observed on the east face of continuity joint at a load of 44 kips, as indicated in Figure 53b with a dark oval. Additional flexural cracks developed during the reload test in the continuity joint at a load of 46 kips, as indicated in Figure 54 with dark ovals. These flexural cracks in the continuity joint developed at a lower load increment during the reload test than the initial cracks observed during the first loading. This would likely be due to the cracks already existing prior to the reload, but which did not fully separate to be visually distinguishable as a crack until the reloading occurred.

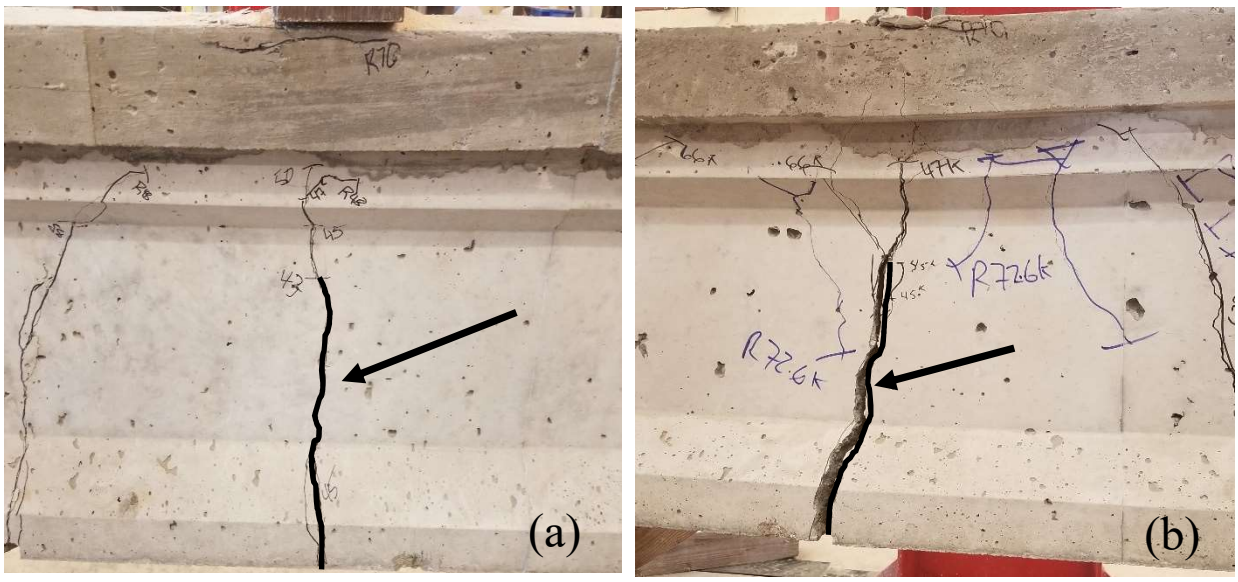

Figure 51. Initial flexural cracking under the load point on the NC1-N girder at 43 kips of load (a) and initial flexural cracking under the load point on the NC1-S girder at 45 kips of load (b). Arrows point to the dark lines that indicate the initial flexural cracks.

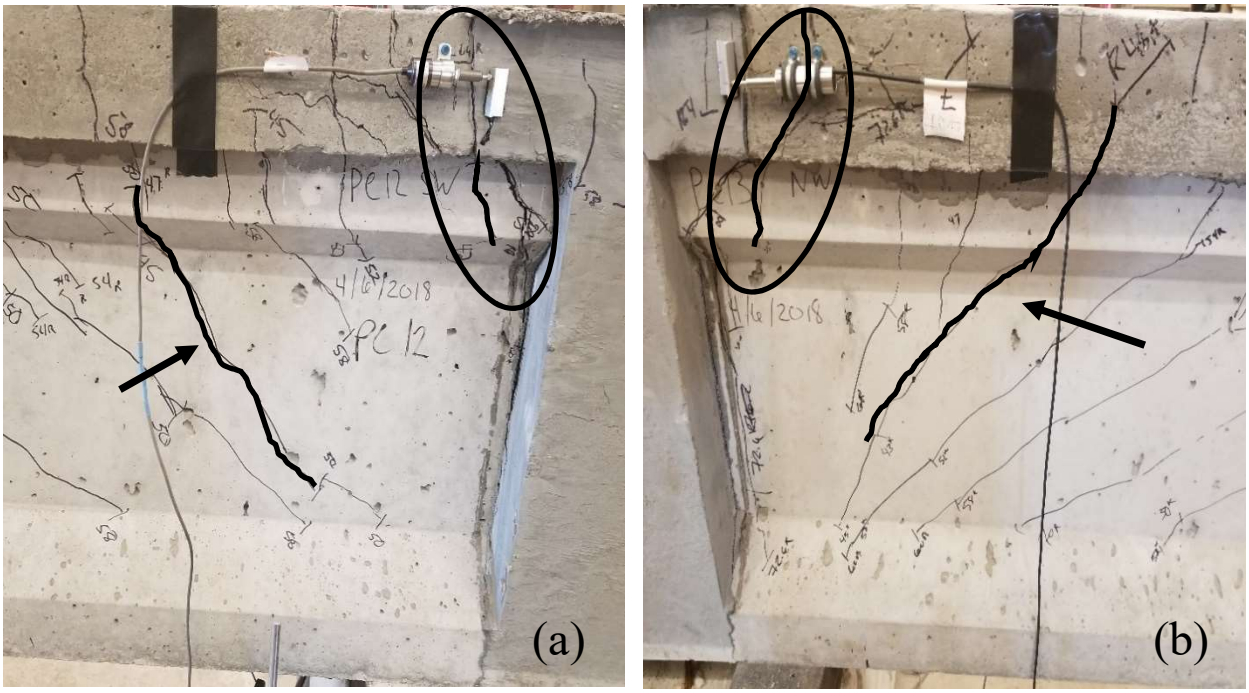

Figure 52. Initial flexural cracking on the NC1-N girder at 43 kips of load and initial flexure-shear cracking on the NC1-N girder at 45 kips of load (a) and initial flexural cracking on the NC1-S girder at 35 kips of load and initial flexure-shear cracking on the NC1-S girder at 43 kips of load (b). Dark ovals indicate the initial flexural cracking near the continuity joint, and arrows point to the dark lines that indicate the initial flexure-shear cracking.

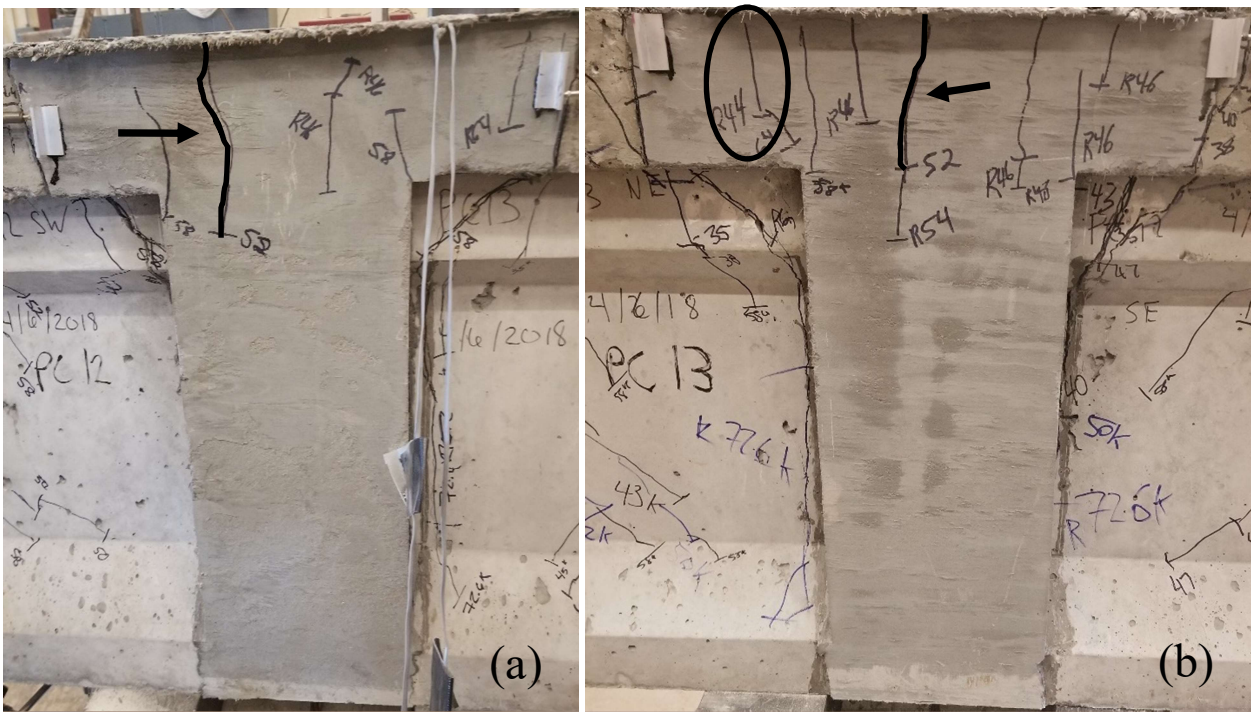

Figure 53. Initial continuity joint flexural cracking on the west face (a) and east face (b) at 52 kips of load. Arrows point to the dark lines that indicate the initial flexural cracks, and the dark oval shows the initial flexural cracks from the reload test. Other reloading cracks are indicated by an R before the load value.

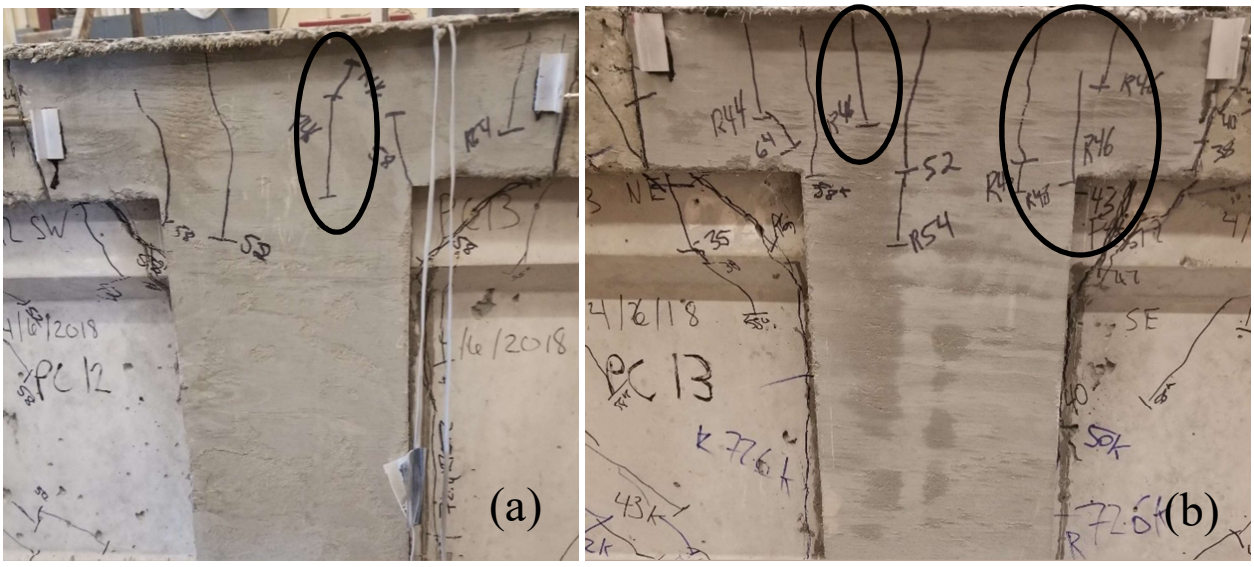

Figure 54. Continuity joint flexural cracking during the reload test on the west face (a) and east face (b) at 46 kips of load. Dark ovals show the initial flexural cracks from the reload test. Other reloading cracks are indicated by an R before the load value.

Cracks that developed between initial cracking and final failure included additional flexural cracks under the point loads, flexure-shear cracks near the joint interface, web shear cracks near the point load, and flexural cracks in the UHPC joint. Most cracks occurring on the NC1 specimen when reaching final failure were flexure-shear and web shear cracks. These cracks developed as the load increased and the flexure-shear cracks began to move away from the joint interface towards the load point. Upon reaching approximately halfway to the load point from the joint, web shear cracks developed in place of the flexure-shear cracks. Figure 55 shows the flexural cracks and web shear cracks between the joint interface and load point for the NC1-N and NC1-S girder.

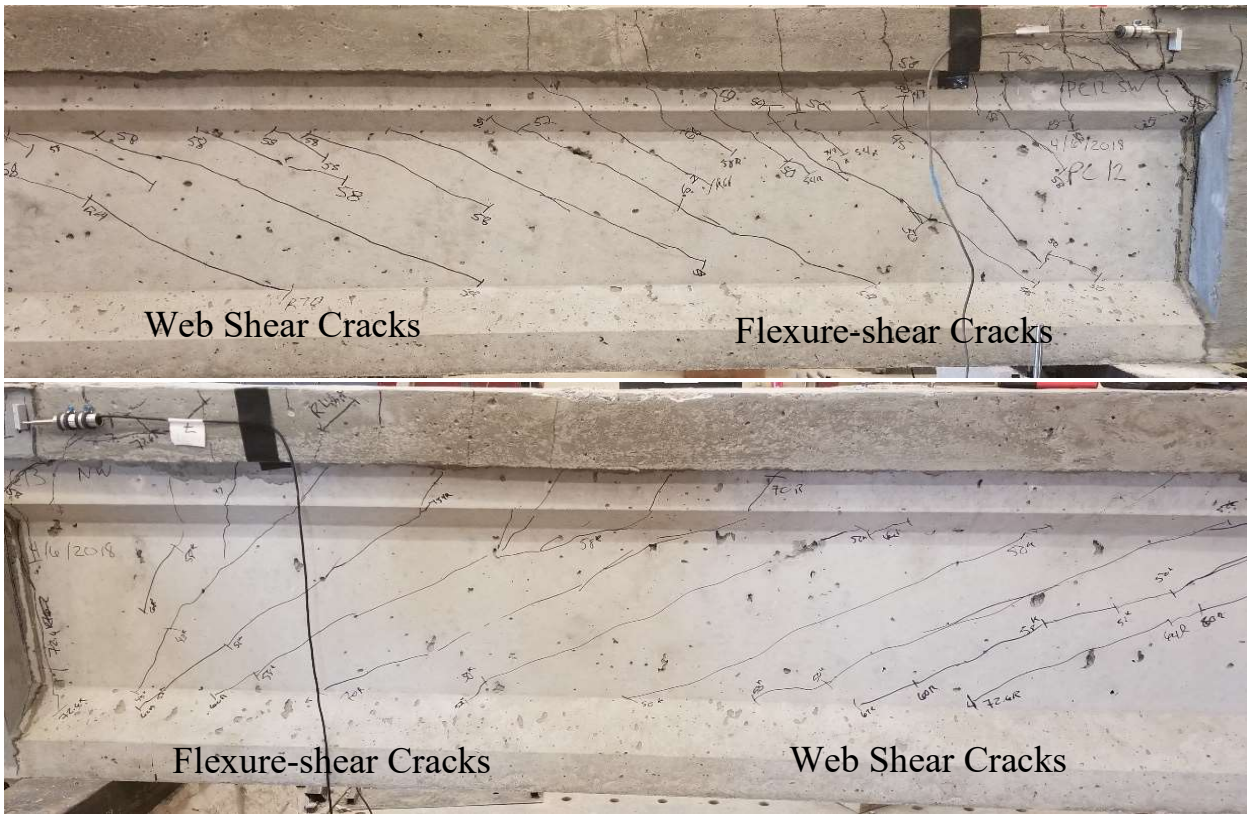

Figure 55. NC1-N girder with flexure-shear and web shear cracks (top). NC1-S girder with flexure-shear and web shear cracks (bottom).

Loading of the specimen was stopped when the prestressing strands in the NC1-S girder ruptured directly under the load point at a load of 73.8 kips. The flexural crack directly under the load point where the prestressing strands ruptured is indicated in Figure 56 with a dark oval. The concrete deck began to crush at the load point in both girders under the loading conditions immediately before the prestressing strands ruptured, as shown by the dark circles in Figure 57. In addition, there was significant widening of the flexural cracks under both load points with additional load application, as shown by dark lines in Figure 57. These conditions were taken to indicate flexural failure of the beam specimens. Allowing the prestressing strands to rupture on the first test specimen helped indicate the capacity of the prestressed concrete girders connected to the continuity joint had been reached, and to prevent the need to take future prestressing strands all the way to rupture.

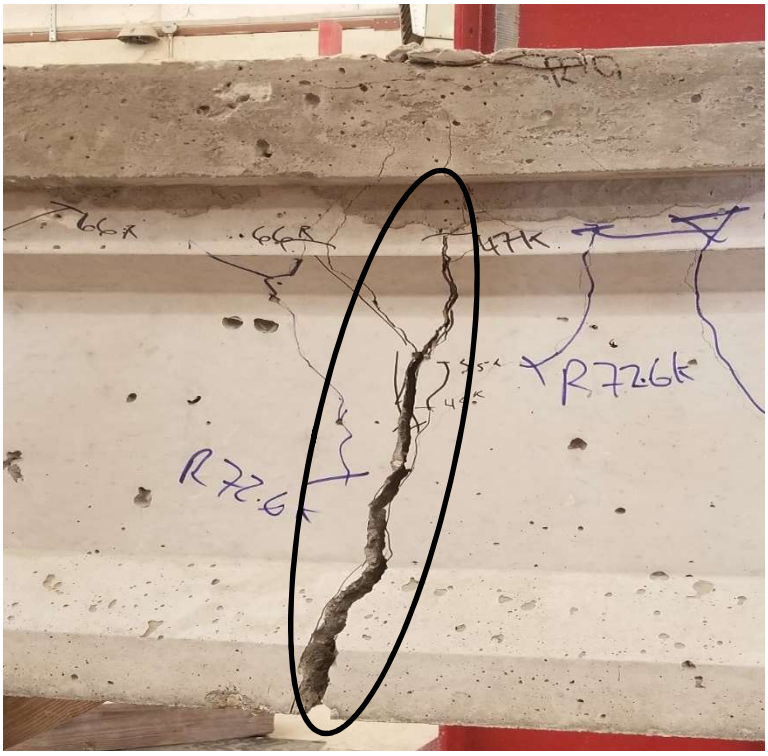

Figure 56. Flexural crack where the prestressing strands ruptured under the load point on the NC1-S girder, indicated by a dark oval

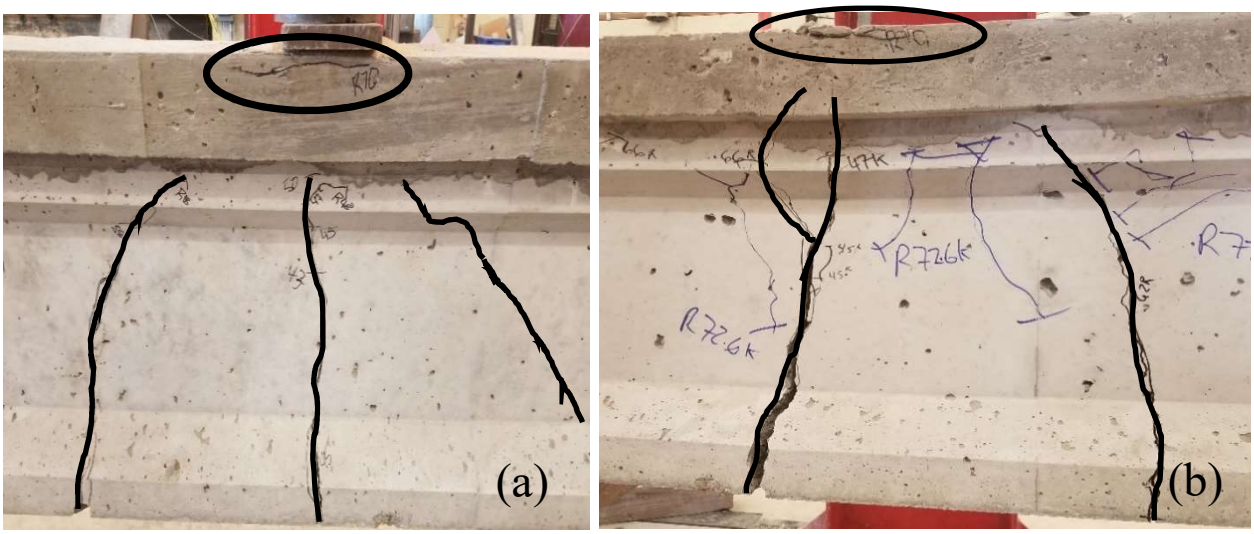

Figure 57. Crushed concrete deck in the NC1-N (a) and NC1-S (b) girder are indicated by a black oval and the final flexural cracks under the load point in the NC2-N (a) and NC2-S (b) girders are indicated by dark lines

The interface between the NC1-N girder and the UHPC joint exhibited flexural cracking along the interface, which resulted in separation of the girder from the joint material, as shown by the dark lines in Figure 58a. Additional separation was observed at the interface between the UHPC joint and the NC1-S girder, but also flexural cracking parallel to the interface, as shown in Figure 58b. The term ”joint separation” will be used throughout the remainder of the document and is defined as the debonding between the concrete deck and UHPC joint interface due to flexural cracking.

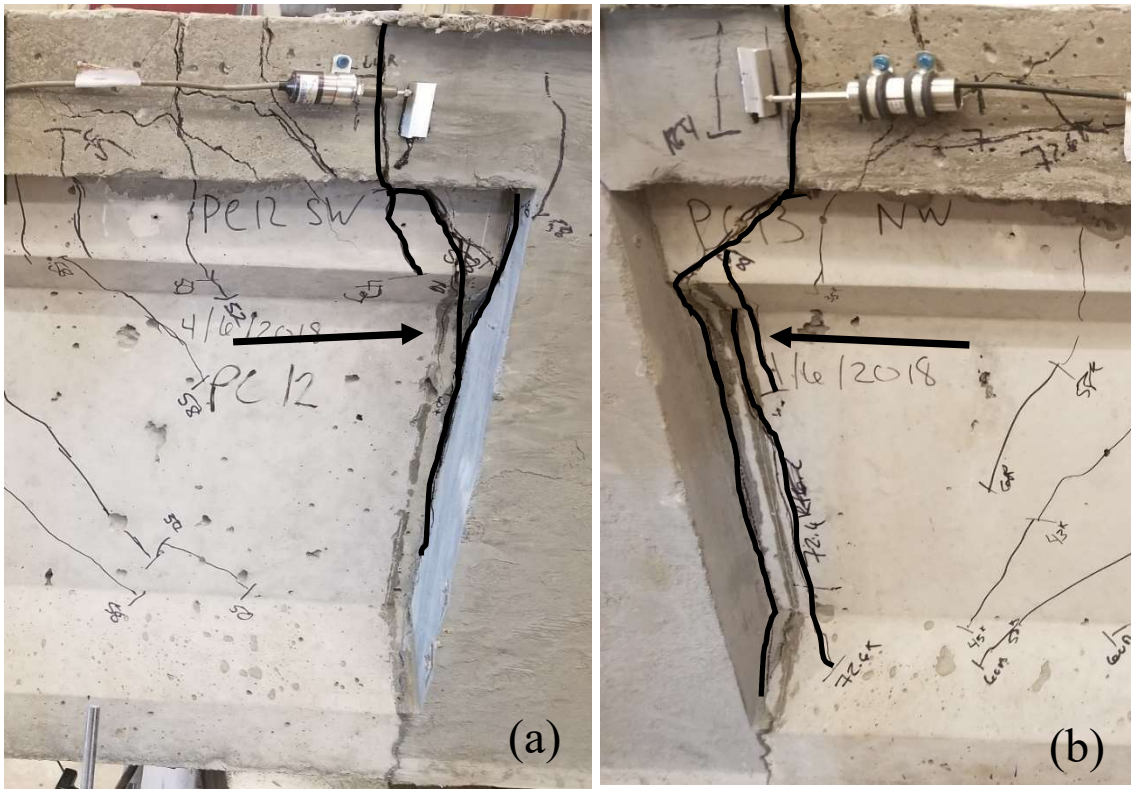

Figure 58. Joint separation at the interface between the NC1-N girder and the UHPC joint (a) and flexural cracking parallel to the interface between the UHPC joint and the NC1-S girder (b) are indicated by dark lines.

Figure 59 shows the load-deflection curve for the NC1-N girder from the reload test. The reload curve does not clearly indicate the girder having a ductile behavior due to initial cracking occurring in the first test. No sudden loss of stiffness indicating cracking is visible in the reload curve. The reload curve beginning to plateau out to 2 inches of deflection after exceeding the maximum load that was reached in the first test indicates that the prestressing strands began to yield. This supports a ductile behavior of the NC1-N prestressed girder during loading up to the ultimate load of 72.5 kips, as the graph was unable to show clear indication of the behavior. Figure 60 shows the reload-deflection curve for the NC1-S girder. The NC1-N and NC1-S girders had the same ductile behavior, but the NC1-S girder's prestressing strands ruptured after the ultimate load of 73.8 kips was achieved. The NC1-S girder deflected an inch more than the

NC1-N girder due to the strands rupturing. The noise in the data visible in both figures comes from the wire pots measuring deflection, and for the future tests they were switched to different data acquisition channels with better signal conditioning to reduce the noise in the signals.

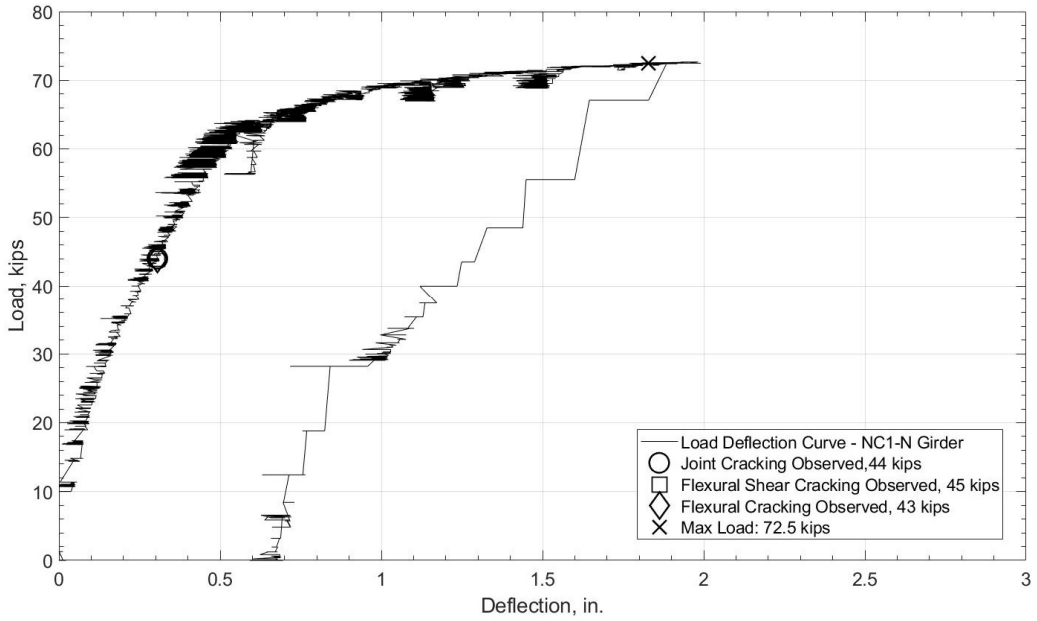

Figure 59. Load-deflection curve for the NC1-N girder, reload test.

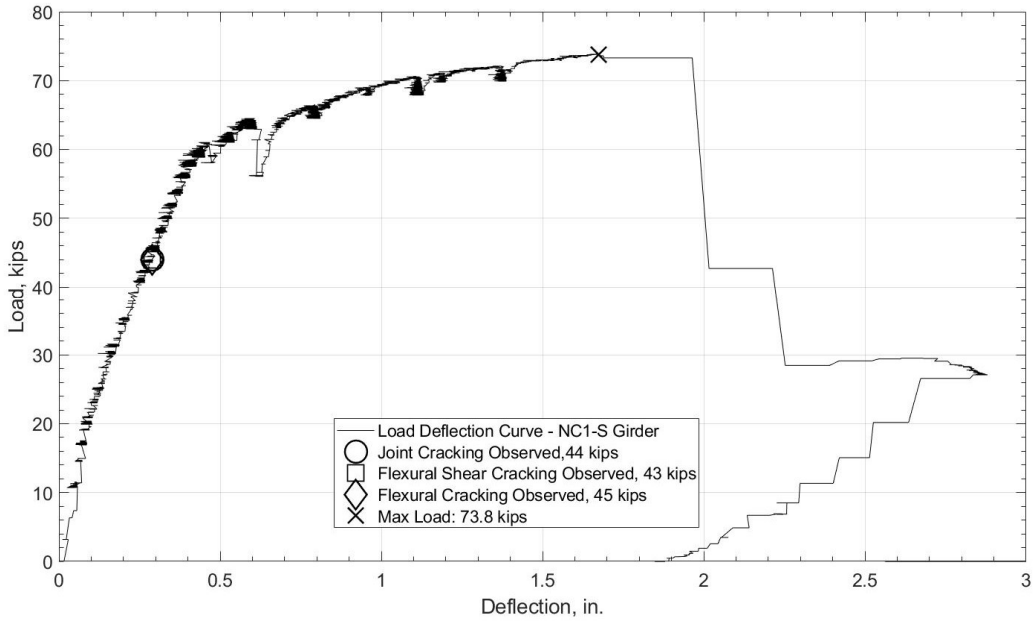

Figure 60. Load-deflection curve for the NC1-S girder, reload test.

Figure 61 shows the load-joint separation curve between the NC1-N girder's concrete deck and the UHPC joint from the reload test. The readings from the LVDTs on the east and west faces of the concrete deck were averaged to get a better representation of the joint separation. Figure 48 shows the location of the LVDTs on the joint interface and are located 2 inches below the top of the deck. The reload curve showed a linear trend from zero back to where the final load of the initial test had stopped. Beyond the 60 kip load joint separation increased significantly with each load increment. At this point the NC1-N girder began to exhibit an increase in deflection, resulting in a less stiff member and creating a hinge at the weak point, that is the joint interface. Figure 62 shows the reload joint separation curve between the NC1-S girder's concrete deck and the UHPC joint. This figure only represents LVDT11 on the west face of the deck. LVDT 7 was not included for any of the six tests, as the data was unreliable. This load joint separation curve

shows the same trends as for the average of LVDT 4 and 9 between the NC-1N girder deck and UHPC joint, but with a smaller magnitude.

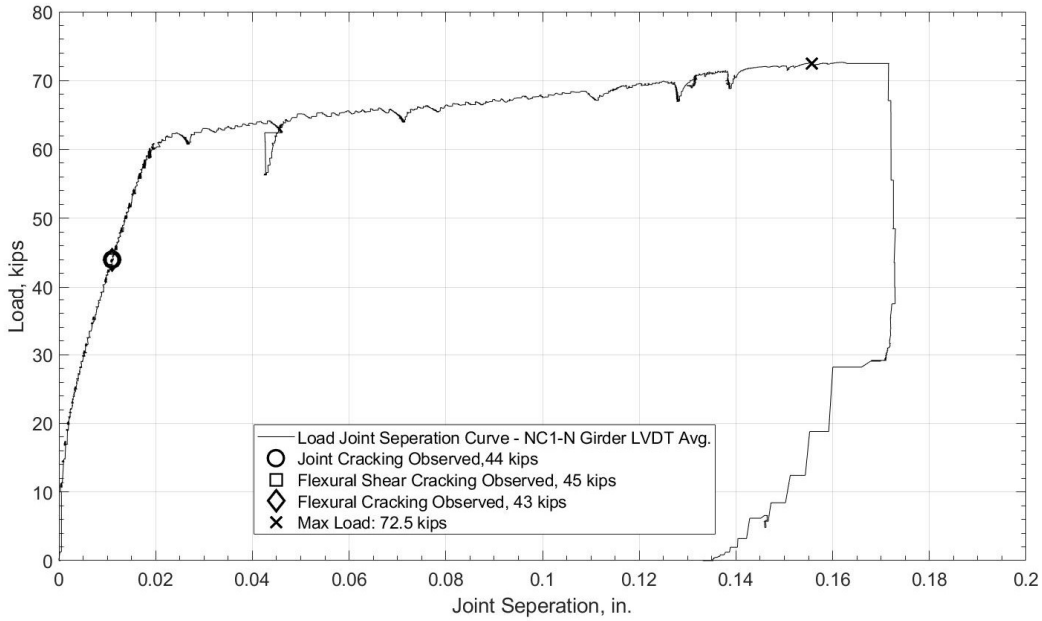

Figure 61. Load-joint separation curve at the NC1-N girder deck to joint interface.

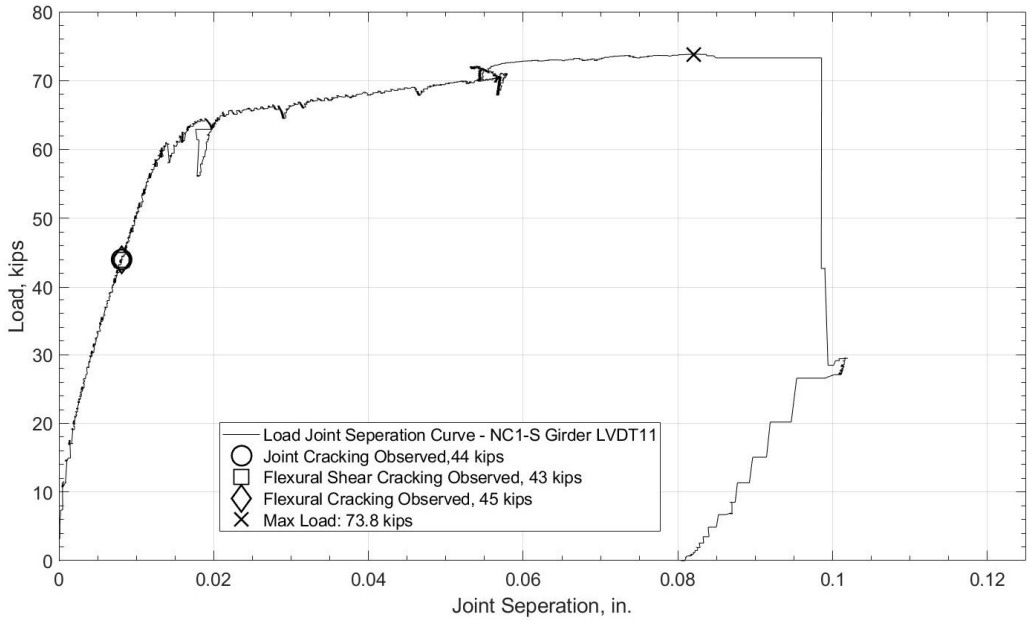

Figure 62. Load-joint separation curve at the NC1-S girder deck to joint interface west face.

4.2.2 Test NC2

Initial flexural cracking was observed directly under the load point on the NC2-N girder at a load of 40 kips, shown in Figure 63a. During the next 5 kip load increment a flexural crack was observed on the NC2-S girder directly under the load point, shown in Figure 63b. In addition, flexure-shear cracks, shown in Figure 64b, had also developed on the NC2-S girder near the continuity joint. Asymmetrical hairline flexural cracks occurred in the continuity joint at the same load increment of 45 kips as shown in Figure 65. The cracking observed on the east face of the joint did not match the west face, as the east face had irregular flexural cracking as indicated in Figure 65b with a dark circle. The second flexural crack did not go to the top of the joint, but instead started below and shifted from the first crack. The NC2-N girder exhibited similar flexure-shear cracks as the NC2-S girder at 47 kips near the joint as shown in Figure 64b.

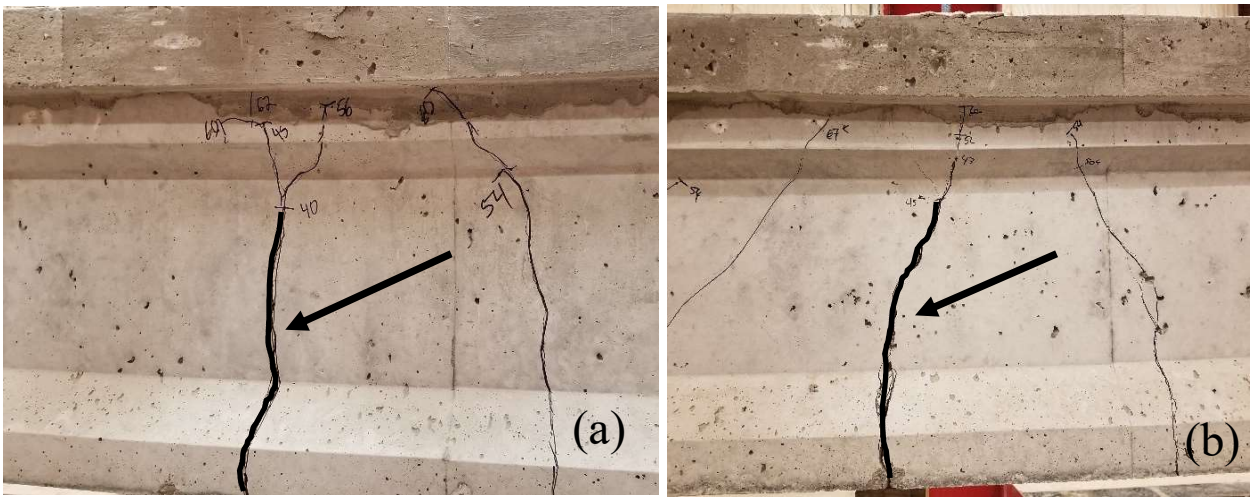

Figure 63. Initial flexural cracking under the load point on the NC2-N girder at 40 kips of load (a) and initial flexural cracking under the load point on the NC2-S girder at 45 kips of load (b). Arrows point to the dark lines that indicate the initial flexural crack.

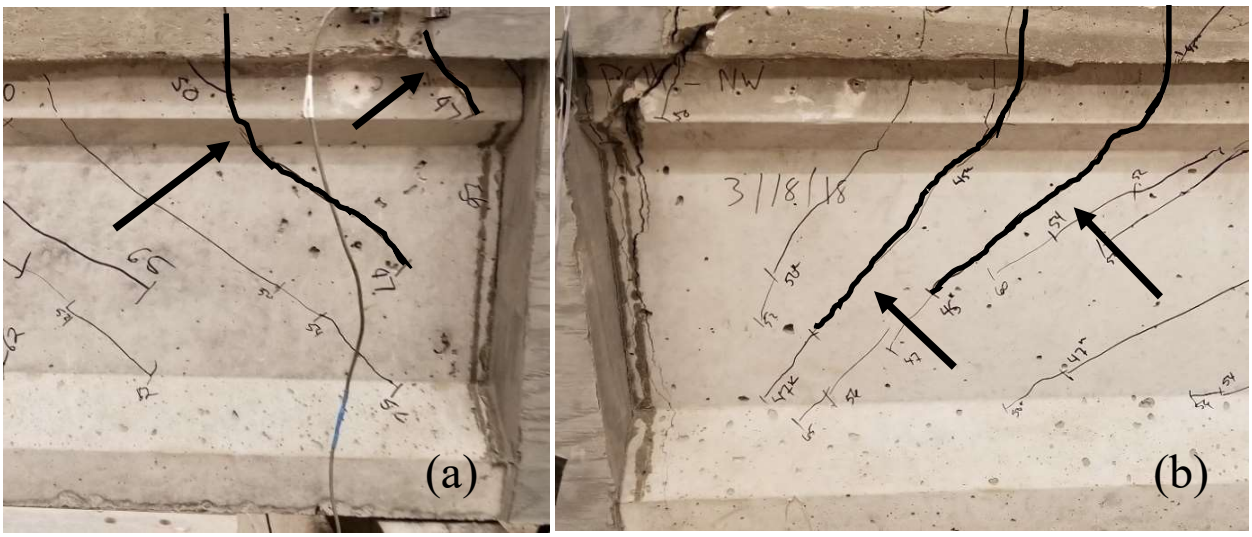

Figure 64. Flexure-shear cracking on the NC2-N girder at 47 kips of load (a) and flexure-shear cracking on the NC2-S girder at 45 kips of load (b). Arrows point to the dark lines that indicate the initial flexure-shear cracking.

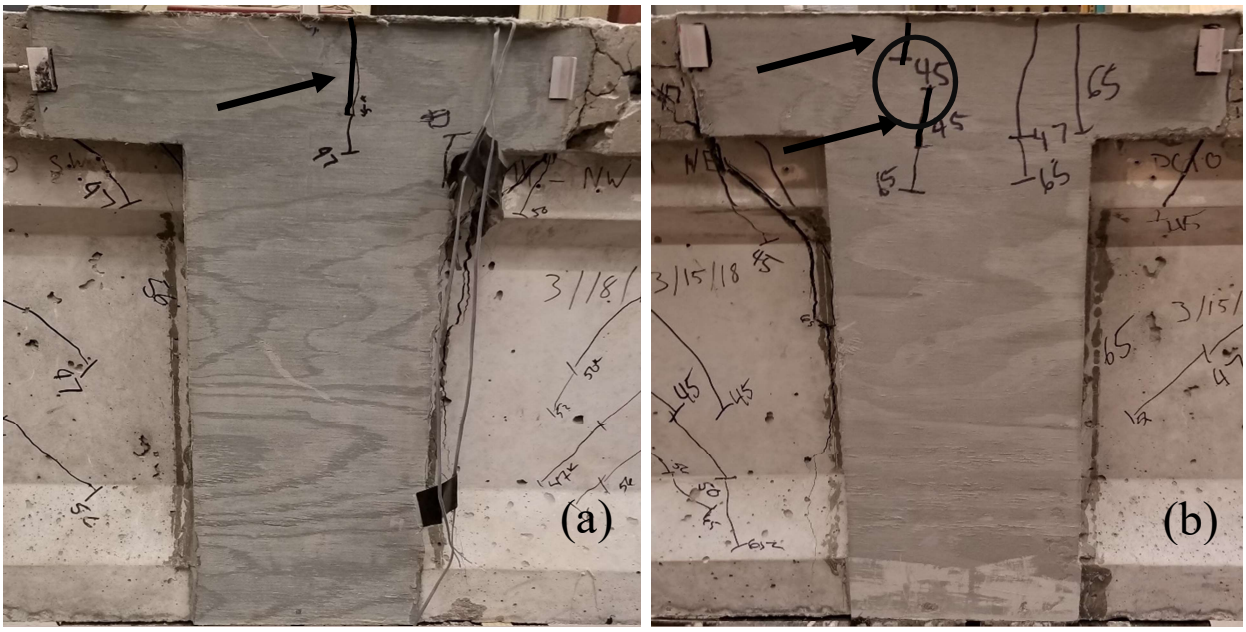

Figure 65. Initial continuity joint flexural cracking on the west face (a) and east face (b) at 45 kips of load. Arrows point to the dark lines that indicate the initial flexural cracks, and the dark circle on the east face (b) shows the irregular flexural cracking.

Cracks that developed between initial cracking and final failure included additional flexural cracks under the point load, flexure-shear cracks near the joint interface, web shear cracks near the point load, and flexural cracks in the UHPC joint. The majority of cracks observed for the NC2 specimen were at final failure were flexure-shear and web shear cracks. These cracks developed as the load increased and the flexure-shear cracks propagated away from the joint interface towards the load point. Beginning approximately halfway to the load point web shear cracks developed in place of the flexure-shear cracks. Figure 66 shows the flexural cracks and web shear cracks between the joint interface and load point for the NC2-N and NC2-S girder.

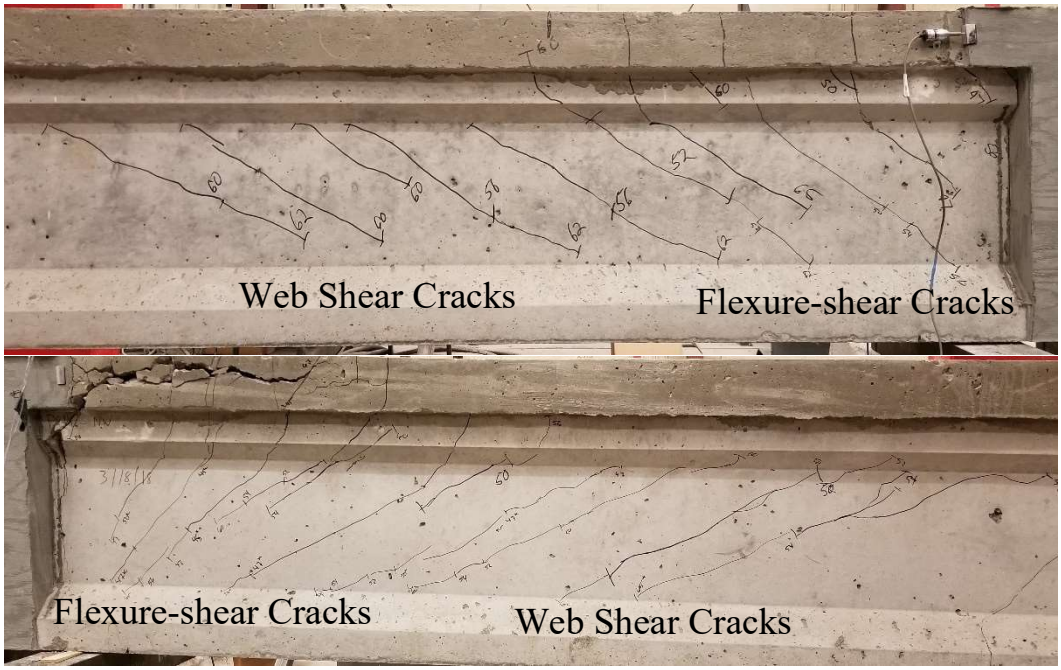

Figure 66. NC2-N girder with flexure-shear and web shear cracks (top) and NC2-S girder with flexure-shear and web shear cracks (bottom).

Loading of the specimen was stopped upon reaching an applied load of 71.5 kips on the NC2-N girder and 72 kips on the NC2-S girder. Under these loading conditions the concrete deck had begun to crush at the load point in both girders, as shown by the dark circles and arrows in

Figure 67. In addition, the flexural cracks under both loads points had significantly widened, as shown by dark lines and arrows in Figure 67. These conditions were taken to indicate flexural failure of the beam specimens and testing was concluded to prevent the prestressing strands from rupturing and causing damage to the testing apparatus.

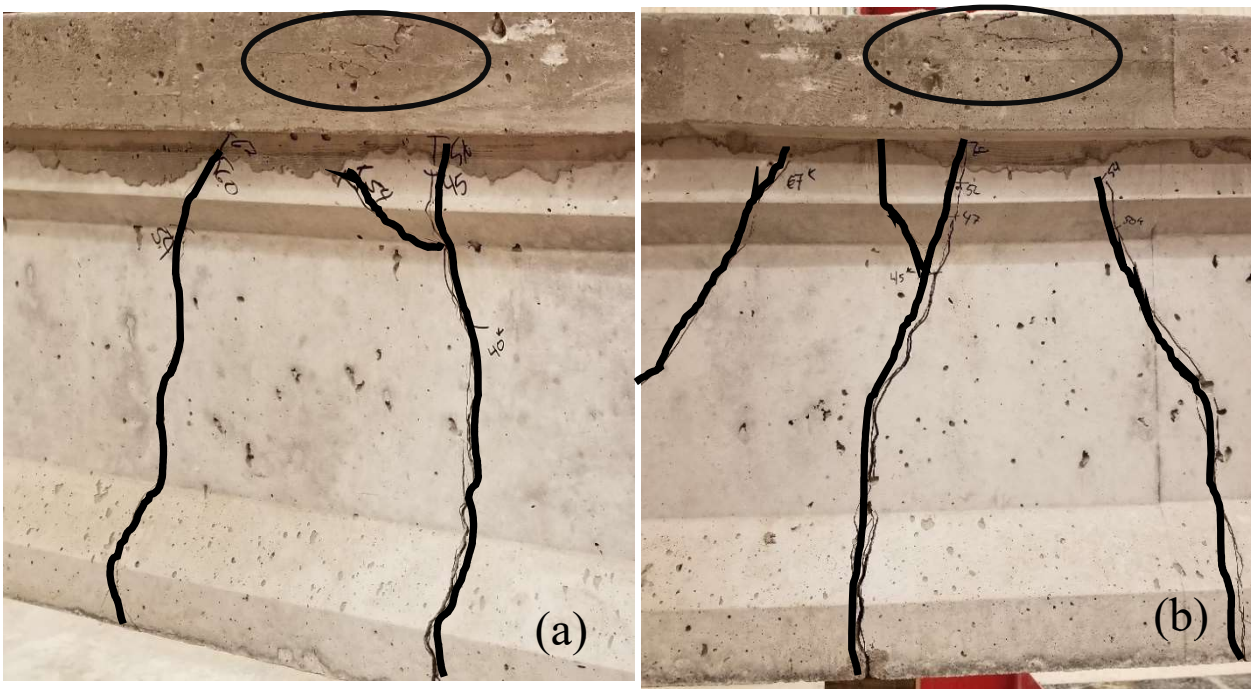

Figure 67. Crushed concrete deck in the NC2-N (a) and NC2-S (b) girders is indicated by a black oval, and the final flexural cracking under the load point in the girders are indicated by dark lines.

Flexural cracking was observed along the interface between the NC2-N girder and the UHPC joint, which resulted in separation of the girder from the joint, as shown by the dark lines in Figure 68a. Less separation was observed at the interface between the UHPC joint and the NC2-S girder, but more flexural cracking parallel to the interface was observed, as shown in Figure 68b.

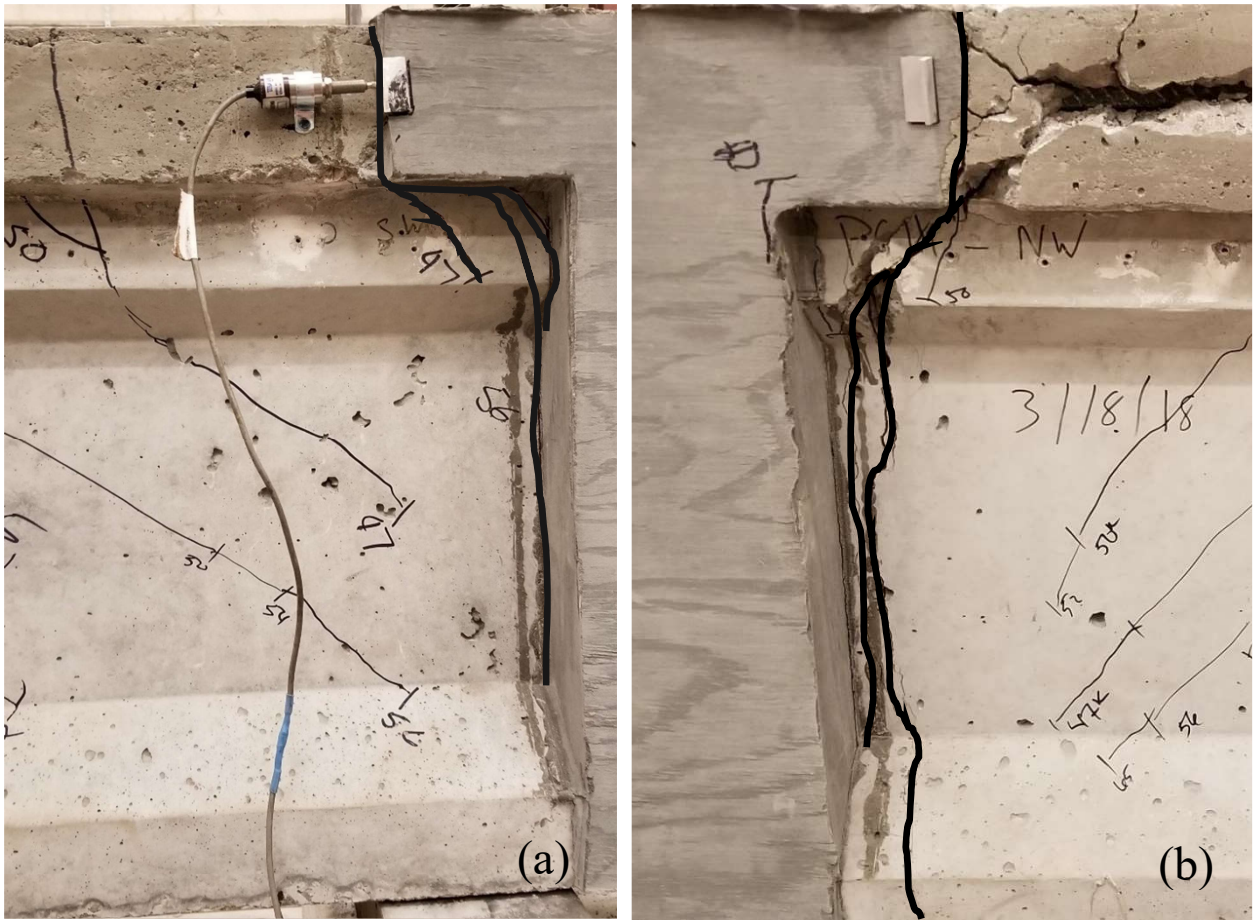

Figure 68. Joint separation at the interface between the NC2-N girder and the UHPC joint (a) and flexural cracking parallel to the interface between the UHPC joint and the NC2-S girder (b) are indicated by dark lines.

The NC2-S girder deck near the joint interface exhibited severe cracking along the side of the deck in the longitudinal direction at the level of the negative moment reinforcement. After testing was complete, the top portion of the deck was removed to determine the cause of this behavior. After the concrete had been removed above the negative reinforcement, it was determined that the rebar had plastically deformed during loading. There was no sign of cracking around the reinforcement entering the UHPC joint, which indicated that the UHPC joint acted as a fixed end for the reinforcement. As the load increased during the test, the girder deflected more

than the relatively rigid joint causing the rebar to follow the same curvature as the girder but remain fixed in the UHPC joint. This caused the rebar to bend sharply upward, and it separated the concrete along the longitudinal negative moment reinforcement in the deck. Figure 69 shows the NC2-S girder deck before and after the excavation of the concrete separation in the deck.

Figure 69. NC2-S girder before excavation of the concrete in the deck (top) and the deck after excavation exposing the reinforcement (bottom)

Figure 70 shows the load-deflection curve for the NC2-N girder. The curve shows a reduction in stiffness that corresponds with the initial flexural cracking observed at 40 kips. Other types of initial cracking did not reduce the stiffness of the girder. This indicates a ductile behavior of the NC2-N prestressed girder during loading up to the ultimate load of 71.5 kips. In addition, the plateau of the load-deflection curve out to 2 inches of deflection indicated the prestressing strands were yielding. Figure 71 shows the load-deflection curve for the NC2-S girder. The NC2-N and NC2-S girders had the same ductile behavior, but with the NC2-S girder having less

deflection at mid-span. The varying deflection of the girders can be related to a difference in the concrete mix, compressive strength, modulus of elasticity, and a difference in prestress loss between the girders. These variables could have caused the NC2-N girder to crack 5 kips earlier in flexure than the NC2-S girder and could have resulted in the NC2-N girder having a reduced stiffness compared to the NC2-S girder. This led to a larger downward curvature, which created more strain in the prestressing strands, and led to even larger deflection in the NC2-N girder.

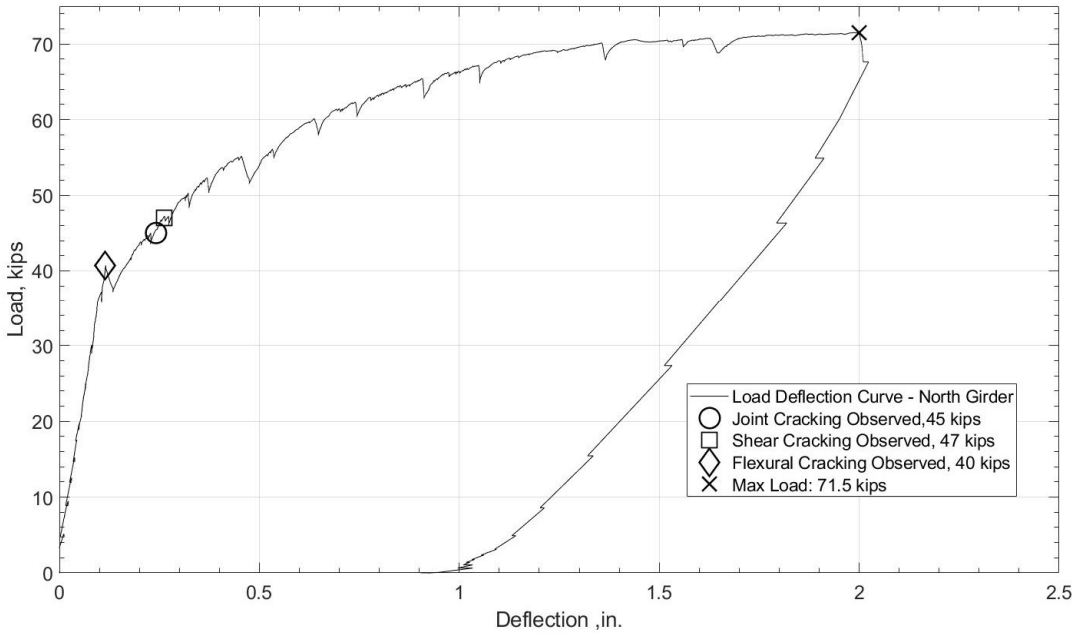

Figure 70. Load-deflection curve for the NC2-N girder.

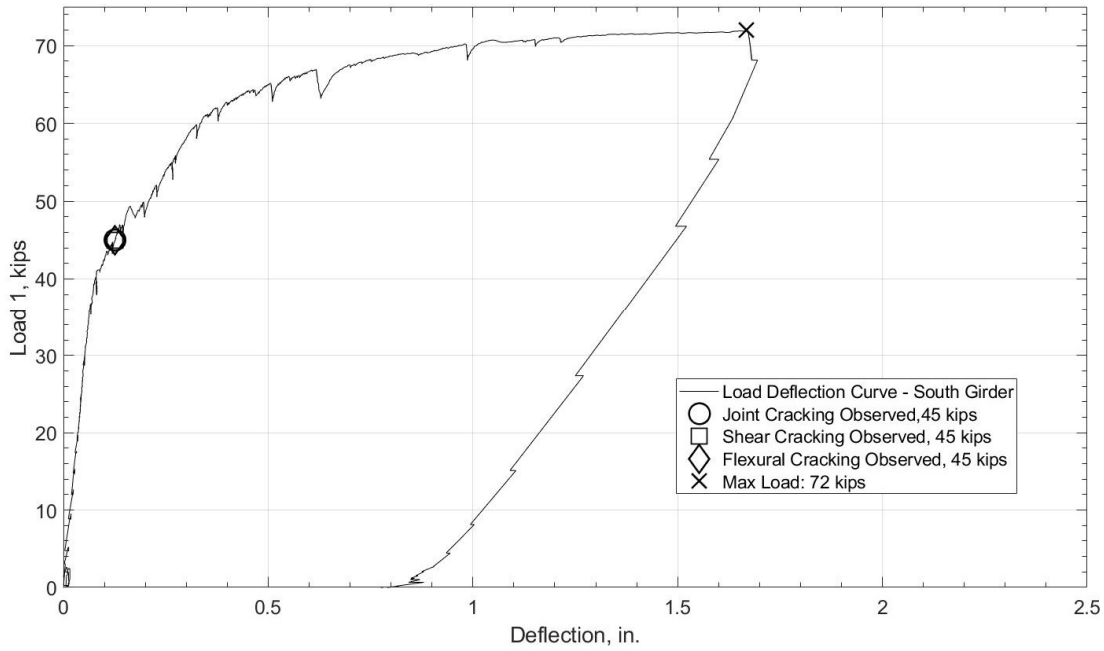

Figure 71. Load-deflection curve for the NC2-S girder.

Figure 72 shows the load-joint separation curve between the NC2-N girder's concrete deck and the UHPC joint. The average of the readings from the LVDTs on the east and west faces of the concrete deck was taken to get a better representation of the joint separation. Figure 48 shows the location of the LVDT's on the joint interface and are located two inches below the top of the deck. The deck joint had minor separation until reaching the initial flexural cracking of 40 kips. After that load, indicated by a diamond shape in Figure 72, the joint separation began to increase significantly with each load increment. It is reasonable that major joint separation could only occur after the girder cracked due to flexure, resulting in a less stiff member and creating a hinge at the weak point; the joint interface. Figure 73 shows the load-joint separation curve between the NC2-S girder's concrete deck and the UHPC joint. This figure only includes results from LVDT11 on the wast face of the deck. This load-joint seperation curve shows the opposite of what was expected. As the girder cracked in flexure, the reduction of girder stiffness appeared to

have no effect on the rate of the joint seperation as the load increased. No major joint seperation occurred until reaching over 60 kips of load, after which the separation rapidly increased until the LVDT gave a faulty reading. The results shown only include data from before the faulty reading occurred.

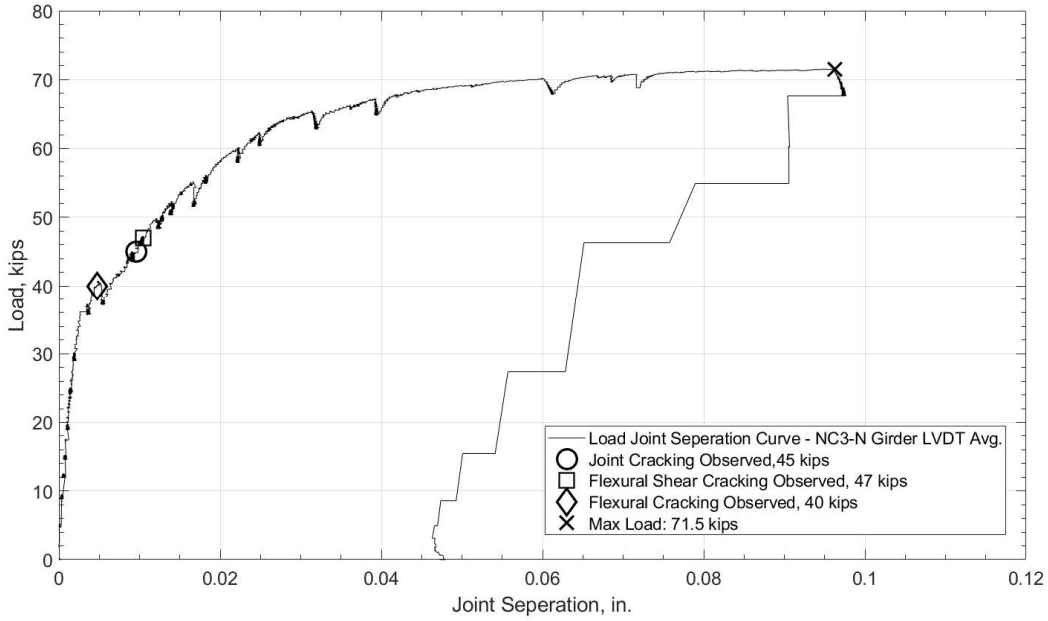

Figure 72. Load-joint separation curve at the NC2-N girder deck to joint interface.

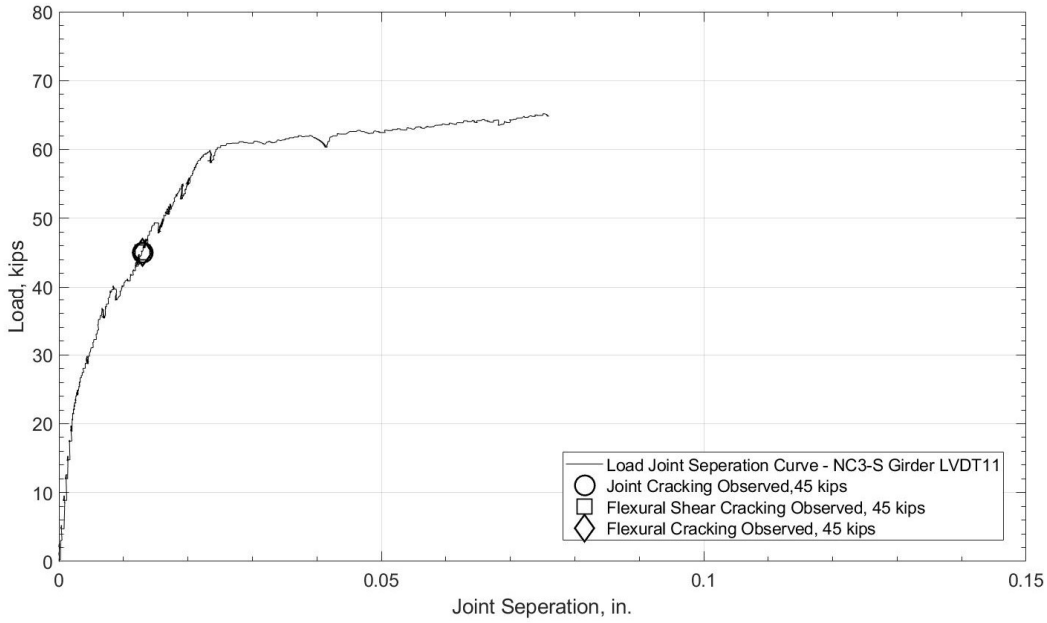

Figure 73. Load-joint separation curve at the NC2-S girder deck to joint interface west face.

4.2.3 NC3 Positive Moment Test

A positive moment test was conducted on the NC3 specimen, in order to test the positive moment region of the UHPC continuity joint. This approach was intended to recreate the time dependent effects that are applied to the continuity joint and create the positive moment that often results in cracking. The supports were removed at the NC3-N and NC3-S joint interface to create a simply supported span with the UHPC joint at the middle of that span. The two loads were then applied in the exact location as the negative moment tests to the girders to create positive moment in the continuity joint region. Initial flexural cracking was observed along the joint interface at a load of 4.5 kips, as indicated with dark lines in Figure 74. As the load progressed, the flexural crack progressed upward along the joint causing joint separation. A flexural crack was observed at 7.2 kips near the joint interface on the NC3-S girder, as indicated in Figure 74b with a dark oval. Upon reaching the 7 kip mark the positive moment test was

stopped to prevent any additional damage to the joint, as this test was conducted only to see the initial cracking behavior of the joint under this loading condition. No flexural cracks were observed in the UHPC joint.

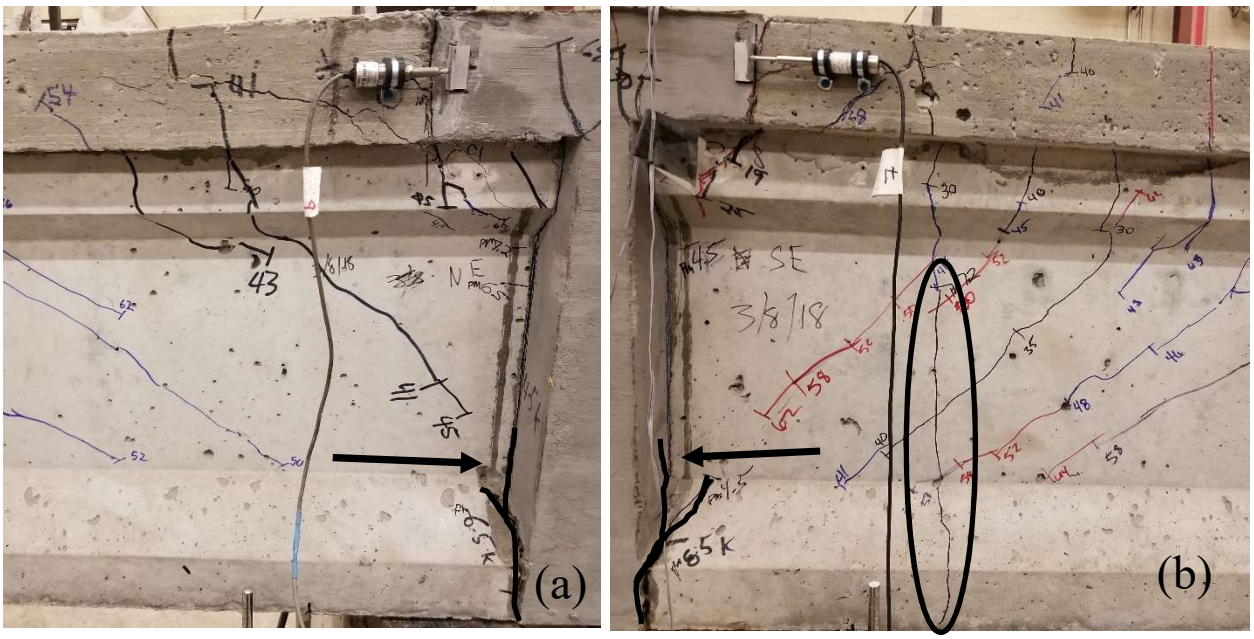

Figure 74. Joint separation at the interface between the NC3-N girder and the UHPC joint during the positive moment test (a) and joint separation at the interface between the NC3-S girder and the UHPC joint (b) are indicated by dark lines. Flexural crack near the joint interface in the NC3-S girder (b) is indicated by a dark oval.

4.2.4 Test NC3

Initial flexural cracking was observed near the joint interface on the NC3-S girder at a load of 19 kips, shown in Figure 76b. After the next load increment asymmetrical flexural cracks were observed in the continuity joint at a load of 25 kips, shown in Figure 77. In addition, a flexural crack had developed in the NC3-N girder near the joint interface , shown in Figure 76a. Initial flexure-shear cracking was observed near the joint interface on the NC3-S glider at a load of 35 kips, shown in Figure 76b. Two cracks were observed at a load of 41 kips, a flexural crack directly under the load point on the NC3-N girder, shown in Figure 75a, and a flexure-shear

crack near the joint interface on the NC3-N girder, shown in Figure 76a. After the next load increment a flexural crack had developed directly under the load point on the NC3-S girder at a load of 46 kips, shown in Figure 75b.

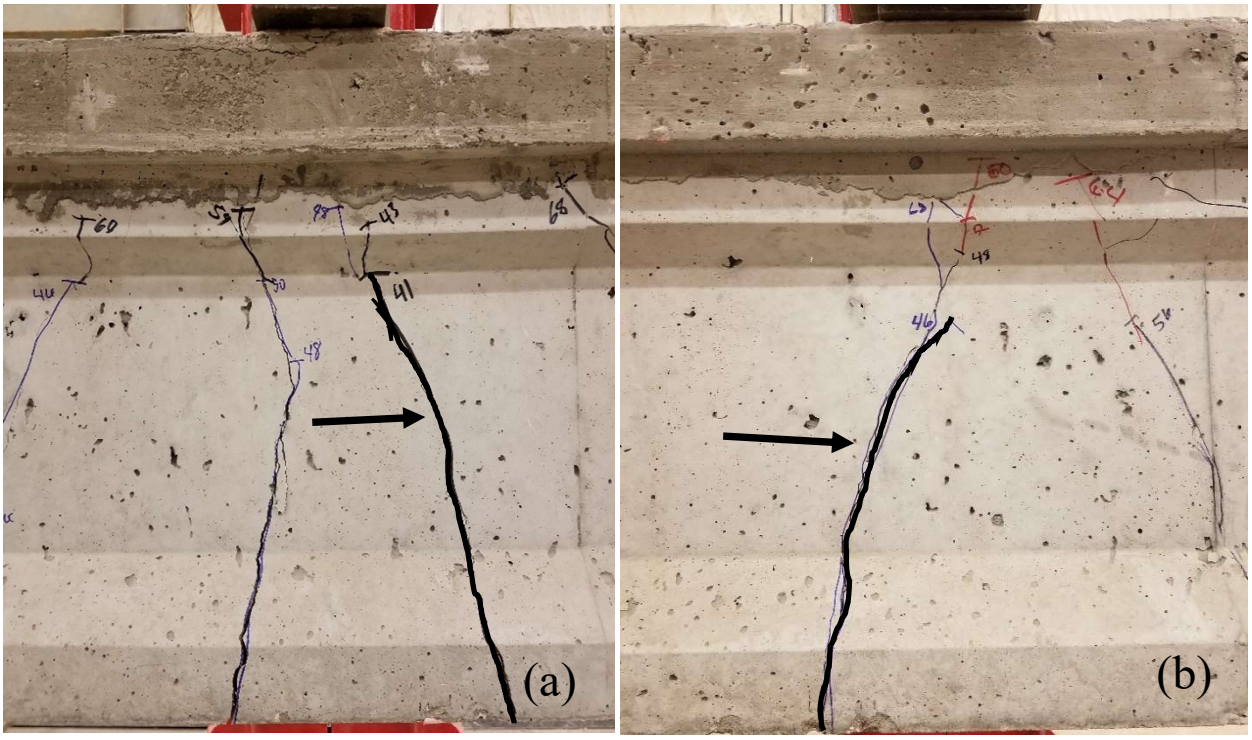

Figure 75. Initial flexural cracking under the load point on the NC3-N girder at 41 kips of load (a) and initial flexural cracking under the load point on the NC3-S girder at 46 kips of load (b). Arrows point to the dark lines that indicate the initial flexural cracks.

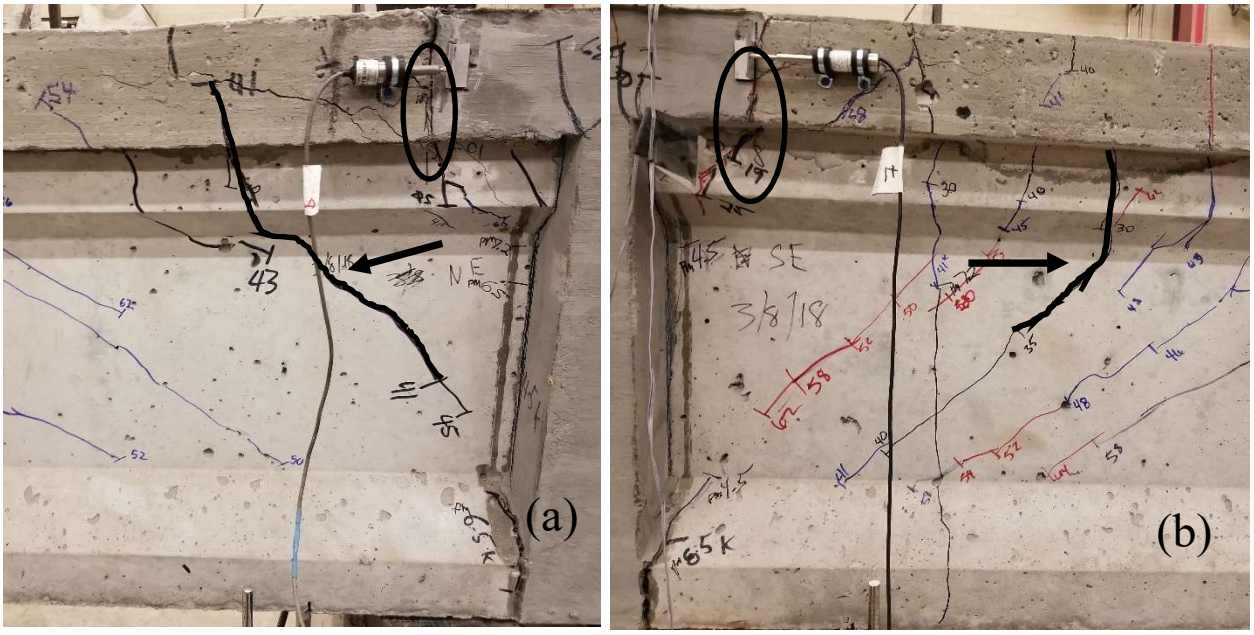

Figure 76. Initial flexural cracking on the NC3-N girder at 25 kips of load and initial flexure-shear cracking on the NC3-N girder at 41 kips of load (a) and initial flexural cracking on the NC3-S girder at 19 kips of load and flexure-shear cracking on the NC3-S girder at 35 kips of load (b). Dark circles show the initial flexural cracking near the continuity joint and arrows point to the dark lines that indicate the initial flexural shear cracking.

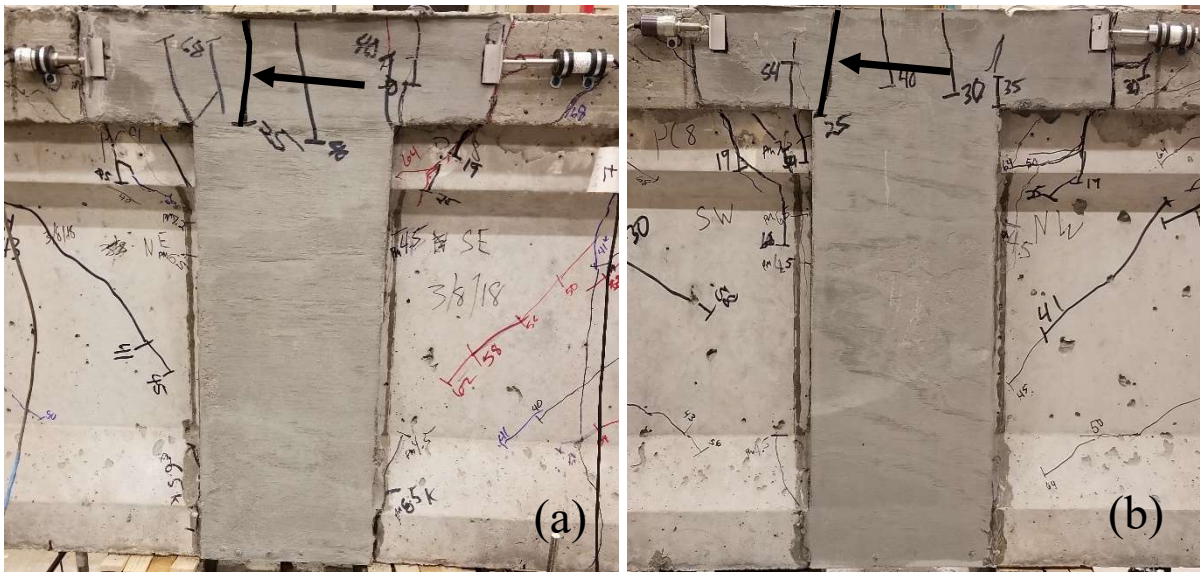

Figure 77. Initial continuity joint flexural cracking on the west face (a) and east face (b) at 25 kips of load. Arrows point to the dark lines that indicate the initial flexural cracks.

Cracks that developed between initial cracking and final failure included additional flexural cracks under the point load, flexure-shear cracks near the joint interface, web shear cracks near the point load, and flexural cracks in the UHPC joint. Most of the cracks observed on the NC3 specimen at final failure were flexure-shear and web shear cracks. These cracks developed as the load increased and the flexure-shear cracks propagated away from the joint interface toward the load point. At approximately halfway to the load point from the joint, web shear cracks developed in place of the flexure-shear cracks. Figure 78 shows the flexural cracks and shear cracks between the joint interface and load point for the NC3-N and NC3-S girders at failure.

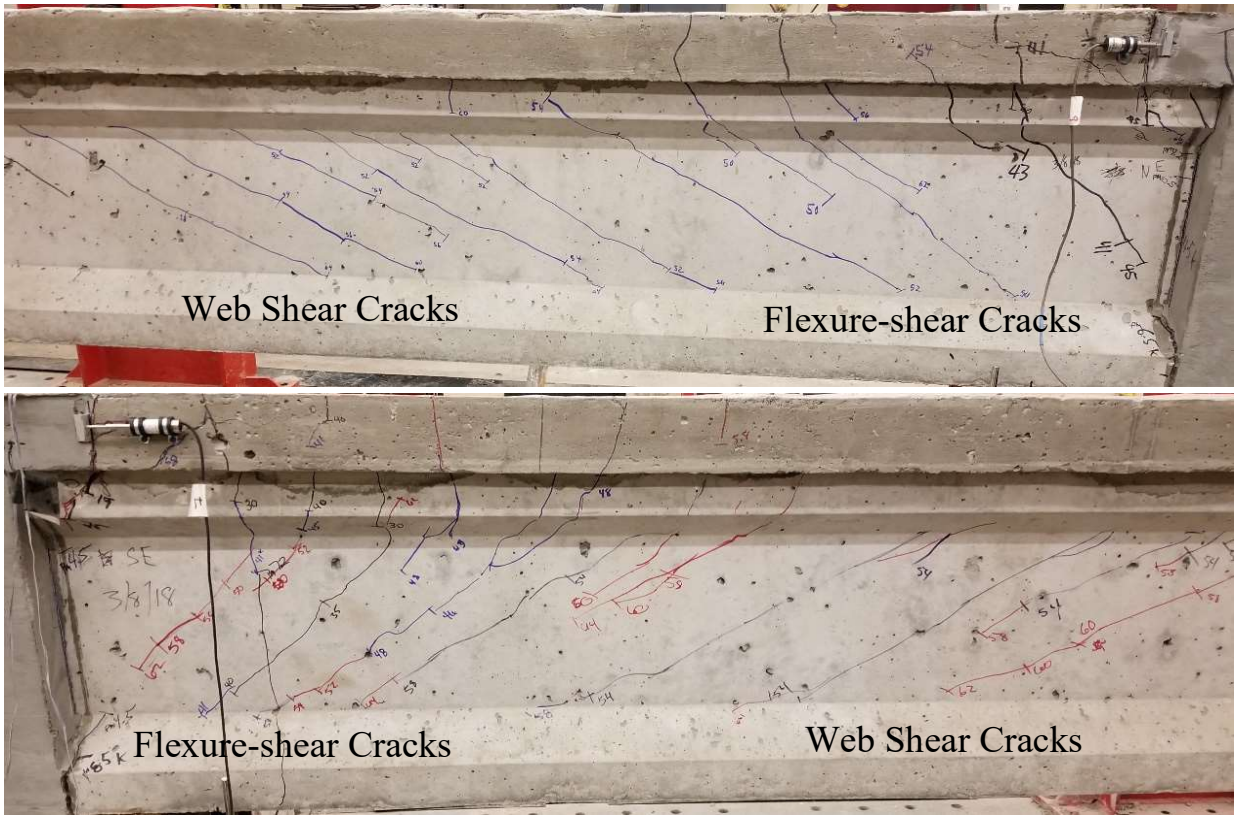

Figure 78. NC3-N girder with flexure-shear and shear cracks top and NC3-S girder with flexure-shear and shear cracks (bottom).

Loading of the specimen was stopped upon reaching an applied load of 69.8 kips on the NC3-N girder and 70.2 kips on the NC3-S girder. Under these loading conditions the concrete deck began to crush at the load point on the NC3-N girder, as shown by the dark circle in Figure 79. There was no visual concrete crushing in the NC3-S girder. In addition, there was significant widening of the flexural cracks under both load points, as shown by dark lines in Figure 79. These conditions were taken to indicate flexural failure of the beam specimens and testing was concluded to prevent the prestressing strands from rupturing and causing damage to the testing apparatus.

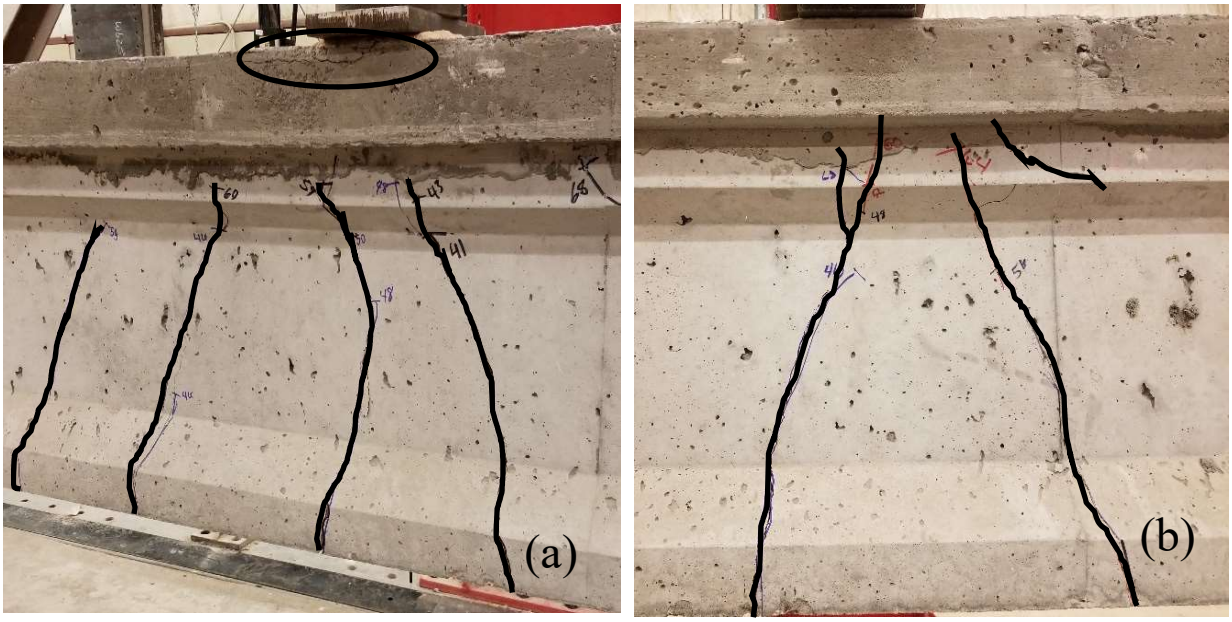

Figure 79. Crushed concrete deck in the NC3-N girder is indicated by a black oval (a) and the final flexural cracking under the load point in the NC3-N (a) and NC3-S (b) girders are indicated by dark lines.

The interface between the NC3-N girder and the UHPC joint had preexisting flexural cracking from the positive moment test, shown in Figure 74a. Flexural cracking occurred along the top portion of the joint interface that extended into the preexisting crack during the final load test. This resulted in separation of the girder from the joint, as shown by the dark lines in Figure 80a.

The same type of flexural cracking occurred at the NC3-S girder and UHPC joint interface, as shown by the dark lines in Figure 80b.

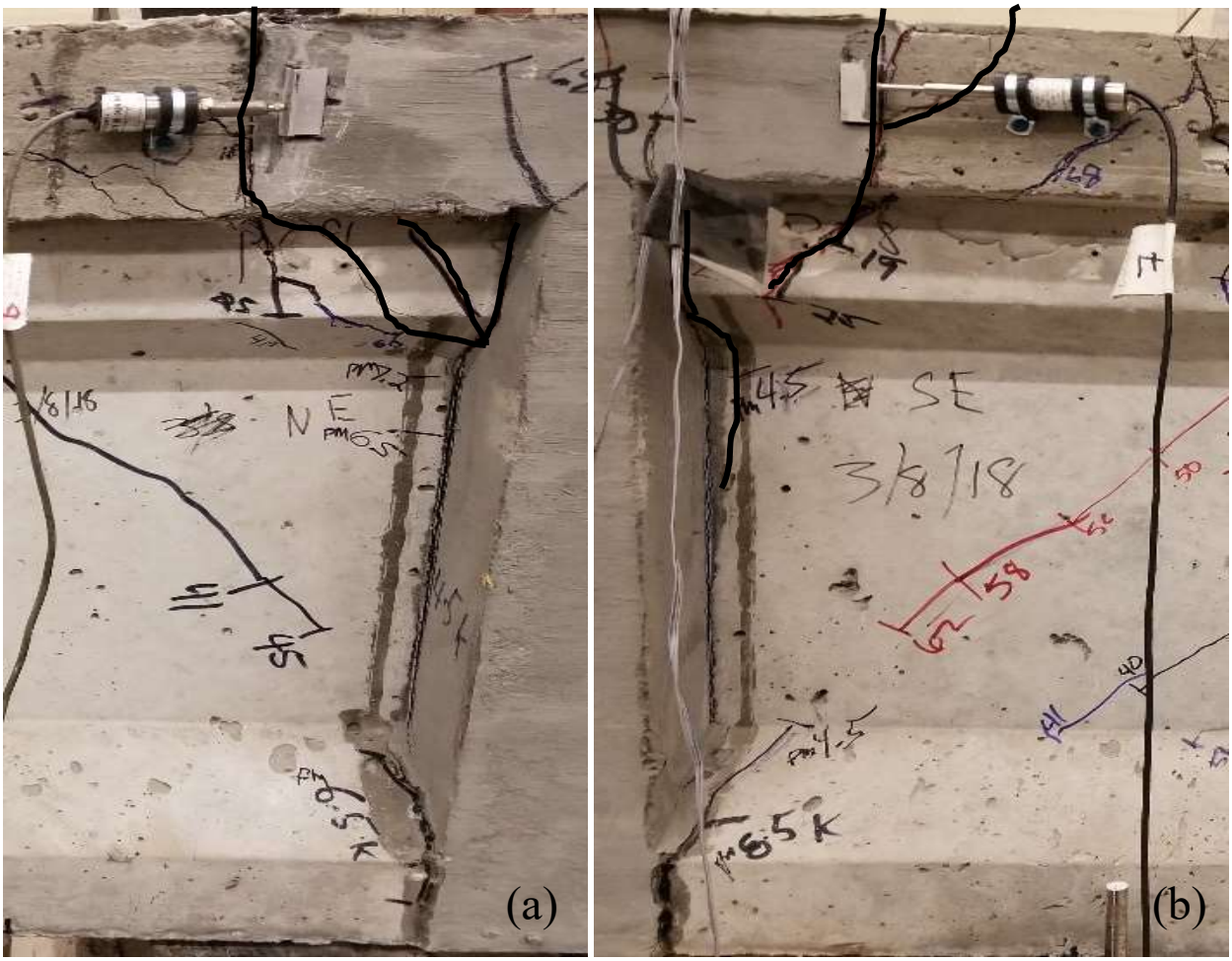

Figure 80. Joint separation at the interface between the NC3-N girder and the UHPC joint (a) and separation at the interface between the NC3-S girder and the UHPC joint (b) are indicated by dark lines.

Figure 81 shows the load-deflection curve for the NC3-N girder. The curve shows a reduction in stiffness that corresponds with the initial flexural and flexure-shear cracking observed at 41 kips. Initial cracking of the UHPC joint did not reduce the stiffness of the girder. This indicates ductile behavior of the NC2-N prestressed girder during loading up to the ultimate load of 69.8 kips. In

addition, the plateau of the load-deflection curve out to 2 inches of deflection also indicated the prestressing strands were yielding. Figure 82 shows the load-deflection curve for the NC3-S girder. The NC3-N and NC3-S girders exhibited the same ductile behavior, but with the NC3-N girder having more than one inch more deflection at mid-span than NC3-S. The varying deflection of the girders can be related to differences in the concrete mix, compressive strength, modulus of elasticity, and a difference in prestress loss between the girders. These variables could have caused the NC3-N girder to crack in flexure 5 kips earlier in load than the NC3-S girder and could have resulted in the NC3-N girder having a reduced stiffness compared to the NC3-S girder. This led to a larger downward curvature, which created more strain in the prestressing strands, and led to larger deflection in the NC3-N girder.

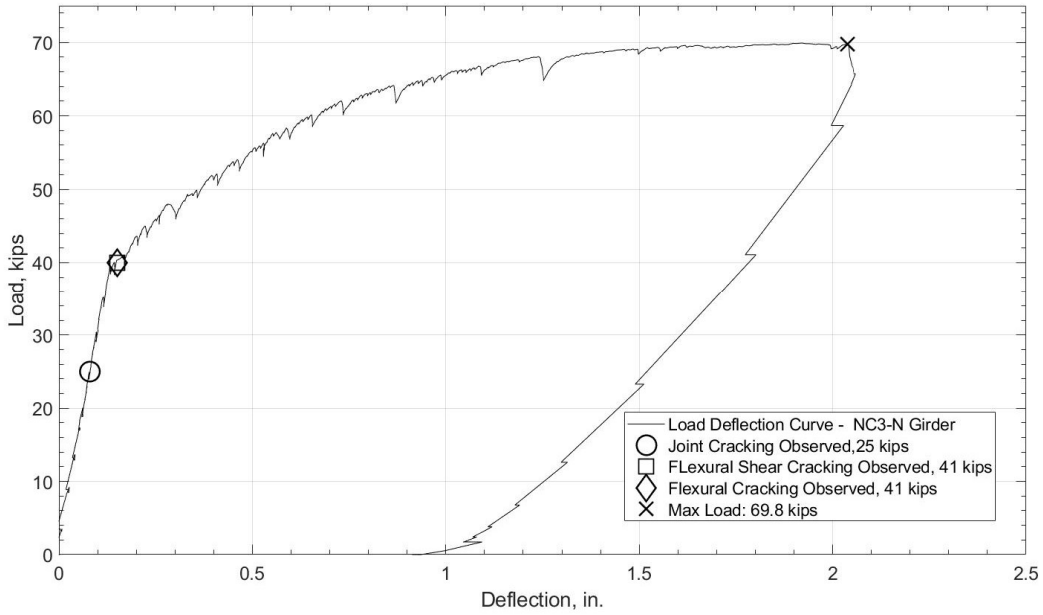

Figure 81. Load-deflection curve for the NC3-N girder.

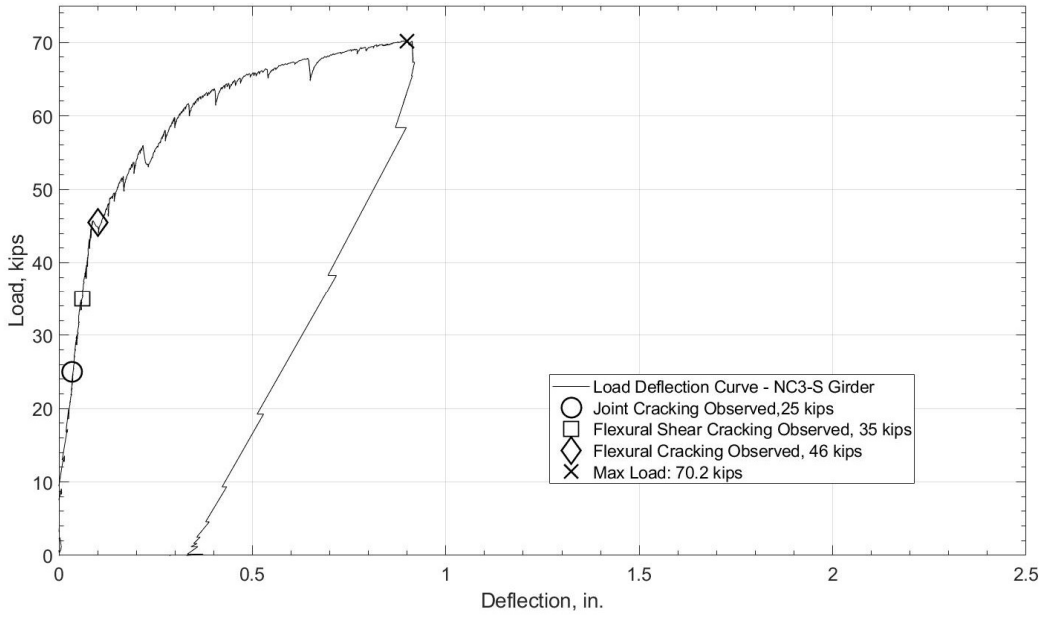

Figure 82. Load-deflection curve for the NC3-S girder.

Figure 83 shows the load-joint separation curve between the NC3-N girder's concrete deck and the UHPC joint. The results from the LVDTs on the east and west face of the concrete deck were averaged to provide a better representation of the joint separation. Figure 48 shows the location of the LVDTs on the joint interface, which were located 2 inches below the top of the deck. The deck joint had minor separation until reaching the 60 kip load mark. As the girder cracked in flexure, the reduction of girder stiffness appeared to have no effect on the rate of joint seperation. The joint began to separate after the 60 kip mark more significnly because the girder began to have more downward curvature, creating a hinge at the weak point; that is the joint interface. Figure 84 shows the load-joint separation curve between the NC3-S girder's concrete deck and the UHPC joint. This figure only presents data from LVDT11 on the west face of the deck. The NC3-N and NC3-S curves closely match one another in behavior expect the NC3-S speration curve shows less seperation occuring. This is most likely due to the NC3-S girder having less

deflection at the mid span of the girder, and the NC3-N girder having more resulting in more joint separation at the NC3-N girder to deck joint interface.

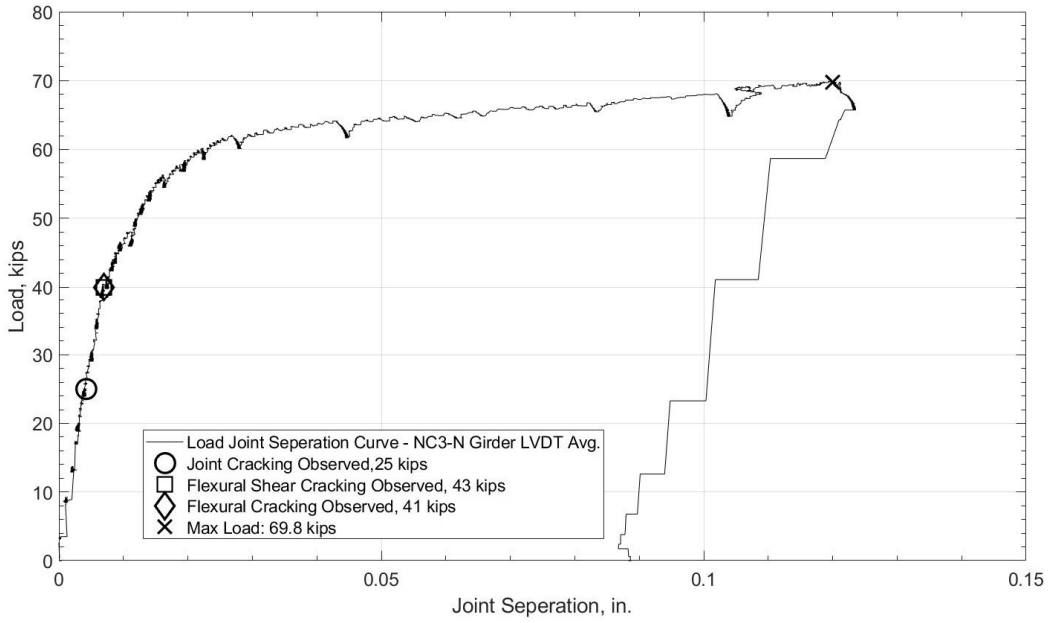

Figure 83. Load-joint separation curve at the NC3-N girder deck to UHPC joint interface.

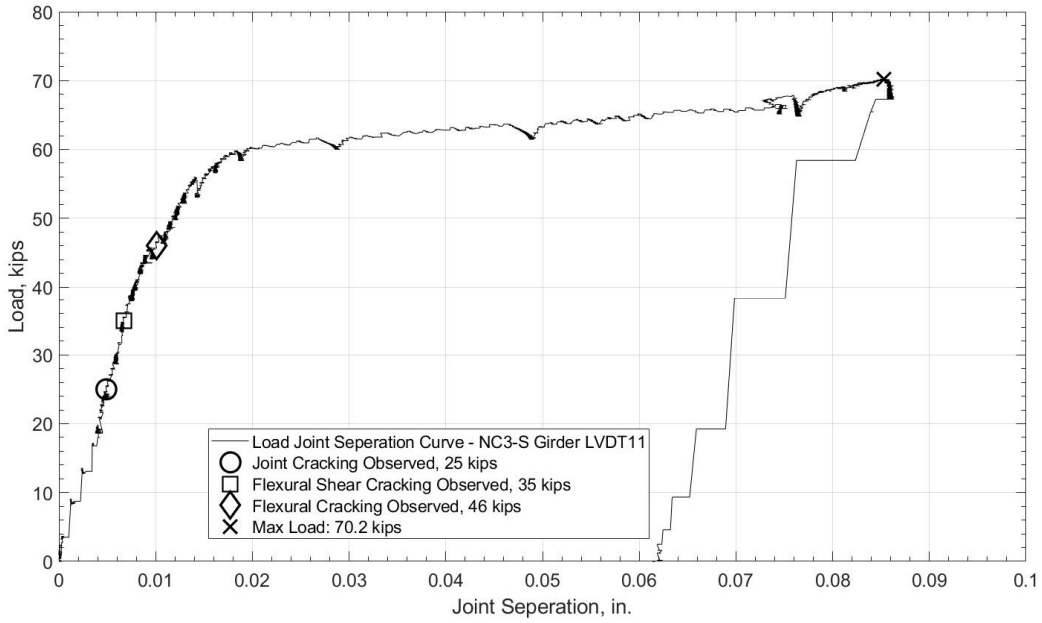

Figure 84. Load-joint separation curve at the NC3-S girder deck to UHPC joint interface.

Overall, the NC3 specimen performed quite well considering the additional positive moment test done to the specimen before the negative moment test was performed. The load-deflection graphs, and the load-joint separation graphs of the NC3 compared quite well to the NC1 and NC2 graphs.

4.3 Retrofit Constructed Specimens

The primary focus of testing the RC specimens was to get a better understanding of how a joint cast to retrofit an existing simply support bridge for live load continuity would perform under loading causing negative moment at the joint. To characterize the performance and behavior of this joint configuration, initial cracking for each region on the specimen, cracking occurring at ultimate load, the load-deflection curves for each girder in the specimen, and the load-joint

separation curves for each joint interface are presented for each RC specimen. The order in which the specimens are presented is the order testing occurred.

4.3.1 Test RC1

Initial flexural cracking was observed near the joint interface on the RC1-N and RC1-S girders at a load of 20 kips, indicated in Figure 86 with dark ovals. An initial flexure-shear crack was observed after the next loading increment near the joint interface on the RC1-S specimen at a load of 25 kips, shown in Figure 86b. A similar flexure-shear crack to that which had developed on the RC-S girder was observed on the RC1-N girder at a load of 30 kips, shown in Figure 86a. A flexural crack was observed directly under the load point on RC1-S girder at a load of 45 kips, shown in Figure 85b. During the following load increment a flexural crack developed directly under the load point on the RC1-N girder, shown in Figure 85a. The first flexural crack observed in the continuity joint occurred on the east face at a load of 60 kips, shown in Figure 87a. On the next load increment a flexural crack developed on the west face of the joint at a load of 62 kips, shown in Figure 87b.

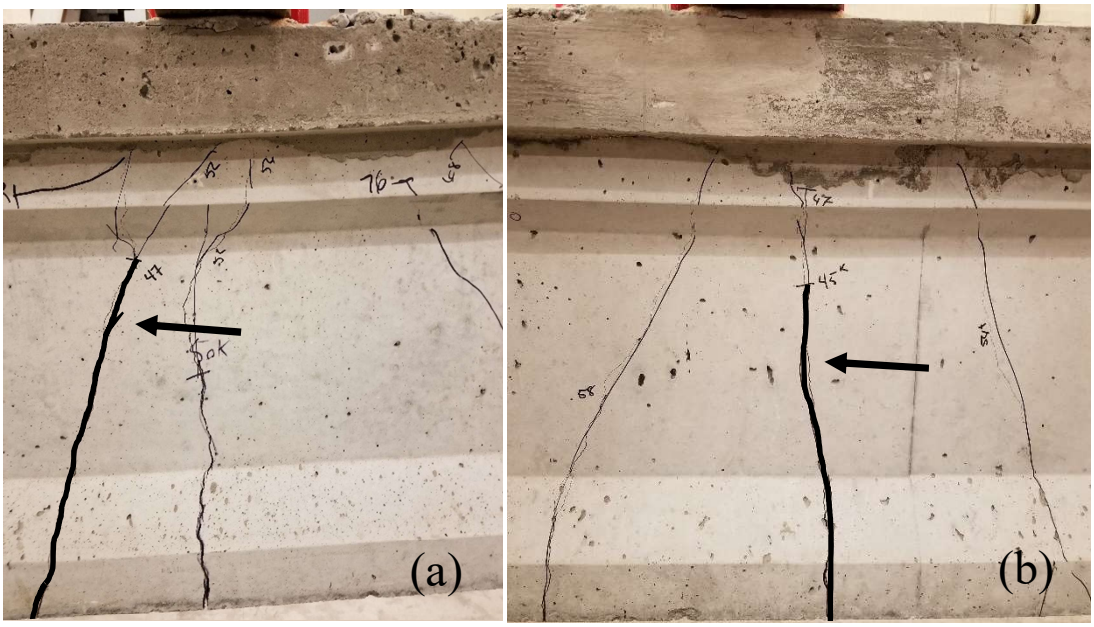

Figure 85. Initial flexural cracking under the load point on the NC2-N girder at 47 kips of load (a) and initial flexural cracking under the load point on the NC2-S girder at 45 kips of load (b). Arrows point to the dark lines that indicate the initial flexural cracks.

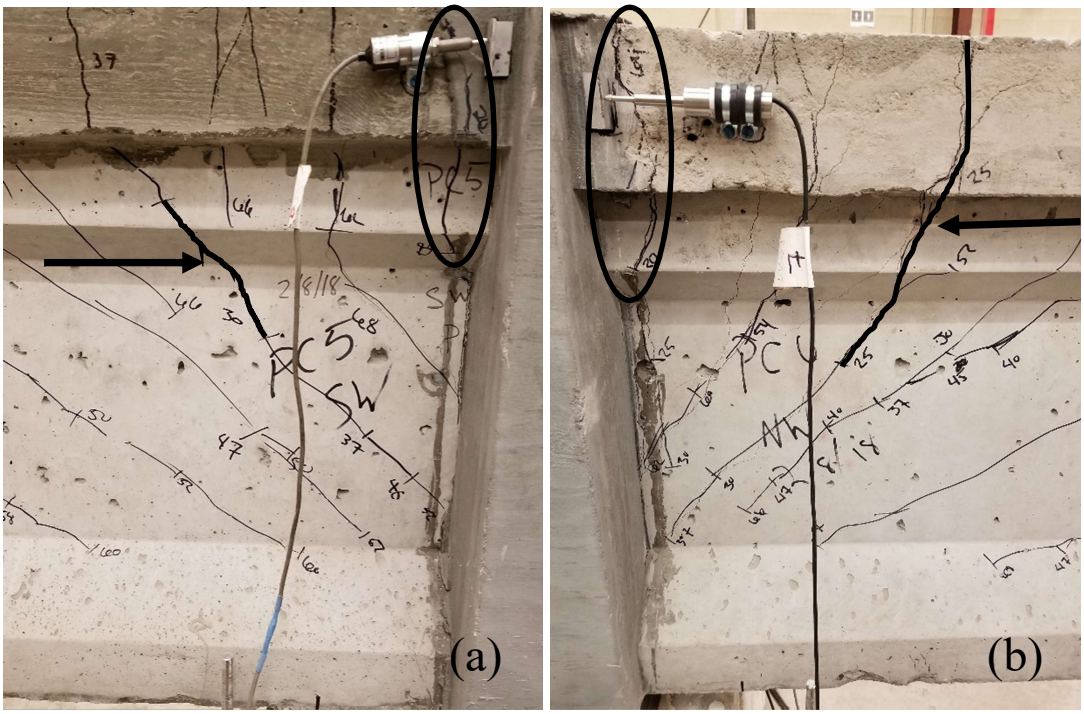

Figure 86. Initial flexural cracking on the NC1-N girder at 25 kips of load and initial flexure-shear cracking on the NC1-N girder at 41 kips of load (a) and initial flexural cracking on the NC1-S girder at 19 kips of load and flexure-shear cracking on the NC1-S girder at 35 kips of load (b). Dark ovals show the initial flexural cracking near the continuity joint, and arrows point to the dark lines that indicate the initial flexure-shear cracking.

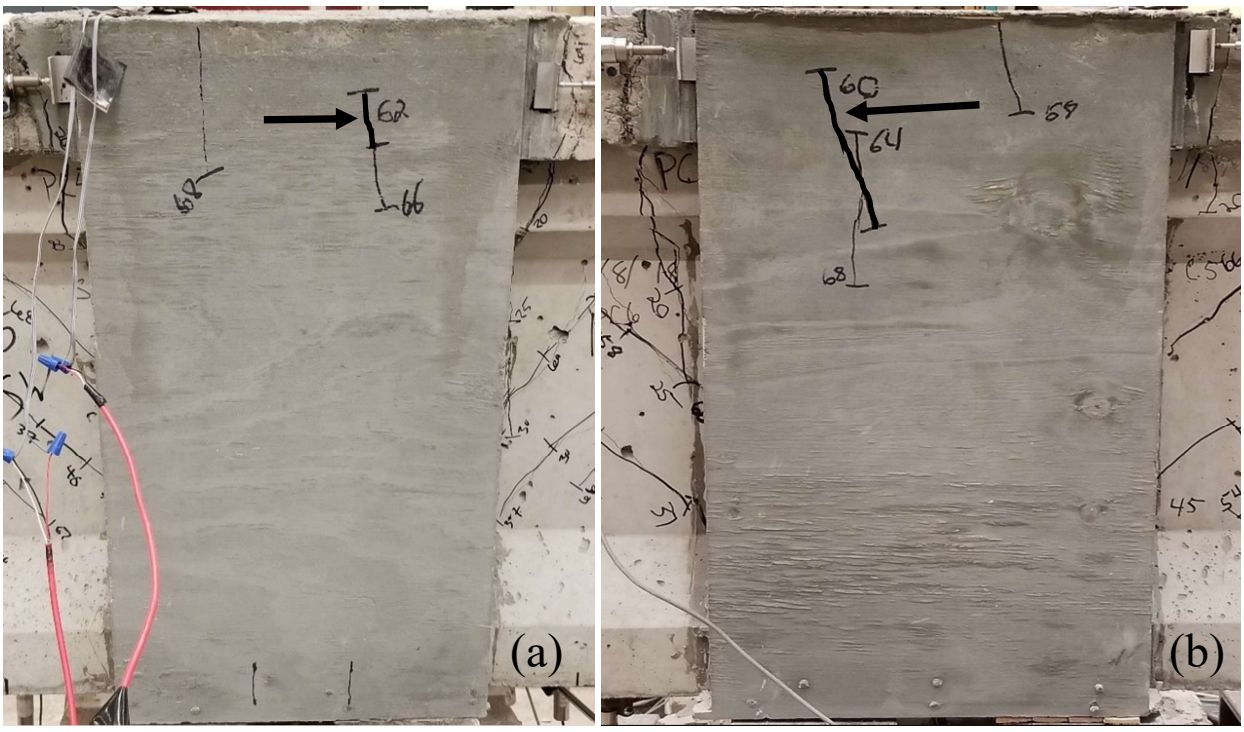

Figure 87. Initial continuity joint flexural cracking on the east face at a load of 62 kips (a) and initial continuity joint flexural cracking on the west face at a load of 60 kips (b). Arrows point to the dark lines that indicate the initial flexure cracks

Cracks that developed between initial cracking and final failure included additional flexural cracks under the point load, flexure-shear cracks near the joint interface, web shear cracks near the point load, and flexural cracks in the UHPC joint. The majority of cracks that occurred between initial cracking and failure were flexure-shear and web shear cracks for the RC1 specimen. These cracks developed as the load increased and the flexure-shear cracks began to move away from the joint interface towards the load point. Upon reaching approximately halfway to the load point from the joint, web shear cracks developed in place of the flexure-shear cracks. Figure 88 shows the flexural cracks and web shear cracks between the joint interface and load point for the RC1-N and RC1-S girders.

Figure 88. RC1-N girder with flexure-shear cracks and web shear cracks at failure (top) and RC1-S girder with flexure-shear cracks and web shear cracks at failure (bottom).

Loading of the specimen was stopped upon reaching an applied load of 76 kips on the RC1-N girder and 75.9 kips on the RC1-S girder. Under these loading conditions the concrete deck began to crush at the load point in both girders, as shown by the dark circles and arrows in Figure 89. In addition, there was significant widening of the flexural cracks under both loads points, as shown by dark lines and arrows in Figure 89. These conditions were taken to indicate flexural failure of the beam specimens and testing was concluded to prevent the prestressing strands from rupturing and causing damage to the testing apparatus.

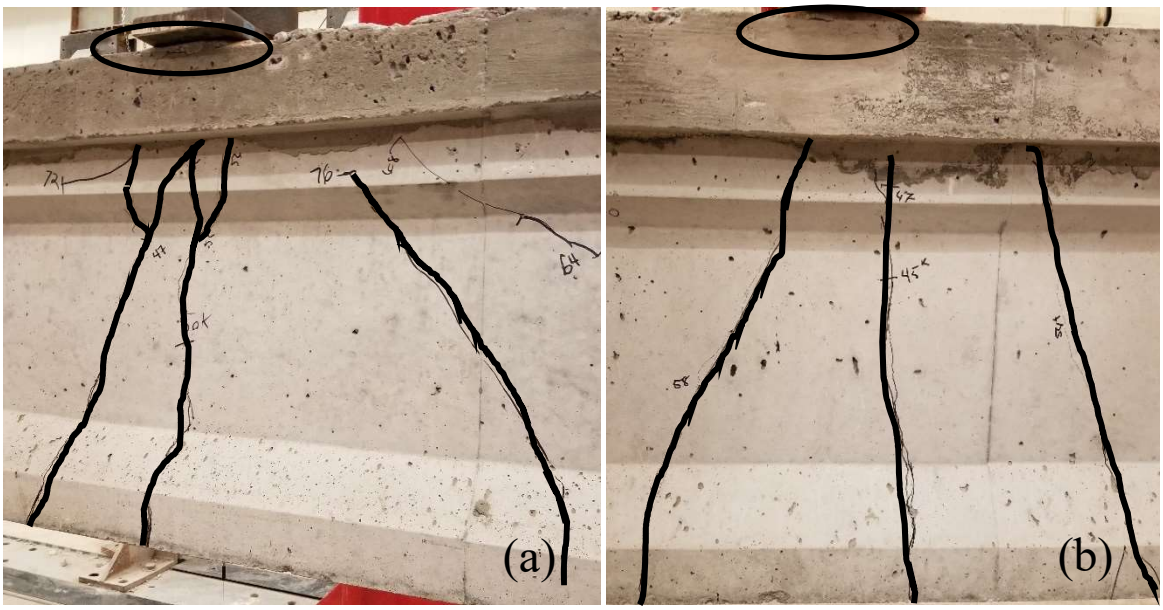

Figure 89. Crushed deck concrete in the RC1-N (a) and RC1-S (b) girders is indicated by a black oval, and the final flexural cracking under the load point in the RC1-N (a) and RC1-S (b) girders is indicated by dark lines.

Flexural cracking occurred at the interface between the RC1-N girder deck and the UHPC joint, which resulted in separation of the deck from the joint. However, the flexural crack from the concrete deck joint interface continued vertically down into the RC1-N girder's flange and then into the web before diverting back towards the joint interface, as shown in Figure 90a. The interface between the RC1-S girder and the UHPC joint exhibited similar flexural cracking to the RC1-N girder and joint interface, as shown in Figure 90b.

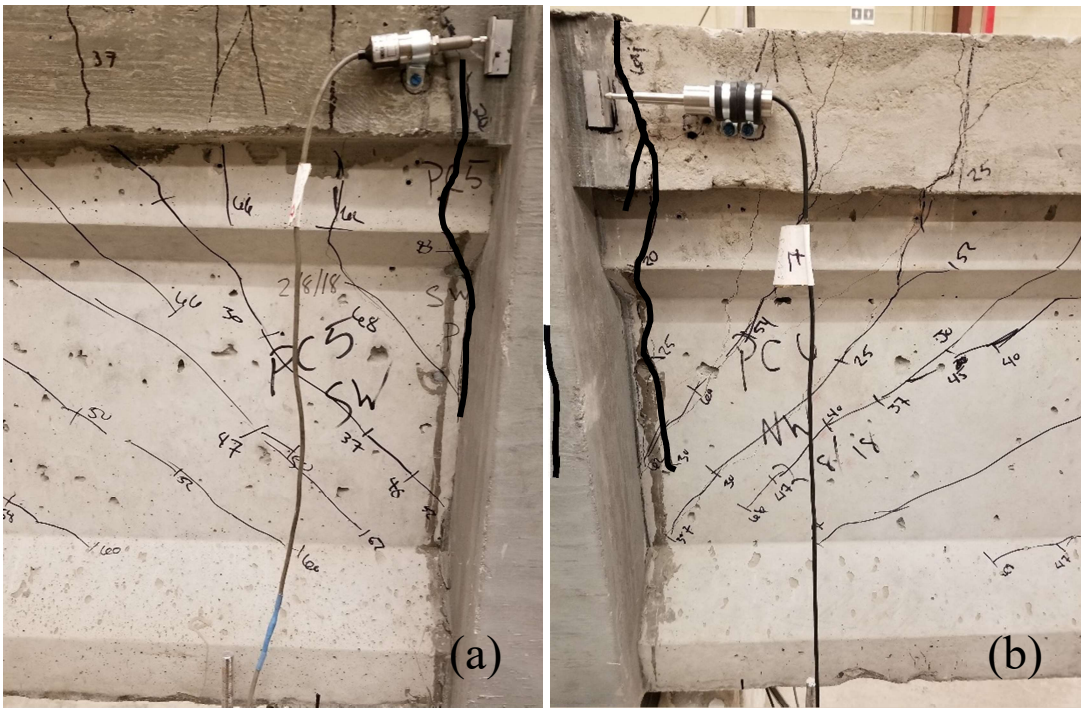

Figure 90. Joint separation at the interface between the RC1-N concrete deck and the UHPC joint with the flexural crack going vertically down in the girder (a) and joint separation at the interface between the RC1-S concrete deck and the UHPC joint with the flexural crack going vertically down in the girder (b) are indicated by dark lines.

Figure 91 shows the load-deflection curve for the RC1-N girder. The curve shows a reduction in stiffness that corresponds with the initial flexural cracking observed at 47 kips. Other types of initial cracking did not reduce the stiffness of the girder. The load-deflection curve indicates a ductile behavior of the RC1-N prestressed girder during loading up to the ultimate load of 76 kips. The plateau of the load-deflection curve out to 1.5 inches of deflection also indicated the prestressing strands were yielding. Figure 92 shows the load-deflection curve for the RC1-S girder. The RC1-N and RC1-S girders had the same ductile behavior, but with the RC1-S girder having less deflection at mid-span. The varying deflection of the girders can be related to potential differences in the concrete mix, compressive strength, modulus of elasticity, and in prestress loss between the girders. These variables could have resulted in the RC1-N girder

having a reduced stiffness compared to the RC1-S girder. This reduced stiffness led to a larger downward curvature, which created more strain in the prestressing strands, and led to larger deflection in the RC1-N girder.

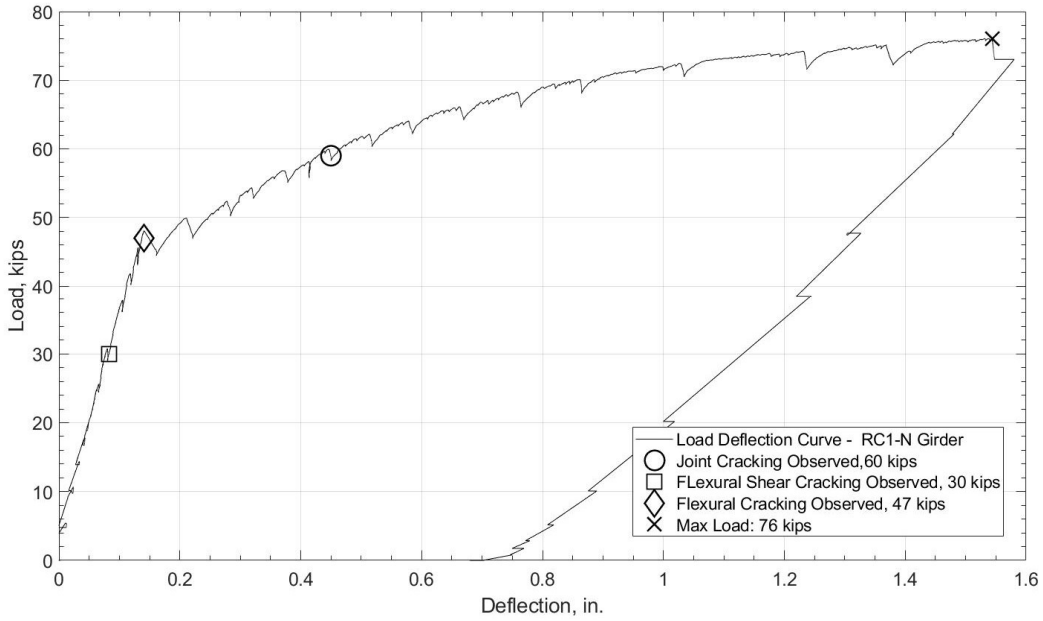

Figure 91. Load-deflection curve for the RC1-N girder.

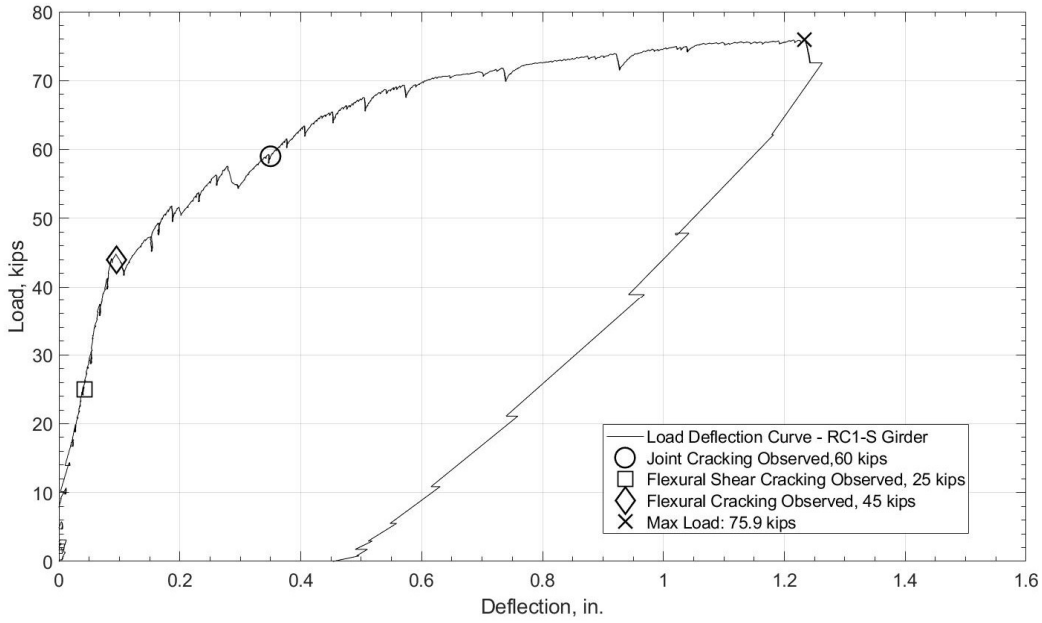

Figure 92. Load-deflection curve for the RC1-S girder.

Figure 93 shows the load-joint separation curve between the RC2-N girder's concrete deck and the UHPC joint. The average of the readings from the LVDTs on the east and west face of the concrete deck was taken to get a better representation of the joint separation. Figure 48 shows the location of the LVDTs on the joint interface which were located 2 inches below the top of the deck. The deck joint had minor separation until reaching the initial flexural cracking of 47 kips. After the 47 kip load, indicated by a diamond shape on Figure 93, the joint separation began to increase significantly with each load increment. This makes sense because major joint separation could only occur after the girder cracked due to flexure, resulting in a less stiff member and creating a hinge at the weak point being the joint interface. The LVDTs on the RC2-S girder's concrete deck did not collect reliable data and the measurements from these instruments were excluded from this section.

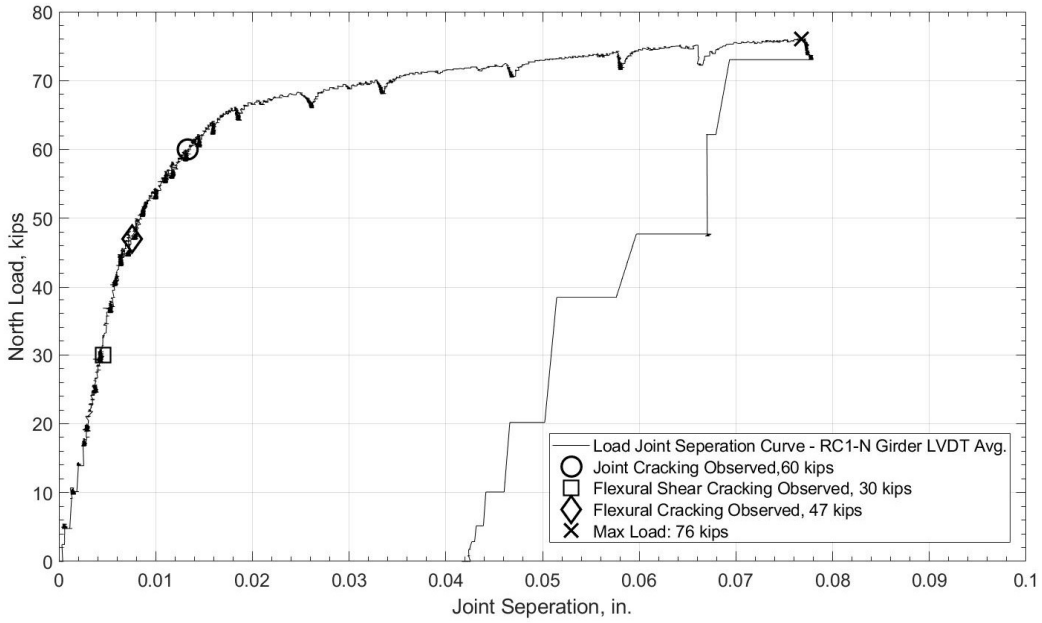

Figure 93. Load joint separation curve at the RC1-N girder deck to UHPC joint interface.

4.3.2 Test RC2

Initial flexural cracking was observed near the joint interface on the RC1-S girder at a load of 19.5 kips, indicated in Figure 95b by a dark oval. Asymmetrical flexural cracks were observed on the continuity joint after the next load increment, at a load of 25 kips, as shown in Figure 96. In addition, two more cracks had developed at 25 kips of load, a flexural crack near the joint interface on the RC2-N girder, indicated in Figure 95a by a dark oval, and a flexure-shear crack near the joint interface on the RC2-S girder, shown in Figure 95b. At the next load increment a flexure-shear crack developed on the RC2-N girder, shown in Figure 94a. Flexural cracking directly under the load point was observed on the RC2-N and RC2-S girders at a load of 44 kips, shown in Figure 94.

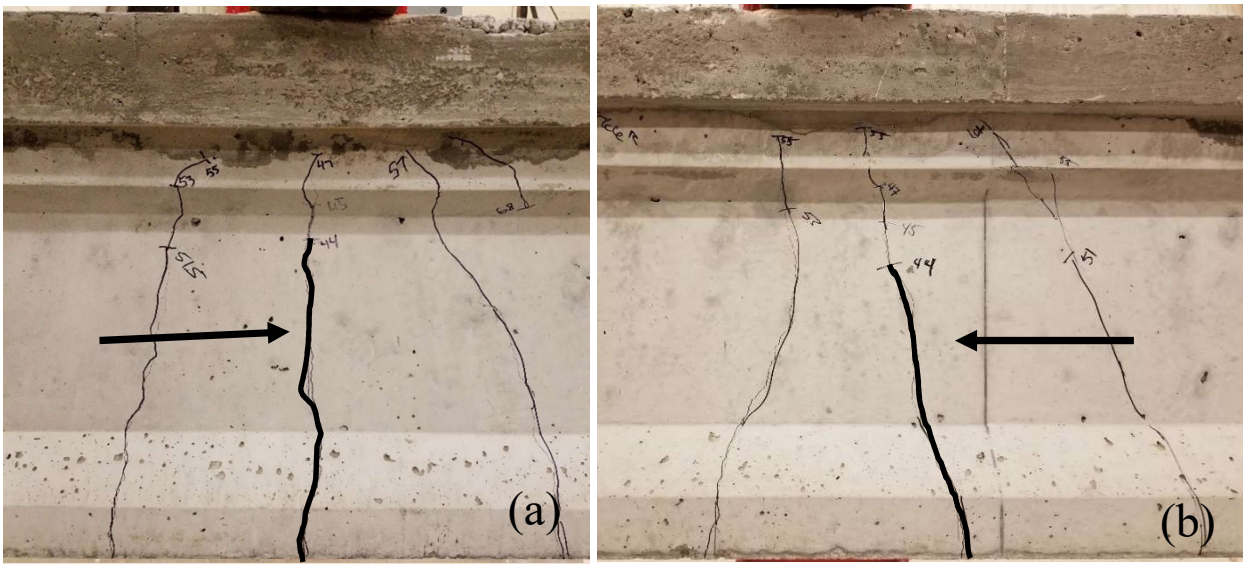

Figure 94. Initial flexural cracking under the load point on the RC2-N girder at 44 kips of load (a) and initial flexural cracking under the load point on the RC2-S girder at 44 kips of load (b). Arrows point to the dark lines that indicate the initial flexural cracks.

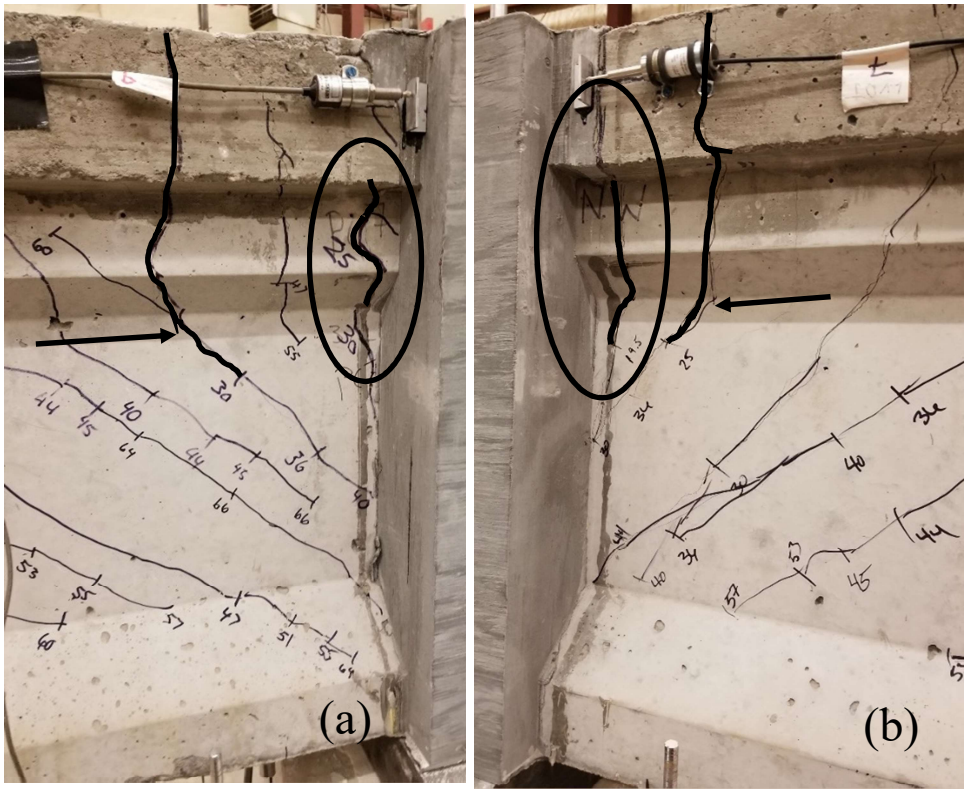

Figure 95. Initial flexural cracking on the RC2-N girder at 25 kips of load and initial flexure-shear cracking on the RC2-N girder at 30 kips of load (a) and initial flexural cracking on the RC2-S girder at 19.5 kips of load and flexure-shear cracking on the RC2-S girder at 25 kips of load (b). Dark ovals show the initial flexural cracking near the continuity joint and arrows point to the dark lines that indicate the initial flexure-shear cracking.

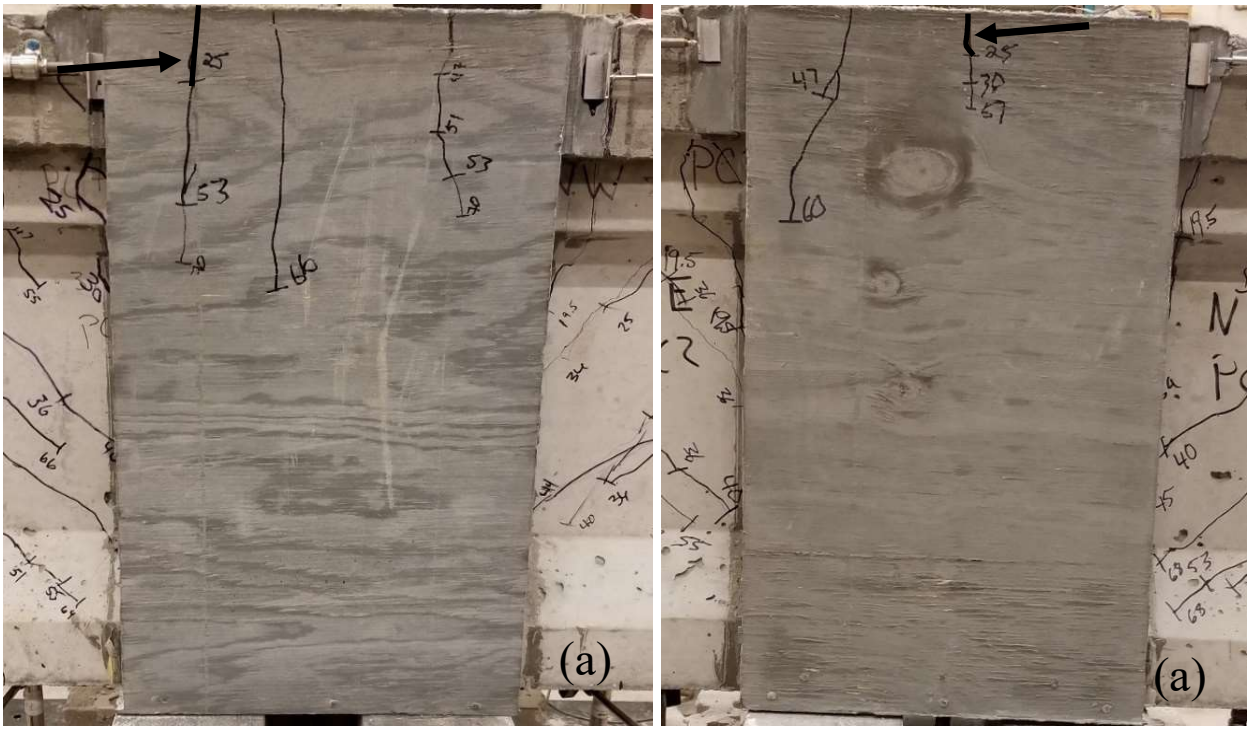

Figure 96. Initial continuity joint flexural cracking on the east face (a) and west face (b) at 25 kips of load. Arrows point to the dark lines that indicate the initial flexural cracks.

Cracking that developed between initial cracking and final failure included additional flexural cracks under the point load, flexure-shear cracks near the joint interface, web shear cracks near the point load, and flexural cracks in the UHPC joint. Most of the cracks that occurred in the RC2 specimen between initial cracking and failure were flexure-shear and shear cracks. These cracks developed as the load increased and the flexure-shear cracks began to move away from the joint interface toward the load point. Approximately halfway to the load point from the joint web shear cracks developed in place of flexure-shear cracks. Figure 97 shows the flexural cracks and shear cracks between the joint interface and load point for the RC2-N and RC2-S girders.

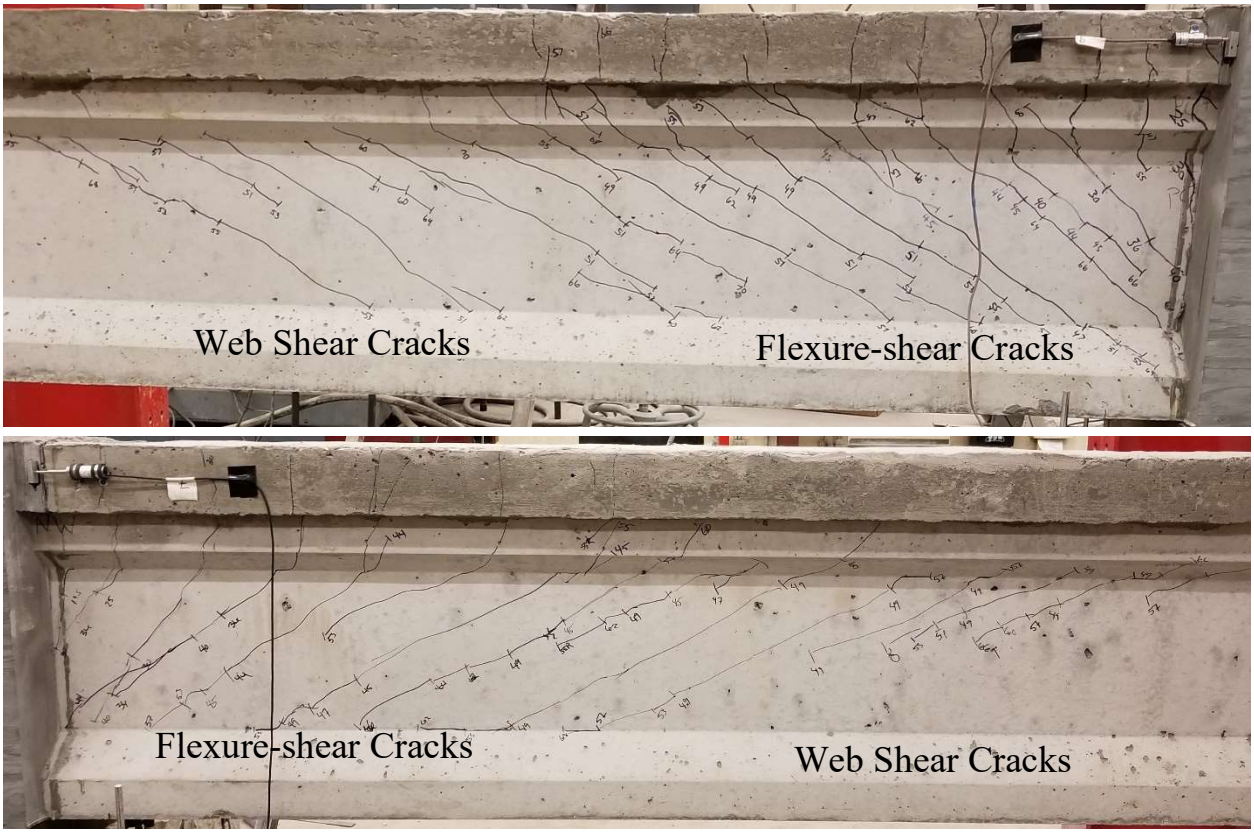

Figure 97. RC2-N girder with flexure-shear cracks and shear cracks (top) and RC2-S girder with flexure-shear cracks and shear cracks (bottom).

Loading of the specimen was stopped upon reaching an applied load of 74.1 kips on the NC2-N girder and 74.2 kips on the NC2-S girder. Under these loading conditions the concrete deck began to crush at the load point in both girders. This is not clear in Figure 98 due to the crushing not being significant on the east face. In addition, there was significant widening of the flexural cracks under both load points, as shown by dark lines in Figure 98. These conditions were taken to indicate flexural failure of the beam specimens and testing was concluded to prevent the prestressing strands from rupturing and causing damage to the testing apparatus.

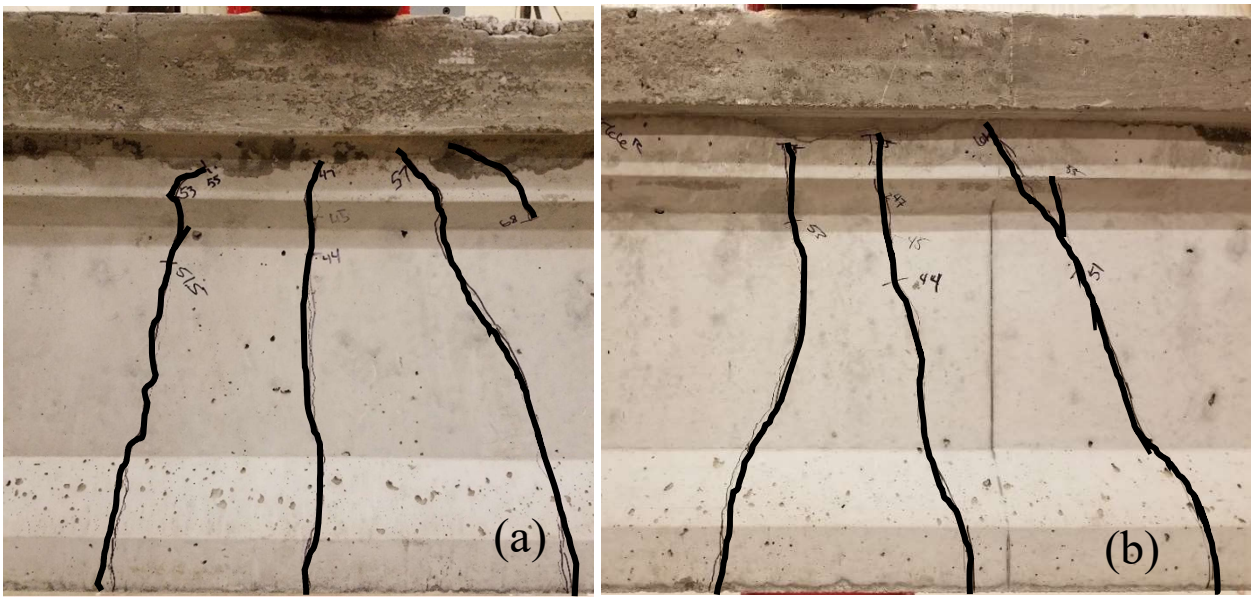

Figure 98. Final flexural cracking under the load point in the RC2-N (a) and RC2-S (b) girders are indicated by dark lines.

Flexural cracking occurred between the RC2-N girder deck and the UHPC joint, which resulted in separation of the deck from the joint. However, the flexural crack from the concrete deck joint interface continued vertically down into the RC2-N girder's flange and then into the web before diverting back towards the joint interface, as shown in Figure 99a. The interface between the RC2-S girder and the UHPC joint had similar flexural cracking to the RC1-N girder and UHPC joint interface, as shown in Figure 99b.

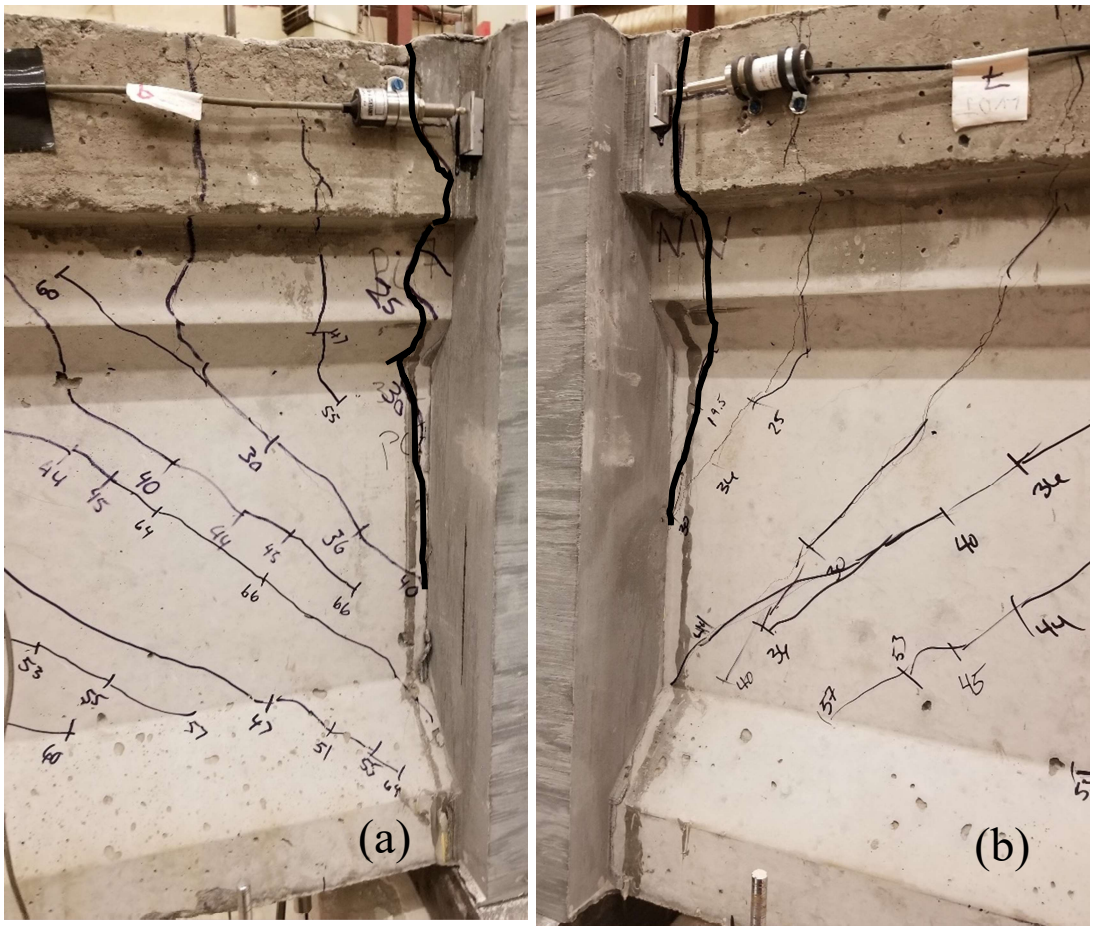

Figure 99. Joint separation at the interface between the RC2-N concrete deck and the UHPC joint with the flexural crack going vertically down in the girder (a) and joint separation at the interface between the RC2-S concrete deck and the UHPC joint with the flexural crack going vertically down in the girder (b) are indicated by dark lines.

Figure 100 shows the load-deflection curve for the RC2-N girder. The curve shows a reduction in stiffness that corresponds with the initial flexural cracking observed at 44 kips. Other types of initial cracking did not reduce the stiffness of the girder. This curve indicates a ductile behavior of the RC2-N prestressed girder during loading up to the ultimate load of 76 kips. In addition, the plateau of the load-deflection curve out to 1.4 inches of deflection also indicated the prestressing strands were yielding. Figure 101 shows the load-deflection curve for the RC2-S girder. The RC1-N and RC1-S girders had similar ductile behavior, but with the RC1-S girder having less

deflection at mid-span. The varying deflection of the girders could be related to differences in the concrete mix, compressive strength, modulus of elasticity, and in prestress loss between the girders. These variables could have resulted in the RC2-N girder having a reduced stiffness compared to the RC2-S girder. The reduced stiffness led to a larger downward curvature, which created more strain in the prestressing strands, and led to larger deflection in the RC2-N girder.

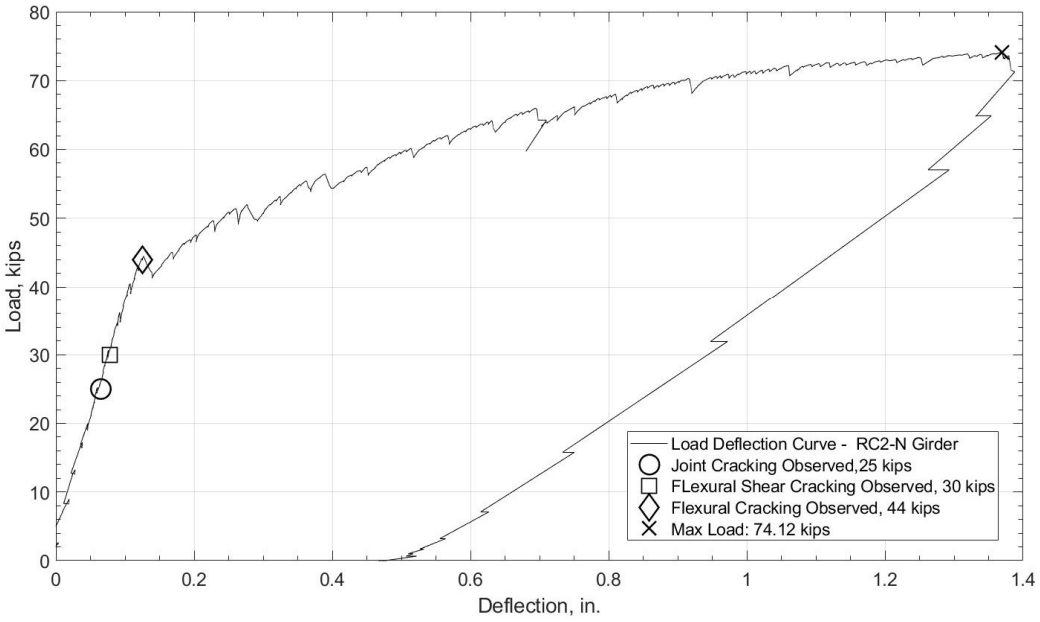

Figure 100. Load-deflection curve for the RC2-N girder.

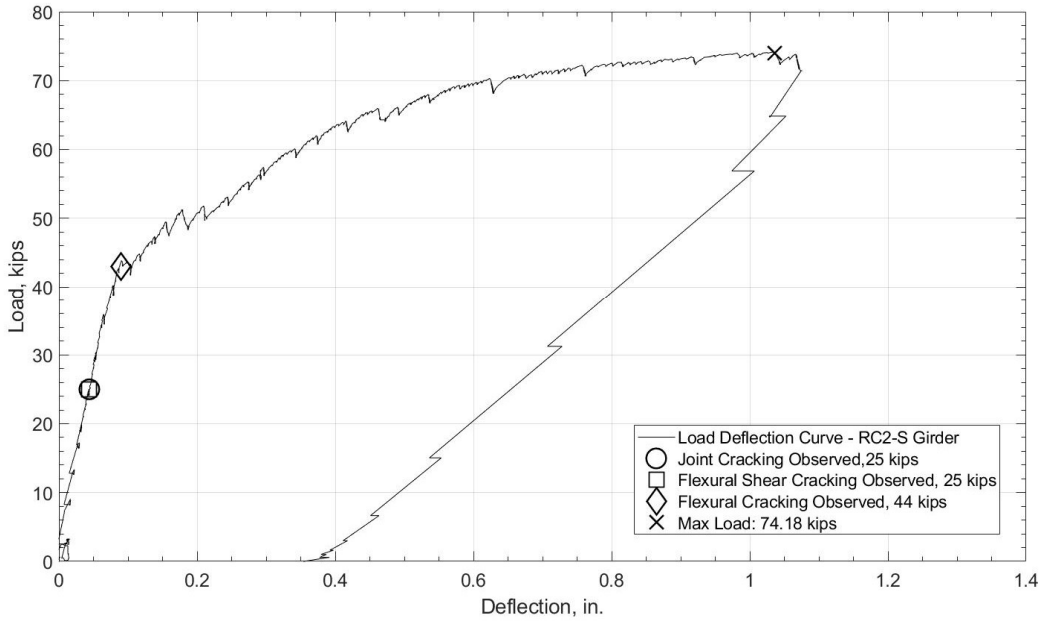

Figure 101. Load-deflection curve for the RC2-S girder.

Figure 102 shows the load-joint separation curve between the RC2-N girder's concrete deck and the UHPC joint. This figure only represents LVDT4 on the wast face of the deck. LVDT9 on the east face did not give accurate data for this test, and was excluded from the results. Figure 48 shows the location of the LVDTs on the joint interface which were located 2 inches below the top of the deck. The deck joint had minor separation until reaching initial flexural cracking at 44 kips of load. After that load, indicated by a diamond shape on Figure 102, the joint separation began to increase significantly with each load increment. This makes sense because major joint separation could only occur after the girder cracked to flexure, resulting in a less stiff member creating a hinge at the weak point being the joint interface. Figure 103 shows the load-joint separation curve between the RC2-S girder's concrete deck and the UHPC joint. This figure only represents LVDT11 on the west face of the deck. This load-joint separation curve shows a similar trend to the RC2-N side of the joint, but with more deflection.

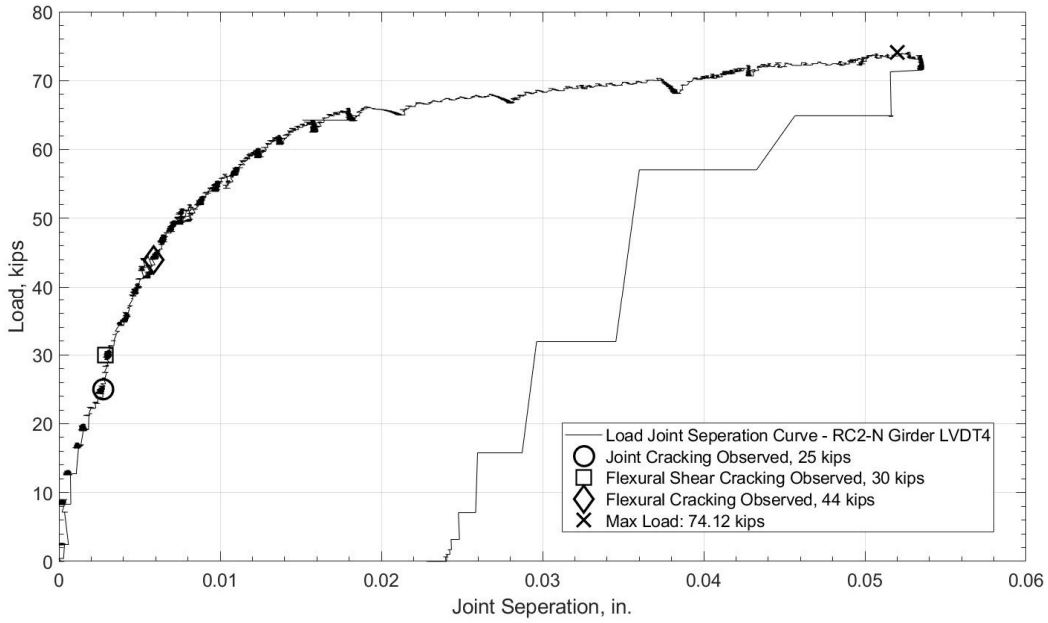

Figure 102. Load-joint separation curve at the RC2-N girder deck to joint interface west face.

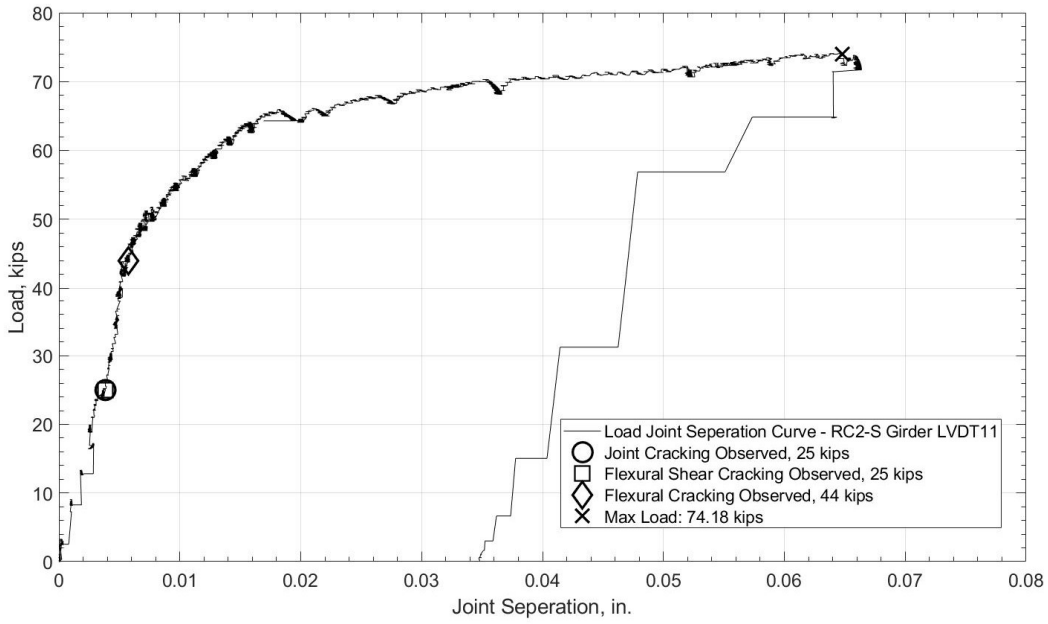

Figure 103. Load-joint separation curve at the RC2-S girder deck to joint interface west face.

4.3.3 RC Positive Moment Test

A positive moment test was conducted on the RC3 specimen, as conducted on the NC3 specimen. Initial flexural cracking was observed along the joint interface at a load of 4 kips, as indicated in Figure 104 with a dark oval. No additional cracks were observed up until this point, however it is possible cracks formed on the girder where the UHPC joint overlaps the girder ends, and the cracks were not visually exposed. In addition, no flexural cracks were observed in the UHPC joint. The positive moment test was concluded after the initial crack was observed to prevent additional damage around the joint interface for the negative moment test.

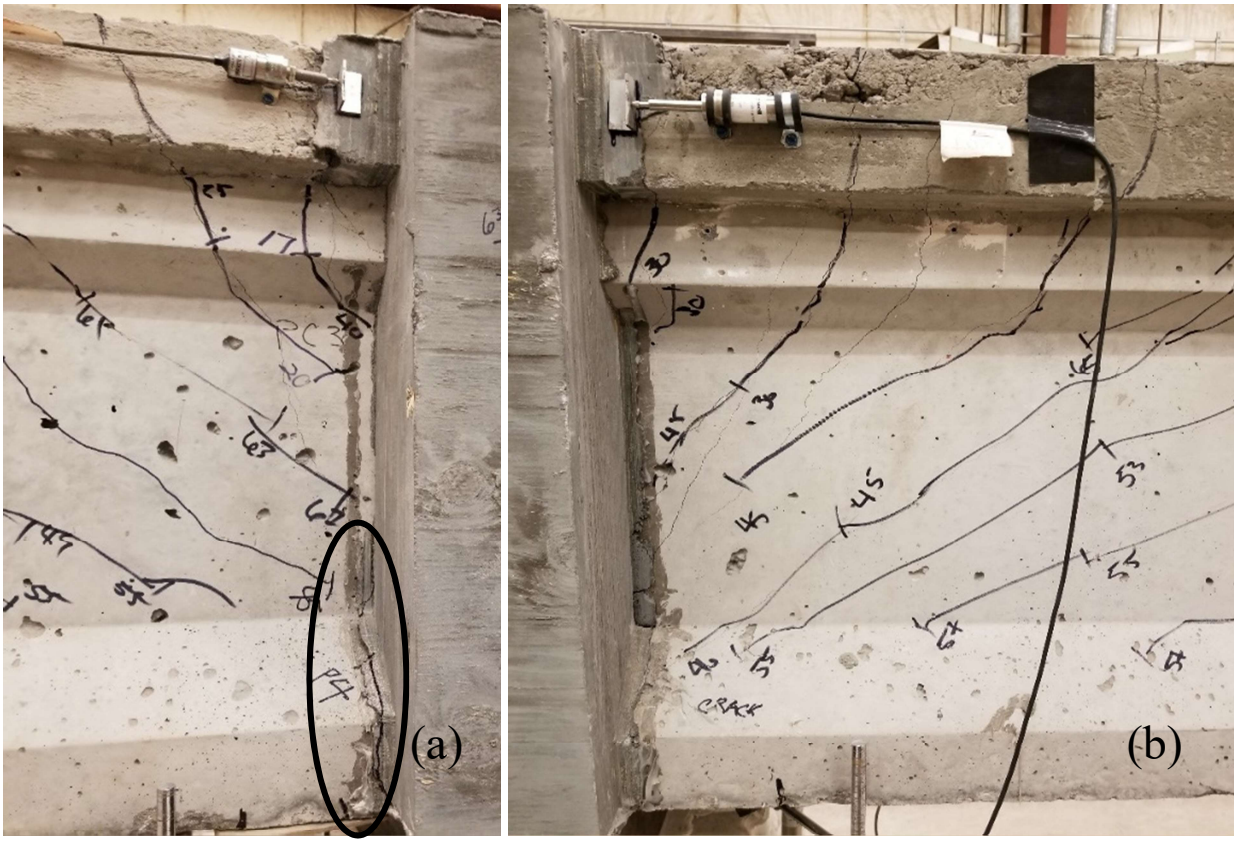

Figure 104. Positive moment joint separation at the interface between the NC3-N girder and the UHPC joint (a) indicated by a dark oval and interface between the NC3-S girder and the UHPC joint showing no visible positive moment cracking (b)

4.3.4 Test RC3

Initial flexural cracking was observed near the joint interface on the RC3-N girder at a load of 17 kips, indicated in Figure 106a with a dark oval. A flexure-shear crack developed in the same girder at a load of 20 kips, shown in Figure 106a. Flexural cracks were observed on the east face of the continuity joint after the next load increment, at a load of 30 kips, shown in Figure 107a. In addition, two more cracks had developed at a load of 30 kips, a flexural crack near the joint interface in the RC3-S girder, indicated in Figure 106b with a dark oval, and a flexure-shear crack near the joint interface in the RC3-S girder, shown in Figure 106b. Flexural cracking directly under the load point was observed in the RC2-N at a load of 45 kips, and in the RC3-S girder at a load of 46 kips, shown in Figure 105. A flexural crack was observed on the west face of the continuity joint at a load of 51 kips, shown in Figure 107b.

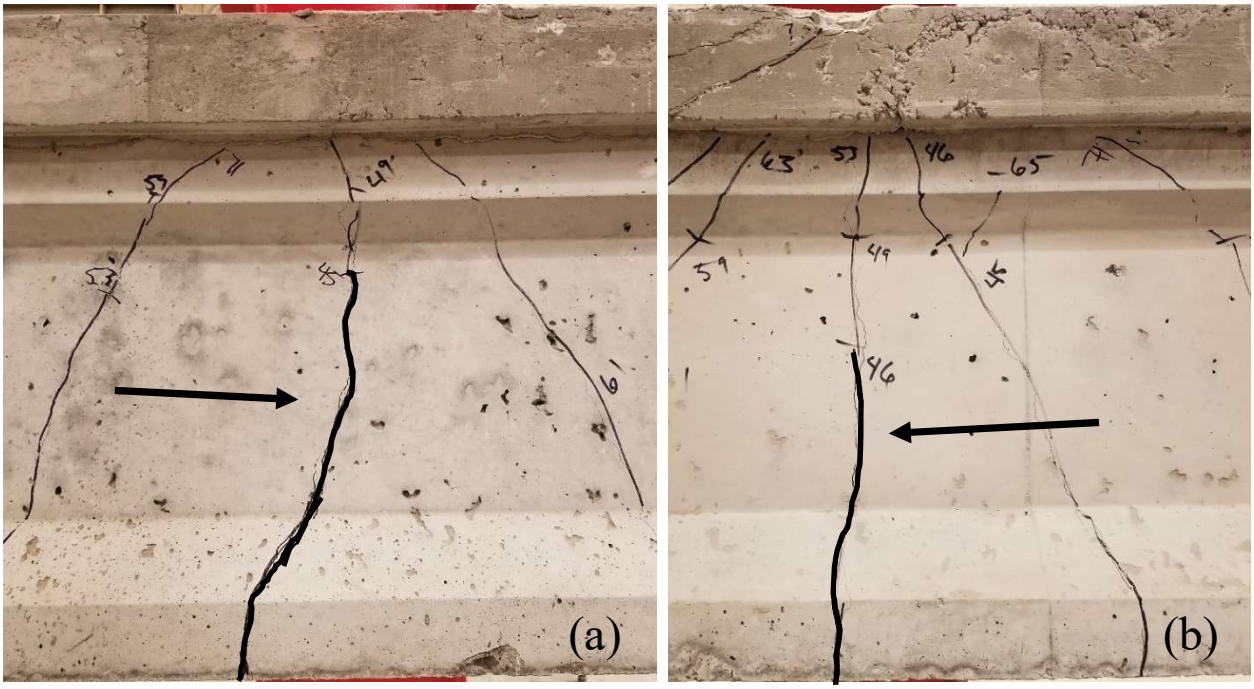

Figure 105. Initial flexural cracking under the load point on the RC3-N girder at 45 kips of load (a) and initial flexural cracking under the load point on the RC3-S girder at 46 kips of load (b). Arrows point to the dark lines that indicate the initial flexural cracks.

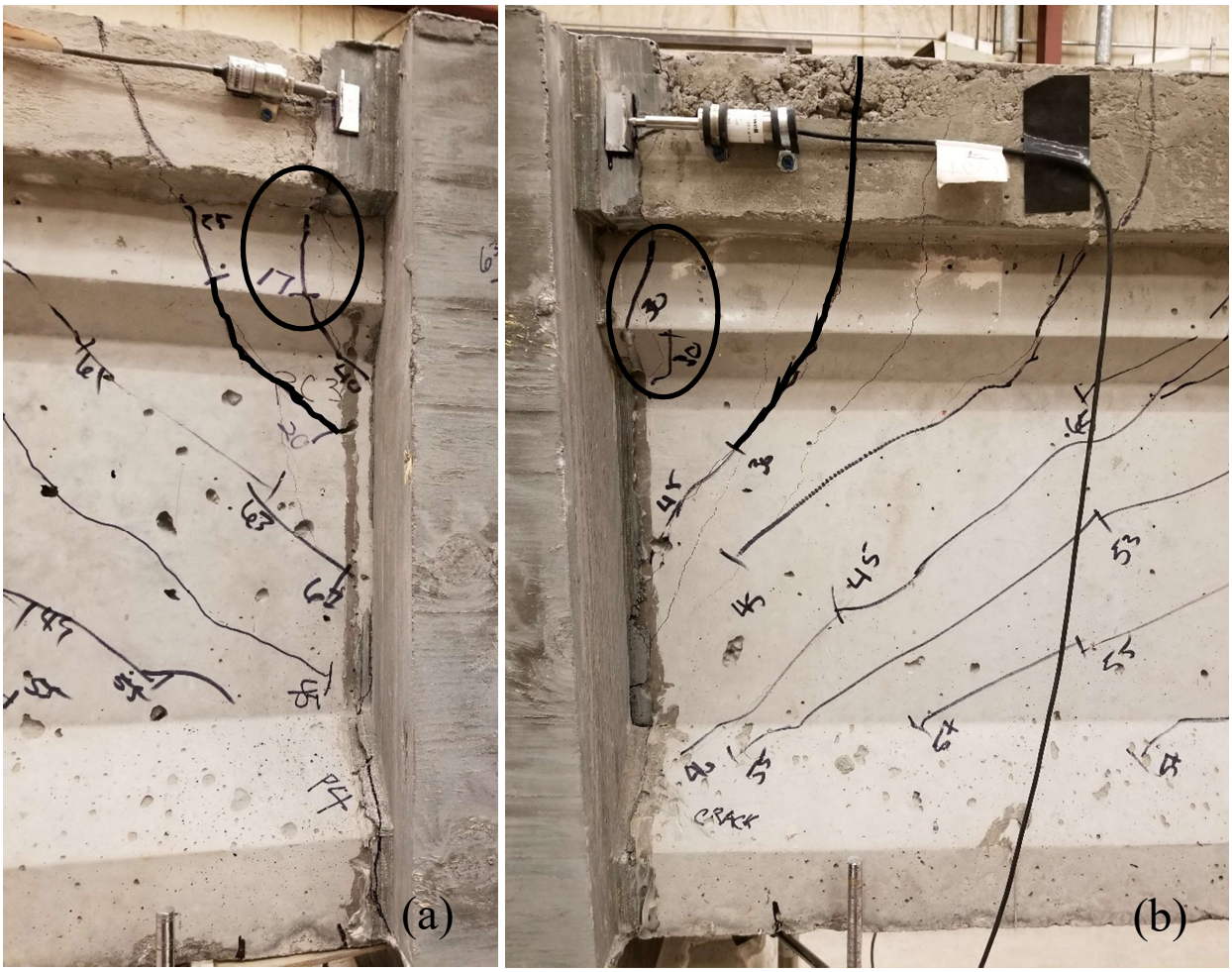

Figure 106. Initial flexural cracking on the RC3-N girder at 17 kips of load and initial flexure-shear cracking on the RC3-N girder at 20 kips of load (a) and initial flexural cracking on the RC3-S girder at 30 kips of load and flexure-shear cracking on the RC3-S girder at 30 kips of load (b). Dark ovals show the initial flexural cracking near the continuity joint and arrows point to the dark lines that indicate the initial flexure-shear cracking.

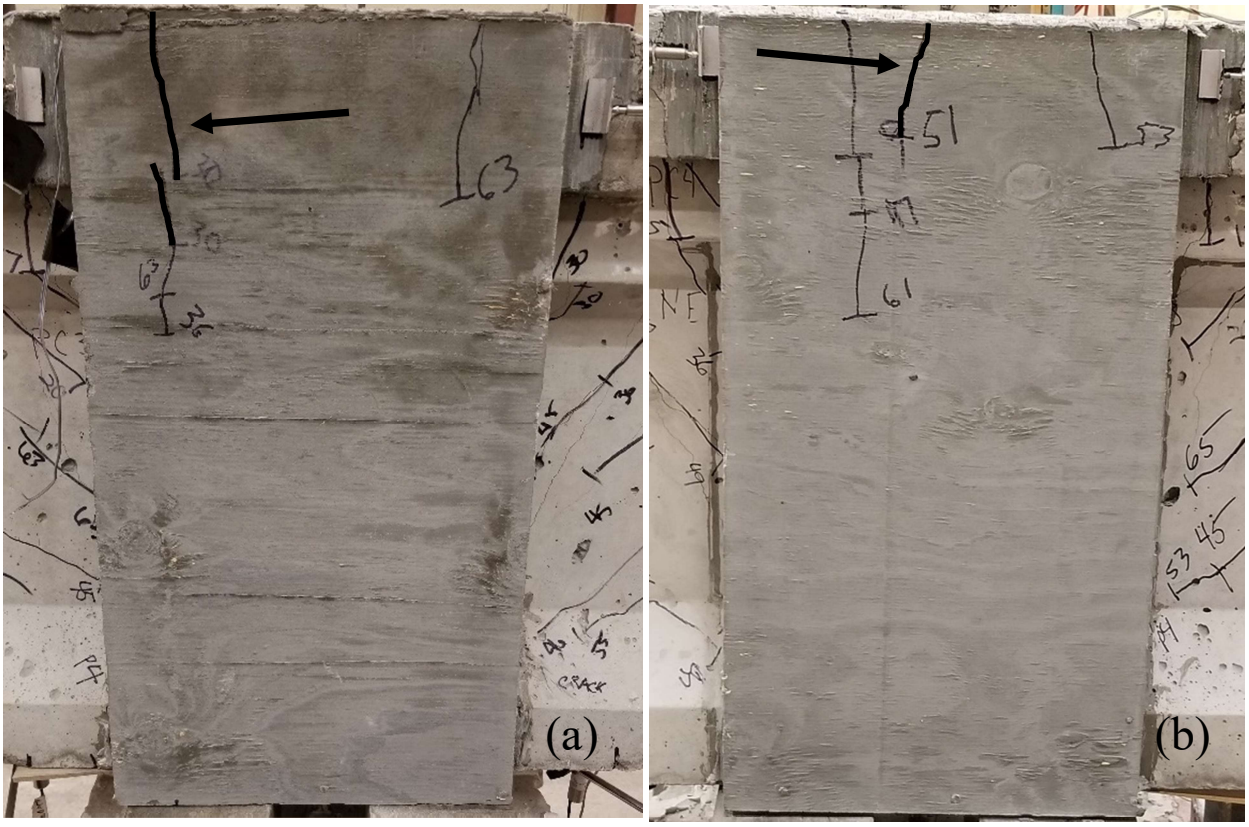

Figure 107. Initial continuity joint flexural cracking on the east face at a load of 30 kips (a) and initial continuity joint flexural cracking on the west face at a load of 51 kips (b). Arrows point to the dark lines that indicate the initial flexural cracking.

Cracking that developed between initial cracking and final failure included additional flexural cracks under the point load, flexure-shear cracks near the joint interface, web shear cracks near the point load, and flexural cracks in the UHPC joint. Most of the cracks that occurred in the RC3 specimen between initial cracking and failure were flexure-shear and web shear cracks. These cracks developed as the load increased and the flexure-shear cracks began to move away from the joint interface toward the load point. Upon reaching approximately halfway to the load point from the joint, web shear cracks developed in place of the flexure-shear cracks. Figure 108 shows the flexural cracks and web shear cracks between the joint interface and load point for the RC3-N and RC3-S girders.

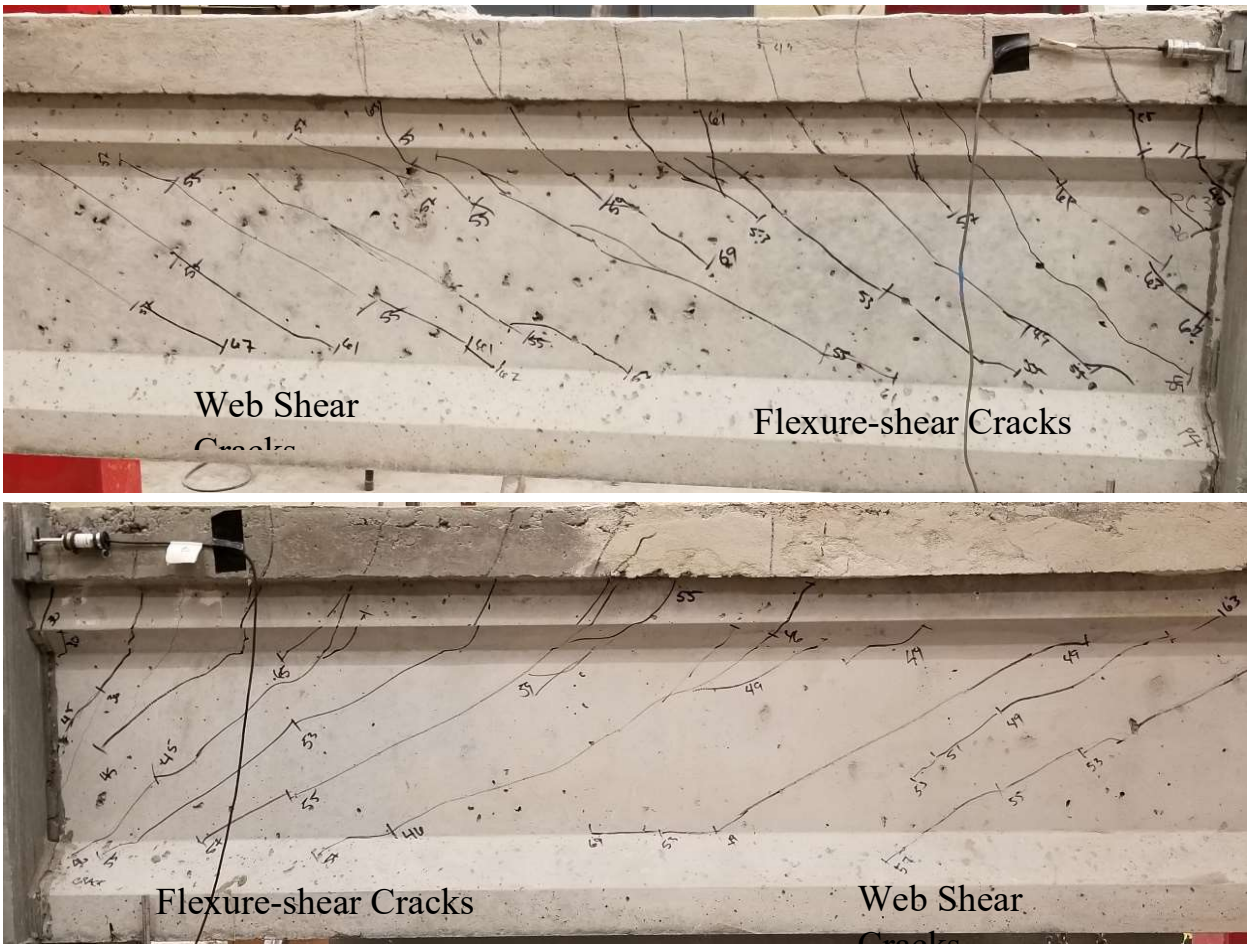

Figure 108. RC3-N girder with flexure-shear cracks and web shear cracks (top) and RC3-S girder with flexure-shear cracks and web shear cracks (bottom).

Loading of the specimen was stopped upon reaching an applied load of 76.1 kips on the RC3-N girder and 73.3 kips on the RC3-S girder. Under these loading conditions the concrete deck began to crush at the load point in both girders, as shown by the dark circles and arrows in Figure 109. In addition, there was significant widening of the flexural cracks under both load points, as shown by dark lines and arrows in Figure 109. These conditions were taken to indicate flexural failure of the beams and testing was concluded to prevent the prestressing strands from rupturing and causing damage to the testing apparatus.

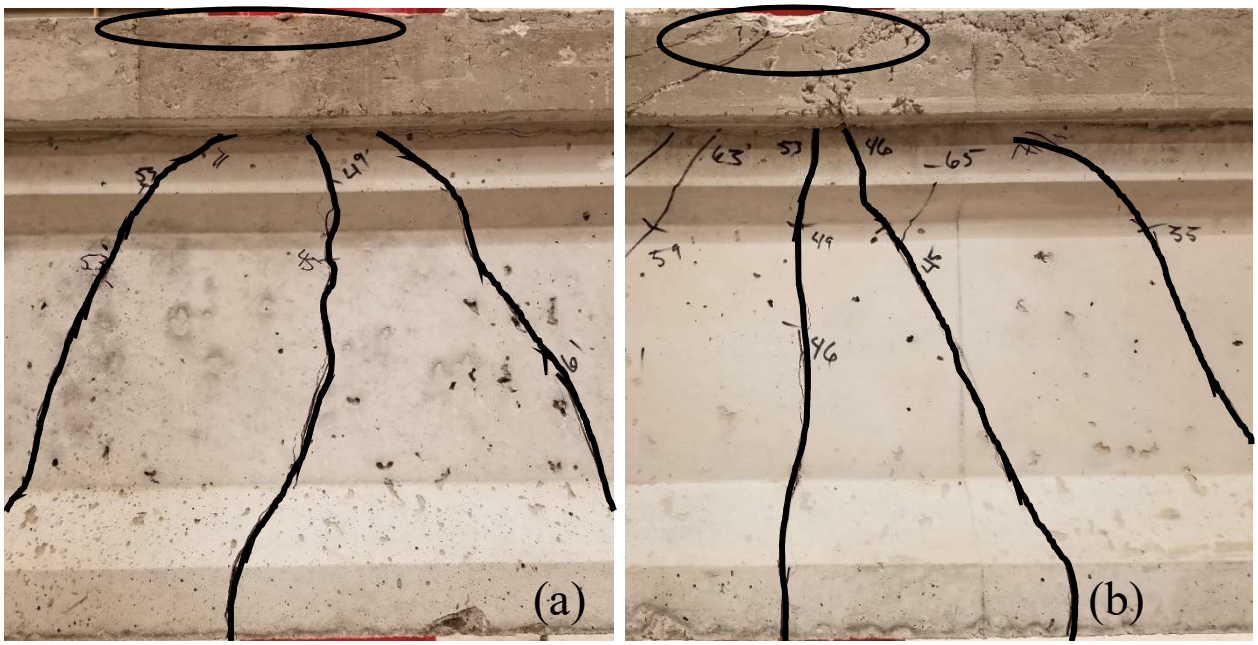

Figure 109. Final flexural cracking under the load point in the RC3-N (a) and RC3-S (b) girders are indicated by dark lines and concrete deck crushing is indicated by dark ovals.

The interface between the RC3-N girder and the UHPC joint had preexisting flexural cracking on the interface from the positive moment test, as shown in Figure 104. Flexural cracking occurred along the concrete deck to UHPC joint interface, which resulted in separation of the deck from the joint, and the flexural crack continued vertically down into the RC3-N girder's top flange and then into the web before going back toward the joint interface, as shown in Figure 110a. There was no clear indication that the flexural cracks from the negative moment test continued into the flexural cracks that had developed from the positive moment test, as had happened in the NC3 specimen. The interface between the RC3-S girder and UHPC joint had similar joint separation at the concrete deck to the RC3-N girder deck joint interface, as shown in Figure 110b. There was no clear indication of joint separation from the positive moment test, and the flexural cracks shown in Figure 110b did not indicate continuation into the joint interface.

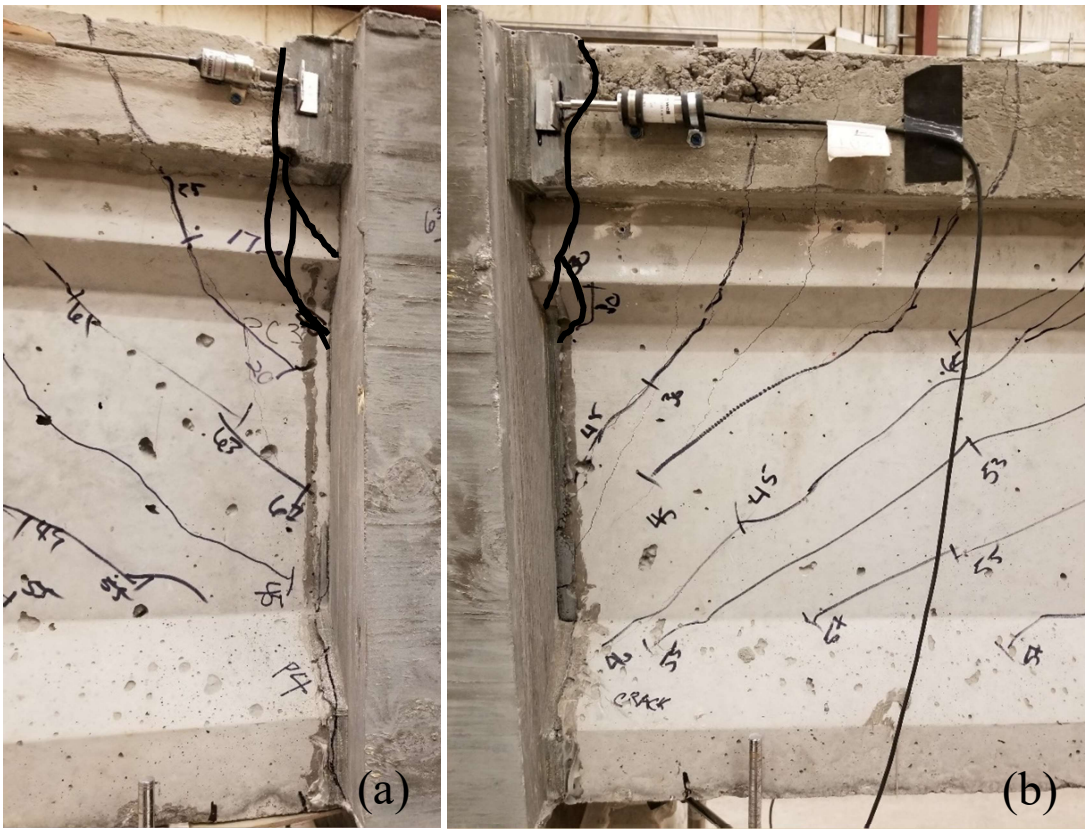

Figure 110. Joint separation at the interface between the RC3-N concrete deck and the UHPC joint with the flexural crack going vertically down in the girder (a) and joint separation at the joint interface between the RC3-S concrete deck and the UHPC joint with the flexural crack going vertically down into the girder (b) are indicated by dark lines.

Figure 111 shows the load-deflection curve for the RC3-N girder. The curve shows a reduction in stiffness that corresponds with the initial flexural cracking observed at 45 kips. Other types of initial cracking did not reduce the stiffness of the girder. This curve indicates a ductile behavior of the RC2-N prestressed girder during loading up to the ultimate load of 76.1 kips. In addition, the plateau of the load-deflection curve out to 1.4 inches of deflection also indicated the prestressing strands were yielding. Figure 112 shows the load-deflection curve for the RC3-S girder. The RC3-N and RC3-S girders had similar ductile behavior, and similar deflection at mid-span.

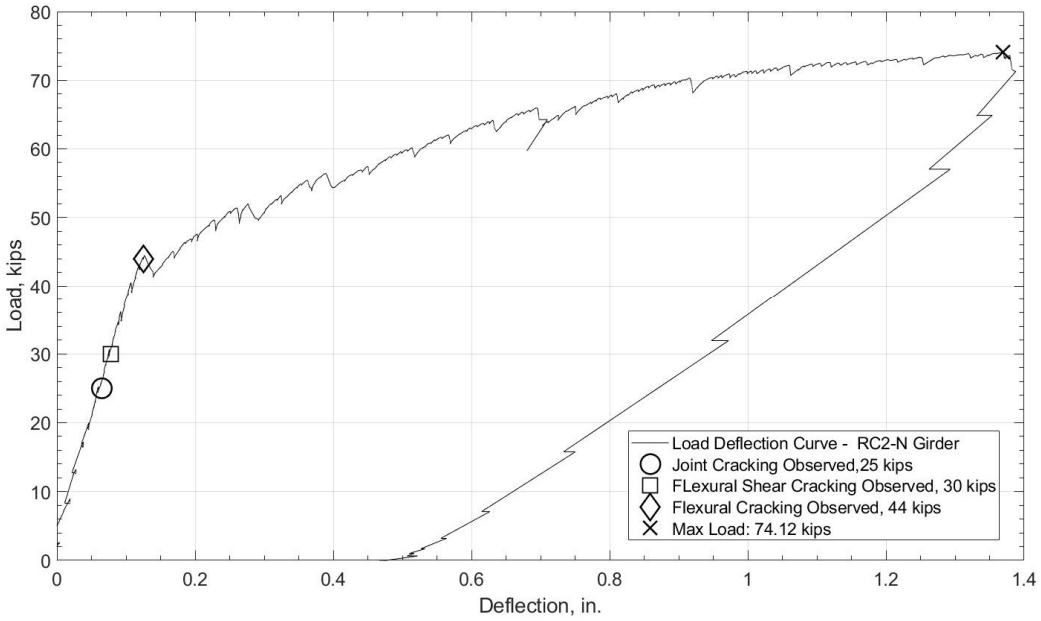

Figure 111. Load-deflection curve for the RC3-N girder.

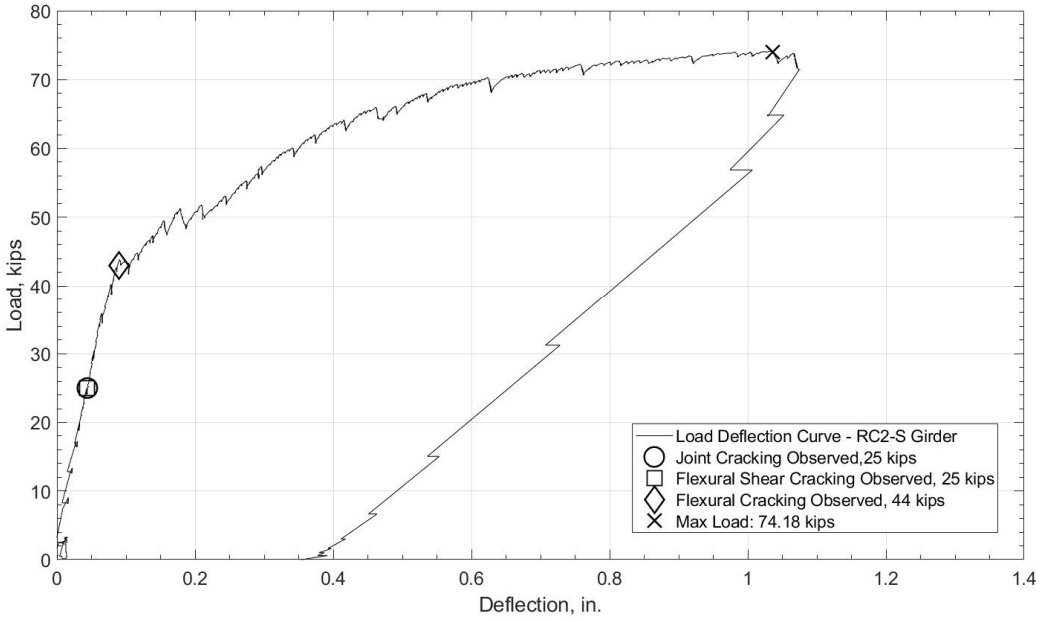

Figure 112. Load-deflection curve for the RC3-S girder.

Figure 113 shows the load-joint separation curve between the RC3-N girder's concrete deck and the UHPC joint. This figure only represents LVDT4 on the west face of the deck. LVDT9 did not give accurate data for this test, and measurements from this sensor were excluded. Figure 48 shows the location of the LVDTs on the joint interface which were located 2 inches below the top of the deck. The deck joint had minor separation until reaching the 60 kip load mark. This load-joint separation curve shows the opposite of what was expected. As the girder cracked in flexure, the reduction of girder stiffness appeared to have no effect on the rate of the joint seperation. The joint began to separate more significantly after the 60 kip mark because the girder began to have more downward curvature, creating a hinge at the weak point, being the joint interface. Figure 114 shows the load-joint separation curve between the RC3-S girder's concrete deck and the UHPC joint. This figure only represents LVDT11 on the west face of the deck. The NC3-N and NC3-S curves closely match one another in behavior except the NC3-S separation curve shows less separation occuring.

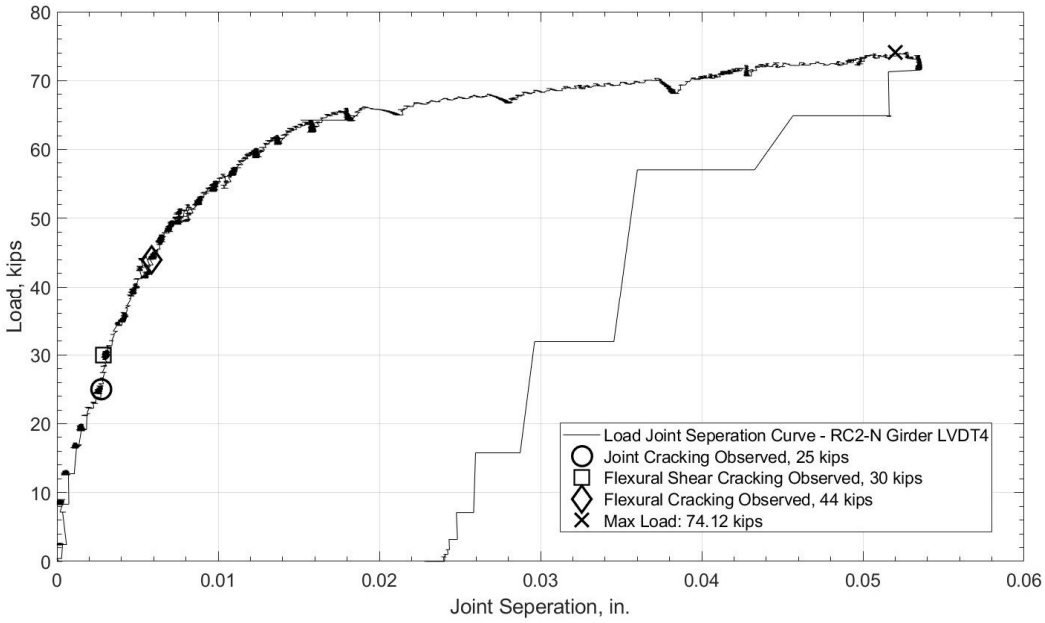

Figure 113. Load-joint separation curve at the RC3-N girder deck to UHPC joint interface west face.

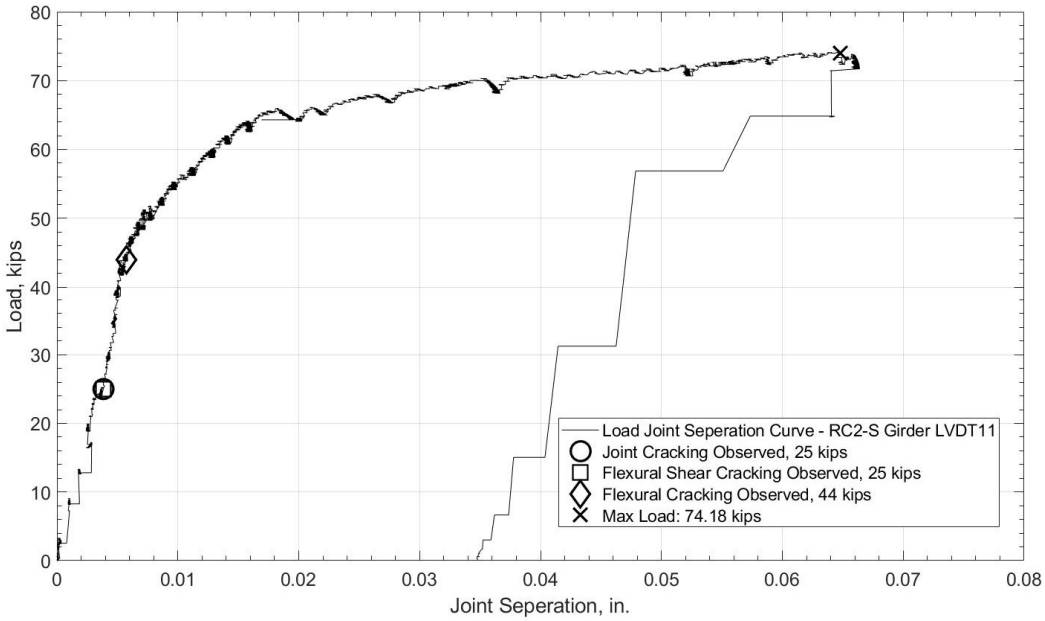

Figure 114. Load-joint separation curve at the RC3-S girder deck to UHPC joint interface west face.

4.4 Strain in the NC joints

Strain gauges were placed on two of the reinforcing bars resisting negative moment within the UHPC joint. The loads applied on the north and south girders were averaged together to get an average load to plot with the strain gauge data. This was done to reduce the amount of load vs. strain graphs, but was still considered reasonable as the north and south load data tracked closely to one another. Figure 115 shows the load-strain curve for the NC1 specimen. This curve shows the strain increasing in the joint as load was applied. This is to be expected, as the girders begin to deflect in downward curvature as more load is applied, which puts the continuity joint in an upward curvature causing a tension stress at the top of the joint, and in return causing strain in the rebar as load increases. Initial cracking observed on the joint did not appear to have any effect on the load-strain curve. Figure 116 shows the load strain curve for the NC2 specimen. This curve is very similar to the NC1 load strain curve, and observed initial joint cracking did not appear to have any effect on the strain in the rebar. Figure 117 shows the load-strain curve for the NC3 specimen. This curve shows similar behavior to the NC1 and NC2 load-strain curves, and initial joint cracking observed on the continuity joint had no apparent effect on the strain in the steel. On all three NC joints the strain did not reach a value of 0.002 strain, which means the rebar in the joint did not yield (assuming Grade 60 steel) and combined with no crushing of the concrete indicates that the joint did not fail. Overall the strain measurements only give a small detail of what the actual strain would be across the joint, as the strain can vary location to location depending on the cracking in the continuity joint.

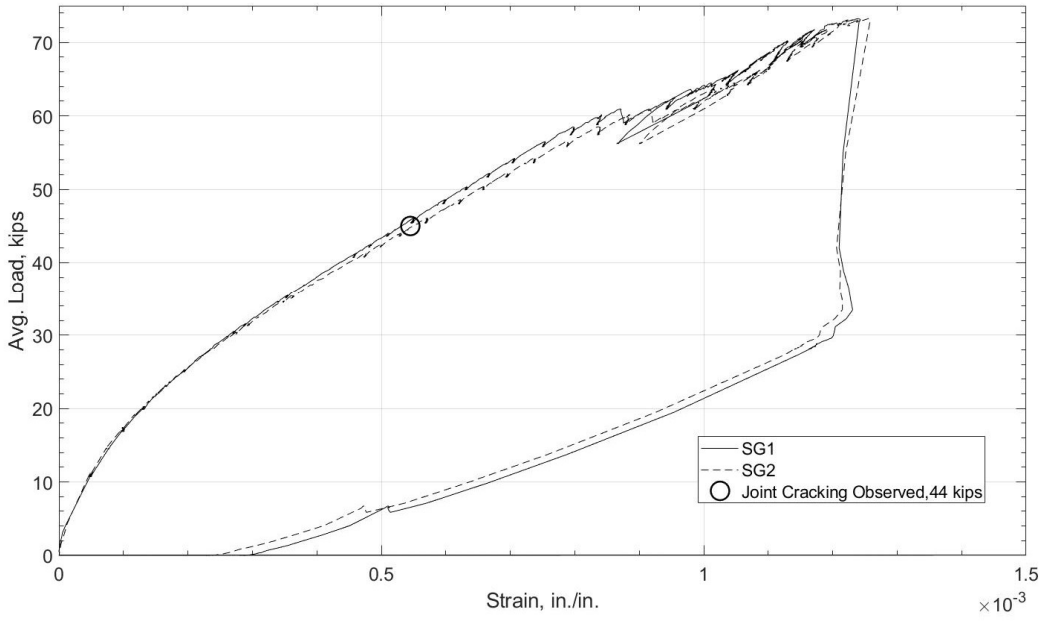

Figure 115. Load-strain curve for the NC1 joint.

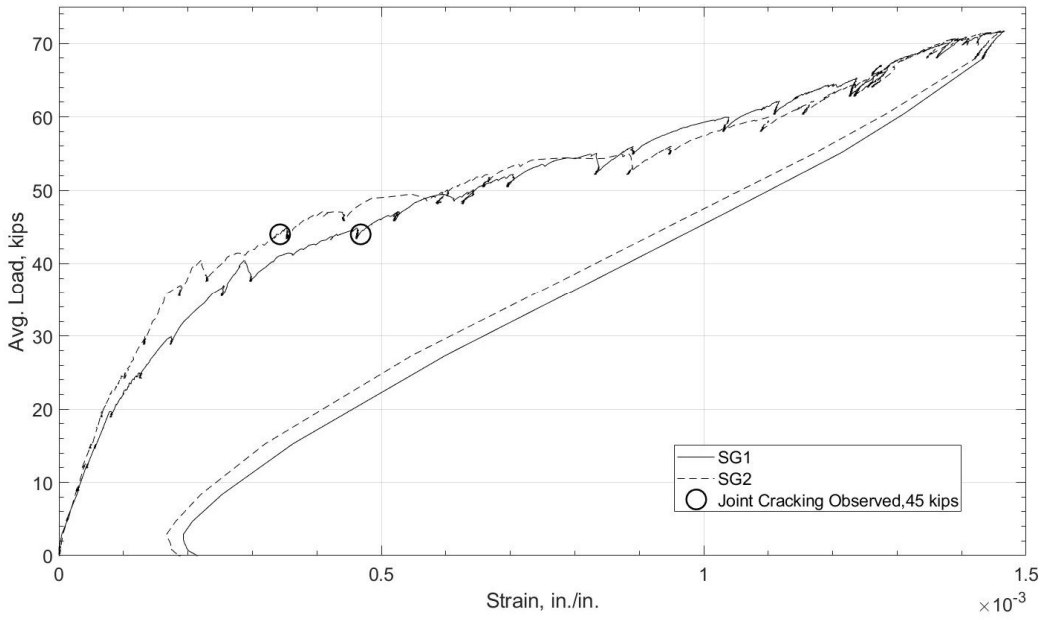

Figure 116. Load-strain curve for the NC2 joint.

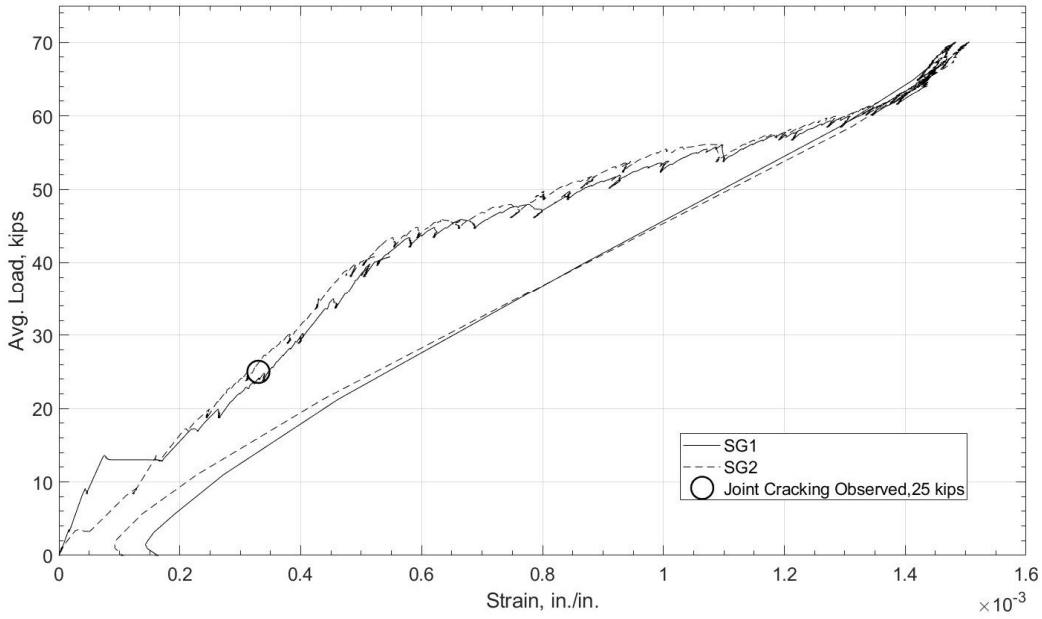

Figure 117. Load-strain curve for the NC3 joint.

4.5 Strain in the RC joints

The load-strain curves for the RC specimens were plotted like the NC load strain curves. The RC joints also tracked similarly the NC joints, as the load increased the strain increased in the joint, which is to be expected. Figure 118 shows the load-strain curve for the RC1 specimen. Initial observed joint cracking did not appear to have any effect on the increase in strain during loading, and both strain gauges tracked together. Figure 119 shows the load-strain curve for the RC2 specimen. Like the RC1 specimen, initial joint cracking did not appear to influence the load strain curve. The strain gauges did not track with one another, as SG1 did not plateau like SG2 had done. Figure 120 shows the load-strain curve for the RC3 specimen. Initial joint cracking had no apparent effects on the strain, as for the RC1 and RC2 load-strain curves. Overall, the RC load-strain curves had similar trends to the NC curves, however, the RC joints had higher strain in the rebar. The max strain in all but one strain gauge read higher than 0.002, meaning the rebar

had yielded at the location of the strain gauges. This could be a result of the fact that the RC joints encase the girders' end region, creating a stiffer joint compared to the NC joints, allowing the girders to take on more load before complete failure. This would allow the RC joints to get closer to complete failure resulting in increased strain relative to the NC joints.

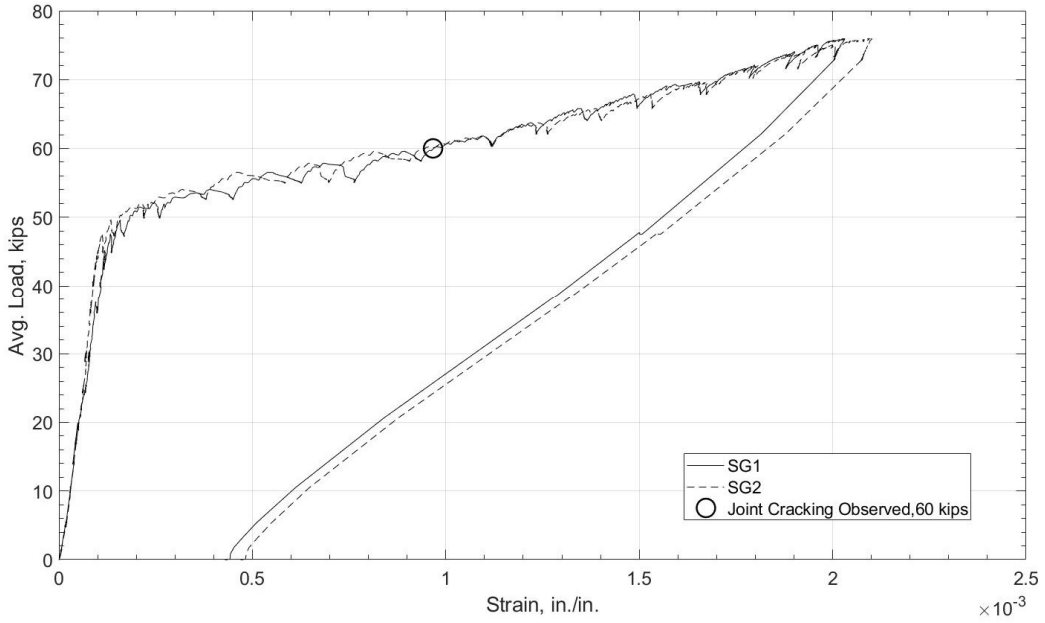

Figure 118. Load-strain curve for the RC1 joint.

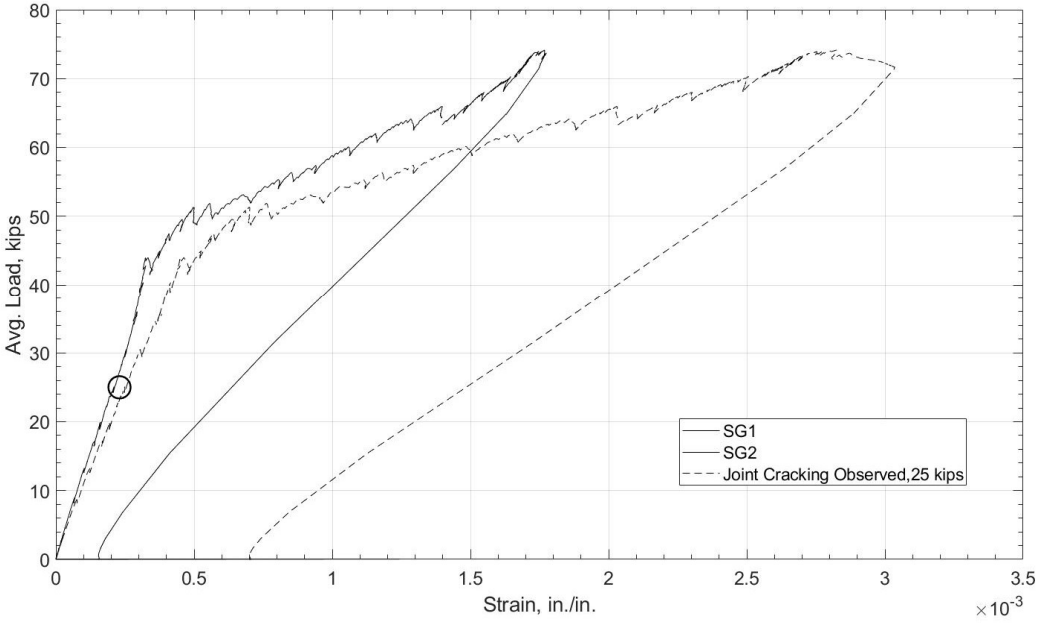

Figure 119. Load-strain curve for the RC2 joint.

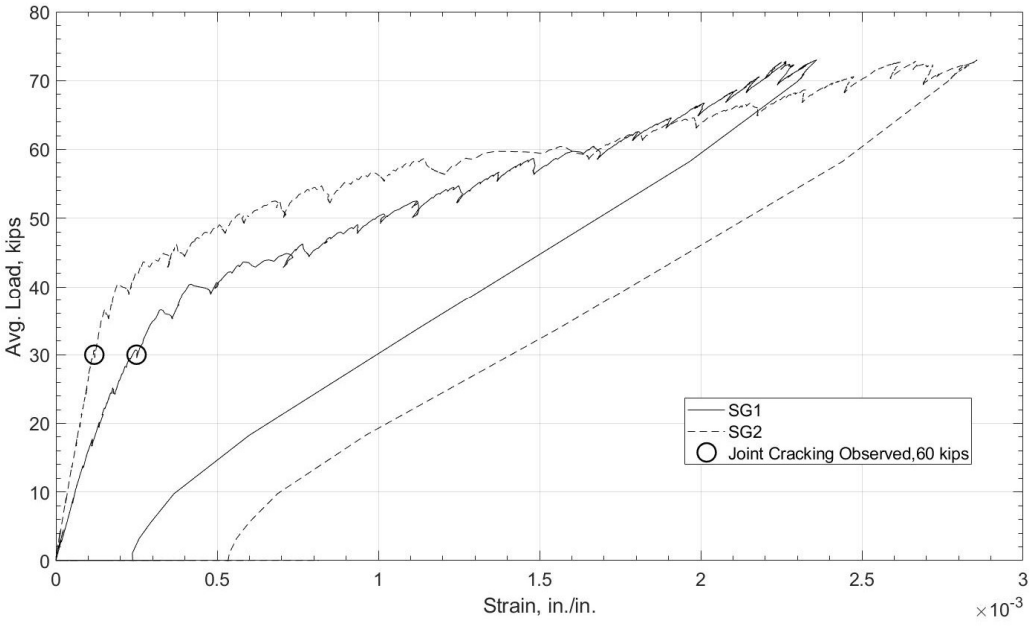

Figure 120. Load-strain curve for the RC3 joint.

4.6 Results Summary

There was not a large variation of the maximum loads between the NC specimens or between the RC specimens. However, the RC specimens had higher maximum loads than the NC specimens. The maximum deflections under the load points showed a consistent trend for the most part between specimens, but not necessarily similar magnitudes between the north and south girders. The deflection behavior was very similar for the RC specimens relative to variations and similarities between specimens. Larger maximum deflections under the load point were measured for the NC specimens compared to the RC specimens. The maximum joint separation was not consistent for the NC specimens or for the RC specimens. Both NC and RC specimens had similar maximum joint separation values overall. There was not a large variation between the two strain gauges in each NC specimen, and the maximum values were very similar when comparing the specimens. This was not the case for the RC specimens, as the strains for one gauge were higher compared to the other for all specimens. The RC specimens exhibited higher maximum strains than the NC specimens in general.

Presented in Tables 10-11 is a summary of the maximum values for the load applied to each girder, deflection at mid-span for each girder, joint separation at each joint interface, and the strain from the rebar in the joint for the NC and RC specimens.

Table 10. Maximum values obtained from testing NC specimens.

Specimen	NC1		NC2		NC3		Average
Girder	NC1-N	NC1-S	NC2-N	NC2-S	NC3-N	NC3-S	
Max Load, kips	72.5	73.8	71.5	72	69.8	70.2	71.6
Max deflection, inches	1.9	2.88	2	1.64	2.04	0.9135	1.90
Max Joint Separation, inches	0.17	0.098	0.096	-	0.012	0.086	0.092
Max strain-SG1	0.00124		0.00147		0.00148		0.00140
Max strain-SG2	0.00125		0.00146		0.00151		0.00141

Table 11. Maximum values obtained from testing NC specimens.

Specimen	R1		RC2		RC3		Average
Girder	RC1-N	RC1-S	RC2-N	RC2-S	RC3-N	RC3-S	
Max Load, kips	76.0	75.9	74.1	74.2	76.1	73.3	74.9
Max deflection, inches	1.58	1.26	1.37	1.07	1.40	1.40	1.35
Max Joint Separation, inches	0.077	-	0.053	0.066	0.08	0.061	0.067
Max strain-SG1	0.00203		0.00177		0.00236		.00210
Max strain-SG2	0.00210		0.00282		0.00286		.00260

Presented in Tables 12-13 are summaries of initial cracking loads for each type of cracking observed in each region of the specimens. These include flexural and flexure-shear cracks under the load points, flexural cracks near the joint interface, and flexural cracks in the joint.

Table 12. Initial cracking for each region of the NC specimens.

Specimen	NC1		NC2		NC3	
Girder	NC1-N	NC1-S	NC2-N	NC2-S	NC3-N	NC3-S
Flexural Crack Under Load Point, kips	43	45	40	45	41	46
Flexural Crack Near Joint Interface, kips	43	35	-	-	25	19.5
Flexure-shear Crack Near Joint Interface, kips	45	43	47	45	41	35
Flexural Crack in Joint, kips	44		45		25	

Table 13. Initial cracking for each region of the RC specimens.

Specimen	RC1		RC2		RC3	
Girder	RC1-N	RC1-S	RC2-N	RC2-S	RC3-N	RC3-S
Flexural Crack Under Load Point, kips	45	47	44	44	45	46
Flexural Crack Near Joint Interface, kips	20	20	25	19.5	17	30
Flexure-shear Crack Near Joint Interface, kips	25	30	30	25	20	30
Flexural Crack in Joint, kips	60		25		30	

4.6.1 Moment Capacity Comparison

The structural analysis program RISA was used to make a model of the NC and RC joint specimens to calculate the moment from the maximum experimental load applied to each individual girder per specimen during testing similarly to what is described for the design values in Chapter 3. This maximum moment from each girder in a specimen was then compared to the nominal moment capacity of an individual prestressed girder with the concrete deck included in the strain compatibility method for prestressed girders. The comparison shows an increase in moment capacity with the spans being continuous in both joint types. Presented in Tables 14-15 are the maximum moment capacity for each girder in a specimen from testing for both joint types, the nominal moment capacity for an individual girder, and the percentage increase for the overall moment capacity.

Table 14. Comparison of maximum experimental moment to the nominal moment of a single span girder for NC specimens.

Specimen	NC1		NC2		NC3	
Girder	NC1-N	NC1-S	NC2-N	NC2-S	NC3-N	NC3-S
Max Experimental Load w/ Continuity Joint, kips	72.5	73.8	71.5	72	69.8	70.2
RISA Max Moment from Max. Experimental load w/ Continuity Joint, kip-ft	211.9	215.6	208.9	210.4	204	205.1
M_n single span girder, kip-ft	145.7		145.7		145.7	
Moment percentage increase w/Continuity Joint	31.2	32.4	30.3	30.8	28.6	29.0

Table 15. Comparison of maximum experimental moment to the nominal moment of a single span girder for RC specimens.

Specimen	RC1		RC2		RC3	
Girder	RC1-N	RC1-S	RC2-N	RC2-S	RC3-N	RC3-S
Max Experimental Load w/ Continuity Joint, kips	76	75.9	74.1	74.2	76.1	73.3
RISA Max Moment from Max. Experimental load w/ Continuity Joint, kip-ft	217.2	216.9	211.8	212	217.5	209.6
M_n single span girder, kip-ft	145.7		145.7		145.7	
Moment percentage increase w/Continuity Joint	32.9	32.8	31.2	31.3	33.0	30.5

Another comparison was done by finding an applied load on both girders in the continuous span model in RISA for both joint types that would result in the nominal moment capacity for an individual girder for both girders in the continuous span. The applied loads that were applied to the model to obtain a moment equal to the nominal moment capacity were 49.8 kips for the NC joint, and 51 kips for the RC joint. Figure 122 and Figure 122 show the results of the RISA model for both joint types with the applied loads. The point loads were then applied to a simply supported girder in RISA to come up with the max moment for that case. The max moment for the applied load of 49.8 kips from the NC joint was 224.1 kip-ft, and the max moment for the applied load of 51 kips from the RC joint was 229.5 kip-ft. These two values far exceed the nominal moment capacity of a single girder, which means if the continuous span was designed with the intent to increase the overall capacity of the bridge and continuity of the joint is lost, the capacity would be significantly reduced, at which point failure could occur.

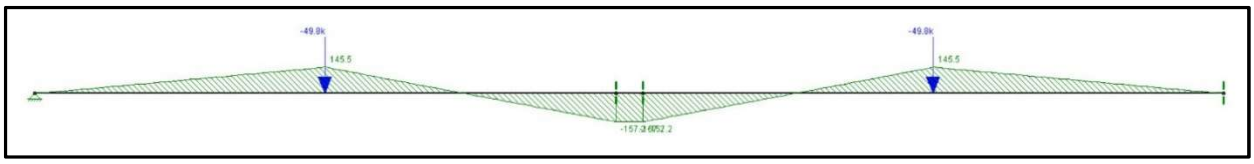

Figure 121.RISA model showing the applied loads to the NC joint configuration to determine the nominal moment capacity of a single span prestressed girder.

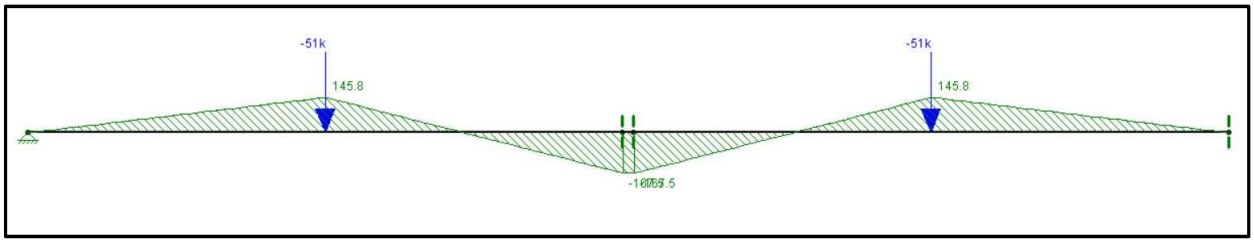

Figure 122. RISA model showing the applied loads to the RC joint configuration to determine the nominal moment capacity of a single span prestressed girder.

The configuration of the positive moment test conducted on the NC3 and RC3 specimens was put into a RISA model to calculate the maximum moment from the two point loads applied during the test. The moment calculated from the NC3 specimen test was 67.5 kip-ft. This moment was 2.1 kip-ft from the calculated joint cracking moment of 69.6 kip-ft. As this was within 3% of the cracking moment, the moment capacity for the negative moment test was very comparable to NC1 and NC2 specimens that did not have a positive moment test conducted. The moment calculated from the RC3 specimen was 37.8 kip-ft. Although the moment at cracking was only slightly above half of the calculated joint cracking moment value, the RC3 specimen still performed similarly to the RC1 and RC2 specimens. Figure 123– Figure 124 show the RISA model with the max load applied in the positive moment tests.

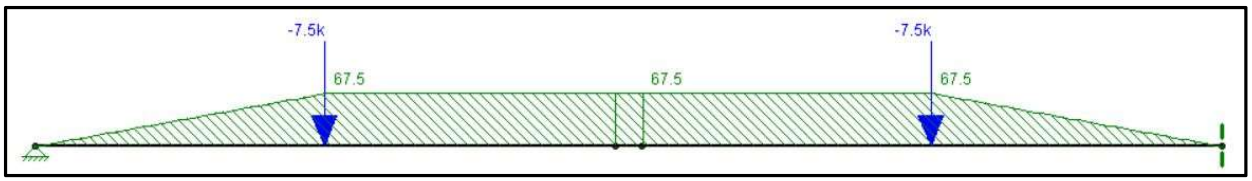

Figure 123. RISA model showing the applied loads to the NC continuity joint configuration from the positive moment test.

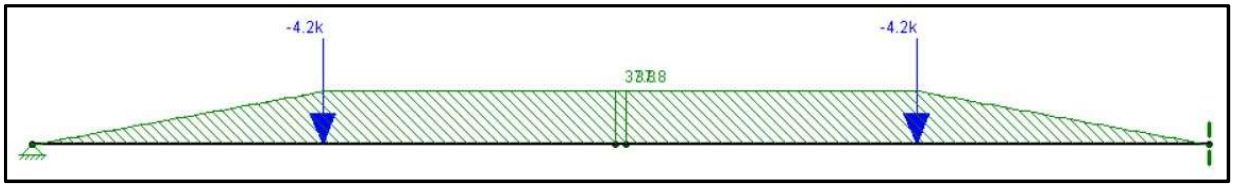

Figure 124. RISA model showing the applied loads to the RC joint configuration from the positive moment test.

5.0 Research Summary

This chapter summarizes the findings, conclusions, and recommendations based on the testing completed from NC and RC specimens presented in Chapter 4. The conclusions are limited to similar conditions within the two types of continuity joints. These conditions are the joint details, UHPC used in the joints, similar reinforcement ratios within the joint, and loading configuration on the girders.

5.1 Findings:

- Both continuity joint configurations resulted in increased flexural capacity for the prestressed girders.
- RC joint specimens had a higher ultimate capacity than NC continuity joint specimens by a percent difference of 4.5%
- RC joint specimens had less deflection at a higher load, than NC joints with less load and had higher deflections under the load point.
- RC joint reinforcing bars had a higher strain than NC continuity joint reinforcing bars by a percent difference of 48.6%.
- RC joint reinforcement yielded within the UHPC with short lap splices.
- NC joint reinforcement reached 70% of the yield capacity within the UHPC with short lap splices.
- NC and retrofit continuity joints had similar joint separation behavior between the concrete deck and UHPC joint.
- Initial flexural cracking under the load point occurred at a load between 40 and 47 kips for all specimens.
- Initial flexural cracking in the UHPC joint material was observed at a wide range of loads in both newly and retrofit connections.
- Both NC and RC specimens exhibited similar crack development over the course of the tests for flexural cracking under the load point, flexure-shear cracking near the continuity joint, and web shear cracking near the quarter-span point between the joint and the load point.
- No visible cracking occurred at the girder ends opposite the continuity joint.
- Significant flexural cracking, flexure-shear cracking, and joint separation was observed at the girder ends connected by the continuity joint
- Both NC3 and RC3 specimens exhibited no flexural cracking in the joint from the positive moment test.

- Both NC3 and RC3 specimens had flexural cracking along and near the joint interface from the positive moment test.
- Capacity of the NC3 and RC3 specimens for negative moment test was not affected by the positive moment test.

5.2 Conclusions:

- The increase of flexural capacity within the girders resulting from the NC and RC connection shows that precast prestressed girders made continuous for live load using a UHPC connection is a structurally superior system for total load capacity compared to two simple spans for the configuration tested.
- RC connections had a smaller joint distance between each girder, with the addition of 6 inches of the girders being embedded in UHPC. This detail provided an increased stiffness at the joint compared to the NC continuity joint allowing for an increased girder capacity, less girder deflection, and an increase in reinforcing bar strain at the joint.
- The loads resulting in the girders' initial flexural cracking under the load point were all within a 7 kip range which leads to a good probability of when flexural cracking should occur when this configuration is loaded regardless of the joint detailing.
- Failure of the system was pushed out of the joint and into the girder for both newly and retrofitted connections as shown by the lack of cracking occurring within the UHPC continuity joint.
- The RC joint configuration appears to be a good option for potentially strengthening existing bridges, if the girders can withstand the additional stresses applied from making them continuous for live load. In addition, the time dependent effects would be non-existent for these bridges and would decrease the amount of stress applied to the joint and girders.
- UHPC is better than conventional concrete for this application by allowing smaller connections with less congested reinforcement due to shortened required splice lengths, This was demonstrated in the RC connection with the reinforcement yielding at ultimate capacity, and by the NC connection reaching 70 percent of the yielding strain.
- Time dependent effects could still cause cracking for a system with UHPC joints, but cracking would more likely occur along the joint interface, or in the girder as demonstrated in the positive moment testing.

5.3 Recommendations:

- While the detail used in this research performed well, other potentially better, methods for attaching rebar shear studs into the girder ends should be investigated for the retrofit connections.

- Shear reinforcement at the girder ends connecting into continuity joints should be increased for new construction joints to withstand the redistribution of stresses caused by the joint compared to a simply supported beam.
- Preexisting girder ends that were not intended for continuity connections should be retrofit with fiber reinforced polymer wrap to increase shear capacity.
- The effects of time dependent deformation induced forces acting on the joint when prestressed girders are connected shortly after prestress release should be investigated further.
- Reinforcing bar splices over the continuity connection should be avoided for NC specimens to eliminate potential variables caused by the splice and highest flexural stress occurring at the same location.
- Results of this project should be compared to tests of similar specimens cast using normal concrete in place of UHPC for the joints.
- The rebar used within the joint should be tested to get the accurate yield stress for more accurate calculations.
- A test should be conducted on a simply supported prestressed girder with the same properties and cross section to get a better comparison of the flexural capacity increase with the use of continuity connections.

References

AASHTO LRFD Bridge Design Specifications, Customary U.S. Units (7th Edition). (2014). American Association of State Highway and Transportation Officials (AASHTO).

ASTM Standard C1437 (2015) "Standard Test Method for Flow of Hydraulic Cement Mortar," ASTM International, West Conshohocken, PA.

ASTM Standard C1856 (2017) "Standard Practice for Fabricating and Testing Specimens of Ultra-High Performance Concrete," ASTM International, West Conshohocken, PA.

Eamon, C., Chehab, A., & Parra-Montesinos, G. (2016). Field Tests of Two Prestressed-Concrete Girder Bridges for Live-Load Distribution and Moment Continuity. *Journal of Bridge Engineering, 21*(5).

Graybeal, B.A. (2006). *Material property characterization of ultra-high performance concrete*. Professional Service Industries, Inc, Turner-Fairbank Highway Research Center, & United States. Federal Highway Administration, Office of Research, Development and Technology, Turner-Fairbank Highway Research Center.

Graybeal, B.A. (2009). *Structural Behavior of a* Prototype UHPC Pi-Girder, FHWA-HRT-09-068, Federal Highway Administration, Department of Transportation, McLean, VA.

Graybeal, B.A. (2009). *Structural Behavior of a 2nd Generation UHPC Pi-Girder*, FHWA-HRT-09-069, Federal Highway Administration, Department of Transportation, McLean, VA.

Graybeal, B.A. (2010). *Field-Cast UHPC Connections for Modular Bridge Deck Elements*, FHWA-HRT-11-022, Federal Highway Administration, Department of Transportation, McLean, VA.

Graybeal, B.A. (2014). Splice Length of Prestressing Strand in Field-Cast Ultra-High Performance *Concrete Connections*, FHWA-HRT-14-041, Federal Highway Administration, Department of Transportation, McLean, VA.

Maya, L., & Graybeal, B. (2017). *Experimental study of strand splice connections in UHPC for continuous precast prestressed concrete bridges*. Engineering Structures, 133, 81-90. doi:10.1016/j.engstruct.2016.12.018.

Miller, R., United States. Federal Highway Administration, & National Cooperative Highway Research Program. (2004). *Connection of simple-span precast concrete girders for continuity* (Report (National Cooperative Highway Research Program); 519). Washington, D.C.: Transportation Research Board.

Oesterle, R., Glikin, J. D., & Larson, S. C. (1989). Design of precast, prestressed bridge girders made continuous / R.G. Oesterle, J.D. Glikin, and S.C. Larson. (Report (National Cooperative Highway Research Program); 322). Washington, D.C.: Transportation Research Board, National Research Council.

Park, H. (2003). Model-Based Optimization of Ultra-High Performance Concrete Highway Bridge Girders, 139, Massachusetts Institute of Technology, Cambridge, MA.

Russell, H., and Graybeal, B. (2013). Ultra- High Performance Concrete: A State-of-the-Art Report for the Bridge *Community*, Report No. FHWA-HRT-13-060, Federal Highway Administration, Department of Transportation, McLean, VA.

Saadeghvaziri, M., Spillers, W., and Yin, L. (2004). *Improvement of Continuity Connection over* Fixed Piers, FHWA-NJ-2004-017, Federal Highway Administration, Department of Transportation, Newark, NJ.

Yuan, J., and Graybeal, B. (2014). Bond Behavior of Reinforcing Steel in Ultra-High Performance Concrete, FHWA-HRT-14-090, Federal Highway Administration, Department of Transportation, McLean, VA.